NASA CR 121107
MTI 72TR32

FLEXIBLE ROTOR BALANCING BY THE INFLUENCE COEFFICIENT METHOD

PART I: EVALUATION OF THE EXACT POINT-SPEED AND LEAST SQUARES PROCEDURES

by

Juergen M. Tessarzik

MECHANICAL TECHNOLOGY INCORPORATED

Prepared for

NATIONAL AERONAUTICS AND SPACE ADMINISTRATION
Lewis Research Center

Contract NAS3-14420

William J. Anderson, Chief
Bearings and Mechanical Power Transfer Branch

1. Report No. NASA CR-121107	2. Government Accession No.	3. Recipient's Catalog No.
4. Title and Subtitle FLEXIBLE ROTOR BALANCING BY THE INFLUENCE COEFFICIENT METHOD, PART I: EVALUATION OF THE EXACT POINT-SPEED AND LEAST-SQUARES PROCEDURES		5. Report Date July 1972 6. Performing Organization Code
7. Author(s) Juergen M. Tessarzik		8. Performing Organization Report No. MTI-72TR32 10. Work Unit No.
9. Performing Organization Name and Address Mechanical Technology Incorporated 968 Albany-Shaker Road Latham, New York 12110		11. Contract or Grant No. NAS 3-14420 13. Type of Report and Period Covered Contractor Report
12. Sponsoring Agency Name and Address National Aeronautics and Space Administration Washing, D. C. 20546		14. Sponsoring Agency Code

15. Supplementary Notes

William J. Anderson, Chief, Bearings and Mechanical Power Transfer Branch, NASA Lewis Research Center, Cleveland, Ohio 44135

16. Abstract

An experimental test program was conducted to extend the verified operating region of the Influence Coefficient Method's Exact Point-Speed procedure for balancing of flexible rotating machinery. Also, the Least Squares procedure (of which the Exact Point-Speed procedure is a particular case) was applied to several test cases which were identical to those investigated by the Exact Point-Speed procedure. A comparison of the effectiveness of both balancing procedures under identical test conditions was thus obtained.

The practical aspects of balancing real, flexible rotors were investigated through inclusion of rotor out-of-roundness data at the measurement probe locations. The computer program was demonstrated to be fully capable of handling out-of-roundness data in the investigation.

Testing was performed predominantly with a machine having a 41-inch (104 cm) long, 126-pound (57 kg) rotor. This rotor was operated over a speed range encompassing three rotor-bearing system critical speeds.

Both balancing procedures were evaluated for several different conditions of initial rotor unbalance. Safe (and slow) passage through all the critical speeds was obtained after two or three balancing runs in most cases.

The Least Squares procedure was found to be generally equivalent in capability to the Exact Point-Speed procedure for the configurations studied. (U)

17. Key Words (Suggested by Author(s))	18. Distribution Statement
Flexible Rotor Balancing, Computer Methods	Unclassified-unlimited

19. Security Classif. (of this report)	20. Security Classif. (of this page)	21. No. of Pages	22. Price*
Unclassified	Unclassified	113	$3.00

* For sale by the National Technical Information Service, Springfield, Virginia 22151

FOREWORD

The investigation reported herein was performed by Mechanical Technology Incorporated under Contract NAS3-14420 for the National Aeronautics and Space Administration, Lewis Research Center, Cleveland, Ohio. Mr. William J. Anderson was the NASA Project Manager, and Dr. Robert H. Badgley was the MTI Project Manager.

The Influence Coefficient Balancing computer programs used for the successful balancing of the test rotor described herein, as well as the analysis upon which the computer programs are based, were written by Dr. Jorgen Lund, Consultant to MTI.

The experimental data reported herein was acquired with the assistance of Mr. Walter Spodnewski, Senior Technician. The computer calculations were conducted by Mrs. F. Gillham, Engineering Analyst.

Page Intentionally Left Blank

ABSTRACT

An experimental test program was conducted to extend the verified operating region of the Influence Coefficient Method's Exact Point-Speed procedure for balancing of flexible rotating machinery. Also, the Least Squares procedure (of which the Exact Point-Speed procedure is a particular case) was applied to several test cases which were identical to those investigated by the Exact Point-Speed procedure. A comparison of the effectiveness of both balancing procedures under identical test conditions was thus obtained.

The practical aspects of balancing real, flexible rotors were investigated through inclusion of rotor out-of-roundness data at the measurement probe locations. The computer program was demonstrated to be fully capable of handling out-of-roundness data in the investigation.

Testing was performed predominantly with a machine having a 41-inch (104 cm) long, 126-pound (57 kg) rotor. This rotor was operated over a speed range encompassing three rotor-bearing system critical speeds.

Both balancing procedures were evaluated for several different conditions of initial rotor unbalance. Safe (and slow) passage through all the critical speeds was obtained after two or three balancing runs in most cases.

The Least Squares procedure was found to be generally equivalent in capability to the Exact Point-Speed procedure for the configurations studied.

Page Intentionally Left Blank

TABLE OF CONTENTS

TABLE OF CONTENTS (concluded)

LIST OF FIGURES

LIST OF FIGURES (continued)

LIST OF FIGURES (continued)

LIST OF FIGURES (continued)

LIST OF FIGURES (concluded)

LIST OF TABLES

SUMMARY

Expanded assessment of the "real world" effectiveness of two related flexible rotor balancing procedures has been obtained from the continuation of a test program begun under NASA contract in 1969. The two balancing procedures investigated were the Exact Point-Speed Influence Coefficient Method (for which some results were already reported previously) and the Least Squares Influence Coefficient Method. The objectives of the herein-reported test program were to experimentally confirm the validity of the balancing procedures for various rotors and unbalance configurations, and to assess the practical aspects of applying the method to an actual flexible-rotor machine.

The major part of the test program was performed with a machine having a 41-inch (104 cm) long, 126-pound (57 kg) rotor, which was supported by two self-acting fluid-film pivoted-pad journal bearings. The rotor had a three-mass configuration, one mass being centrally located between bearings, the remaining two masses being overhung at each end of the rotor. For some of the tests the rotor was modified through removal of one of the overhung masses at one end of the rotor, which reduced rotor weight to 110 pounds (50 kg).

The rotor was operated at speeds up to 15,000 rpm. Three rotor-bearing system critical speeds were encountered within this speed range. The first two critical speeds were essentially "rigid body" criticals. The third critical, which occurred at about 11,000 rpm for the three-mass rotor and at a somewhat higher rotational speed for the two-mass rotor, was the first flexural critical of the rotor. Rotor damping at the flexural critical was very low for the three-mass rotor due to the journal bearings being located at the nodal points of the rotor. The test machine thus provided an excellent (severe) challenge for evaluation of the influence coefficient balancing method.

The following conditions of initial rotor unbalance were investigated for the three-mass configuration rotor:

I. Rotor with substantial unbalance added along the rotor in a corkscrew configuration (weights spaced 90° angularly apart, progressing in a corkscrew fashion from one end of rotor to other); see Figure 14.

II. Rotor with substantial unbalance added along the rotor in an in-line, in-phase configuration (single axial plane, weights all on same side of shaft centerline); see Figure 25.

III. Rotor with substantial unbalance added along the rotor in an in-line, out-of-phase configuration (single axial plane, weights on overhung masses on same side of shaft centerline but opposite from weights on central mass); see Figure 31.

For the two-mass rotor, one rotor unbalance configuration was investigated:

IV. Rotor with substantial unbalance added to the overhung disc; see Figure 36.

Additionally, the effect of rotor out-of-roundness at the measurement locations upon balancing effectiveness was evaluated experimentally for the two-mass rotor with unbalance weights placed at the overhung disc.

Satisfactory rotor balance was achieved for all unbalance arrangements and for both rotor configurations with reasonable effort.*

For two test cases (II and III) the three-mass rotor was balanced with only two series of trial weight runs when the Least Squares procedure was used. The two-mass rotor, which exhibits more bearing damping at the approach to the third critical speed and therefore a much less rapid rise in rotor amplitudes, was satisfactorily balanced after one series of trial weight runs by either of the two balancing procedures investigated.

Comparison of all test results, including those from previously presented work, reveals the Least Squares procedure to be generally as capable as the Exact Point-Speed procedure. Furthermore, tests with substantial out-of-roundness at the measuring stations have clearly demonstrated that the capability to subtract rotor out-of-roundness is essential when proximity probes are used to acquire vibration data. Failure to account for eccentricity or out-of-roundness of the rotor surface at the measurement probe locations will severely affect final balance quality.

The dependency of the balancing procedures upon accurate instrumentation to obtain phase and amplitude measurements during trial weight runs was demonstrated during one phase of the experimental program.

Application of the Influence Coefficient Method (either the Exact Point-Speed or the Least Squares Procedure) to specific flexible rotor balancing problem situations in commercial machinery appears warranted. Finally, with respect to balancing technology, the capability of either procedure to balance flexible rotors which must operate through several flexural critical speeds may now be evaluated.

---

* To some extent, the definition of "reasonable effort" in flexible rotor balancing will always remain relative, and must await the availability of "effectiveness data" relative to many or all other flexible rotor balancing methods.

INTRODUCTION

The need for well-developed flexible rotor balancing technology, together with the economical and technical benefits which are expected to result from this capability once it becomes available to technical users, have been amply described in References 1 and 2. This report documents the results of a continuing effort to assess new and untried flexible rotor balancing procedures and evaluate their effectiveness for "real-world" applications. A previous report (Reference 1) described in detail the Influence Coefficient Method adapted for flexible rotor balancing, and particularly the Exact Point-Speed procedure, which is computationally the simplest application of this method to flexible rotor balancing. Reference 1 also presented experimental results where a fluid-film bearing supported rotor was balanced for safe (and slow) passage through the third (first flexural) critical speed. Three particular combinations of intentional unbalance added to the test rotor were examined.

This report continues with additional results obtained by the same balancing procedure for the original test rotor which is characterized by a three-mass configuration, and then proceeds to a modified rotor where one overhung end mass was removed to produce significant changes in rotor vibration amplitudes and response mode shapes.

The new procedure for flexible rotor balancing evaluated in this report is termed the Least Squares balancing procedure. It is also based upon the Influence Coefficient Method, but differs computationally from the previously examined Exact Point-Speed balancing procedure in that it is not limited to the solution of a square matrix (and thus to a limited amount of trial weight data for a given number of rotor balancing planes). Instead, the Least Squares procedure minimizes the squares of the residual amplitudes when the balancing data fed into the program exceeds the square matrix requirement. Practically, this capability will allow the use of multiple sets of trial weight data which were acquired in one run, but at several different rotational speeds. (A brief treatment of the mathematical derivation of the Least Squares balancing procedure is given in Reference 3, Appendix A.)

Balancing tests performed with the aid of the Least Squares procedure duplicated those which were done by the Exact Point-Speed procedure (including those performed previously and reported in Reference 1). A realistic comparison of the relative effectiveness of both procedures has thus been obtained.

THEORY OF LEAST SQUARES BALANCING PROCEDURE

The Least Squares balancing procedure differs from the Exact Point-Speed balancing procedure only by virtue of one significant addition to the latter: a calculation of the minimized sum of the squares of residual amplitudes for a 'nonsquare' matrix of influence coefficients.

The application of the Influence Coefficient Method to the balancing of flexible rotors was described in detail in Reference (1). Also shown in Reference (1) (page 9) was the square matrix requirement for solution of the equation

$$\{w_R\} = [\alpha] \cdot \{U_p\}$$

where

w_R = rotor amplitude in rotating coordinates
α = influence coefficients
U_p = unbalance moments in plane p

Only where the number of measurements (v = number of speeds x number of sensors) is equal to the number of balancing planes (n) can $\{w_R\}$ be made zero. The method thus was called the "Exact Point-Speed" procedure in References (1) and (2).

A discussion of the relationships of the Exact Point-Speed balancing procedure (square matrix, v=n) to the Least Squares balancing procedure (where $v > n$) is given in Reference (3), Appendix A.

The computer program implementing the Least Squares balancing procedure contains substantially the same features for increased experimental accuracy and convenience which are incorporated in the Exact Point-Speed computer program described in Reference (1). These features are as follows:

1. A provision to read instrumentation calibration factors for amplitude and phase angle measurements directly into the program. This feature eliminates the need for manual conversion of instrumentation output voltages into displacement and phase angle units.

2. A provision to include phase angle off-set. Such a feature allows for a non-zero angle between the reference axial plane and the plane(s) containing the trial weight holes. Thus, the calculated angular locations for the balancing correction weights are relative to the actual trial weight holes in each plane, decreasing chances for error. This feature was extensively used for all the correction weight calculations.

3. A provision for specifying shaft out-of-roundness at the measuring locations. Subtraction of the synchronous harmonic of shaft out-of-roundness from displacement transducer signals at the measuring stations may well

make the difference between a rotor that can be successfully balanced and one that cannot. Such a correction becomes increasingly important as the ratio of shaft out-of-roundness to unbalance displacement amplitude increases. This feature was investigated in the course of the experiments described in this report.

4. Provisions for making trial weight runs with the weight placed first in one (specified) radial position in each trial weight plane, and then placed 180^{o} opposite from the original position in the same axial plane. Trial weight runs with the weight placed first in one location and then 180^{o} away can yield significant increases in experimental accuracy. This is because the averaging of two amplitude vectors obtained by separate and opposing trial weight placements acts to reduce the experimental error. All of the experimental results documented in this report were obtained by means of this technique. A cursory examination of the effect of omitting either one of the trial weight data sets (data for either 0^{o} or 180^{o}) is given in this report.

A description of the experimental procedure by which the Influence Coefficient balancing method is implemented may be found in Appendix A.

FLEXIBLE ROTOR BALANCING TEST APPARATUS

The basic mechanical apparatus used for the herein-described balancing tests had originally been designed and built for turbulent journal bearing tests and for rotor unbalance response measurements. It had recently been used for balancing tests by the Exact Point-Speed procedure (Reference 1). Since it was not modified for the tests described herein, the results of these tests may be readily compared with those reported in Reference 1. The system was specifically designed to amplify the effects of rotor unbalance, thus providing an excellent vehicle for experimental rotor balancing tests.

Test Rotor Configuration - Three-Mass Version

The three-mass test rotor shown in Figure 1a was 41 inches (104 cm) long and had a nominal bearing diameter of 2.500 inches (63.5 mm). The rotor [2]* was basically symmetrical about its mid-point and had a three-mass configuration with the two end masses [3] overhung from each of the journal bearings. The center span between bearings was 25 inches (63.5 cm).

The center mass, 6 inches (152.4 mm) in diameter by 6 inches (152.4 mm) long, was integral with the shaft. The detachable end masses [3], also 6 inches (152.4 mm) in diameter but only 3 inches (76.2 mm) long, were shrunk onto the shaft and secured by locknuts [33]. The weight of the center mass, exclusive of the 2.5-inch (63.5 mm) diameter shaft section, was 36 pounds (16.3 kg); that of each end mass, 19 pounds (8.6 kg). Total rotor weight was 126 pounds (57 kg). Rotor material was nitrided Nitralloy 135 (modified).

The test rotor was in the above described configuration for all of the previously conducted tests which were reported in Reference 1. During some of the tests reported herein, the rotor configuration was changed through removal of an end mass, as described below.

Test Rotor Configuration - Two-Mass Version

In its altered form (Figure 1b) the rotor had one steel end mass removed and replaced by a lightweight aluminum disc. The aluminum disc weighed only 2.5 pounds (1.13 kg) and the complete rotor in this configuration weighed 109.5 pounds (49.7 kg).

The aluminum disc, which replaced the steel end mass opposite the drive end for some of the tests, had a similar though not identical arrangement of tapped holes for balancing weights as the steel masses had. The number of small holes on the larger radius had been doubled and a complete second set of large holes (3/8-16 thread) was provided on a smaller radius of 1.75 inch (44.4 mm).

---

* In this section, numbers in brackets refer to detail part numbers in Figure 1.

Figure 2 shows a photograph of the aluminum end disc installed on the rotor in the Flexible-Rotor Balancing Test Rig.

Features Common to Both Rotors — Three- and Two-Mass Versions

The test rotor was equipped with a row of axial, tapped holes [34,35] on each side of each mass. The tapped holes, 15 degrees apart, were on a 2.625-inch (66.7 mm) radius from the center of the shaft. The holes contained 10-32 threads, except for two opposing 3/8-16 threaded holes in each set which were used for trial weight placement. The large and the small holes were in-line in all three rotor masses.

One of the end discs was equipped on one-half of its outer diameter with a narrow (1/4-inch; 6.3 mm) reflective foil. The other half of the circumference of the disc was painted dull black. The circumferential mid-point position on the reflective strip was the reference point on the rotor from which the angles for maximum dynamic displacement at the other rotor stations were measured (phase angles).

The reflective segment extended between the two large trial weight holes, which were arbitrarily marked zero degrees and 180 degrees, as shown in Figure 3. Consequently, the reference point (the mid-point of the reflective strip) actually led the zero degree position marked on the disk by 90 degrees. This required that 90 degrees be subtracted from all phase angle measurements, which was equivalent to making the reference position and the zero degree position on the rotor coincident. (The same result could have been obtained by rotating the reflective strip on the disk, until it covered the arc 90-0-270 degrees). The test rig setup is shown in Figure 4, and the relationship among the reference mark, the trial weight locations, and the angular markings on the rotor is shown in Figure 3.

Test Rotor Support Bearings

The test rotor was radially supported by two identical tilting-pad type journal bearings, shown in Figures 5 and 6. Each of the bearings consisted of four radially rigid pads [6]*, with each pad extending over an 80 degree arc and with a pivot position of 44 degrees (55 percent) from the leading edge. The pivot configuration was that of a fixed sphere (integral with the pivot [8]) in contact with a cylindrical surface. The ball-in-cylinder pivot geometry allowed the pad to tilt in both the pitch and roll directions. Thus, it permitted the pads to track both translatory and conical shaft motions. The latter capability is particularly useful in a test machine, because it allows the experimenter greater latitude in setting the maximum permissible orbits without fear of contact between the shaft and the edges of the pads.

Pad length in the axial direction was 2.5 inches (63.5 mm) and the radial clearance between each pad (at the pivot location) and the shaft was 0.00187 inch (0.0475 mm). (Calculated journal bearing fluid-film radial stiffness as a function of rotor speed is presented and discussed below). Horizontal and vertical radial stiffnesses are identical for the bearings, which were oriented

* In this section, numbers in brackets refer to detail part numbers in Figure 5.

in the load-between-pivots configuration.

The lubricating fluid for the journal bearing was Dow Corning 200, with a kinematic viscosity of 0.65 cS at 77°F (25°C). The bearings were operated in a flooded condition with a maximum temperature rise of 10°F (5.5°C).

Axial positioning of the test rotor was provided by two externally-pressurized air-lubricated thrust bearings located on both sides of the rotor center mass. Locations of the thrust bearings are indicated in Figure 1 and in Section B-B of Figure 5.

Mechanical Features of the Apparatus

The test machine (Figure 1) was mounted on a structural steel base weighing approximately 3,200 pounds (1455 kg). The base was isolated from the floor by rubber pads. (These details of the base assembly are mentioned here only for reasons of documentation. There is no inherent requirement of either the Exact Point-Speed procedure or the Least Squares procedure relative to the type of machinery base used.) Bolted to the top plate of the base was an aluminum jig plate [20]* to which were fastened the individual housings [9 and 11] for the journal and thrust bearings, and the proximity probe holders [4] which held capacitance probes [31] used to measure motions of the end masses [3]. Also mounted to the same plate was the electric drive motor [30].

The journal bearing housings [3] were equipped with seal rings [5] on both sides. Each of these rings had a clearance seal adjacent to the bearing housing with an outboard annular scavenging cavity. Outside the scavenging cavity was a labyrinth seal to restrict entry of air into the cavity. Bearing fluid leaking into the cavity was pumped back into the sump by two separate electrically-driven pumps. A positive-displacement pump driven by an air motor forced the bearing fluid through a water-cooled heat exchanger and back into the journal bearing housings. Journal bearing supply pressure was controlled to ensure a flooded condition. Journal bearing temperature was measured by thermocouples welded to the back of the two lower pads in each bearing.

The drive motor [30] was a 30-hp, 30,000-rpm, 600-Hz, 600-volt electric motor, powered from a variable frequency generator set. The test rotor was coupled to the drive motor by a crowned spline coupling [14,15,16]. The teeth on the shaft part of the coupling [15] were crowned so that the coupling could accommodate up to an 0.030-inch (0.76 mm) radial misalignment between the axes of the motor and the test shaft without shaft restraint.

Instrumentation

The instrumentation required to run the test machine consisted of pressure gages indicating thrust bearing air supply pressure, journal bearing fluid supply pressure, drive motor bearing air-mist lubrication pressure, thermocouples indicating journal bearing pad and bearing fluid temperature, and a speed counter for shaft rotational speed. To assure safe rotor operation under heavy unbalance

---

* In this section numbers in brackets refer to detail part numbers in Figure 1.

loads, vertical and horizontal capacitance-type proximity probes were installed in two locations along the rotor axis for orbit indications. These orbits were monitored during test runs through oscilloscope observation.

The instrumentation required for acquisition of balancing data consisted of four capacitance-type proximity probes for the measurement of vertical rotor displacements and one optical probe for the identification of angular rotor positions (phase angle). The locations of the proximity probes and the optical probe along the rotor axis are shown in Figures 7 and 8.

A schematic of the complete data acquisition system as it was used for the flexible rotor balancing tests described in this report is shown in Figure 9.

The instrumentation system used for the balancing tests described in this report differs from the system described in Reference 1 only in the level of automation of the data recording system. In addition to the magnetic tape system which was used for the plotting of simultaneously-recorded rotor displacement amplitudes from various rotor stations, a paper printout system was added for faster and more accurate displacement probe readouts.

In the test rig, only the vertically mounted capacitance probes were used for balancing purposes. The selection of the vertical plane instead of the horizontal plane for displacement measurements was an arbitrary decision.

At this time, no fixed rule is available for specifying a priori the required number of measuring stations along the axis of the rotor for balancing by the procedures investigated. In fact, this topic deserves further study. The computer program for the Exact Point-Speed procedure allows the substitution of data obtained at different speeds for data obtained at different rotor locations, provided that the product of the number of measuring stations and the rotational speeds at which trial weight data are taken is equal to the number of balancing planes in which correction weights are to be added. Balancing of the test rotor by the Exact Point-Speed procedure was predominantly done in three planes. (A description of the reason which led to this development is given under Test Results.) However, balancing of the same rotor by the Least Squares procedure was mostly done in four planes. Consequently, four measurement stations were always used when trial weight data was obtained. The data from each station was recorded so that different combinations of speeds and measuring stations could be selected, as desired, for computations of correction weight values.

The fifth signal required for the balancing operation (commonly referred to as the reference signal) was used to relate a fixed angular position on the rotor (the equivalent of the commonly used 'mark') to the angular position at which maximum dynamic displacement occurred at each of the four measurement stations. This angular relationship, called phase-angle, was obtained as follows: Half of the circumference of one of the end masses was covered with a reflective foil and the other half painted dull black. Each time the reflective arc passed under an optical proximity sensor (MTI Fotonic sensor, Model KD-38) a constant but adjustable voltage was generated. This square-wave signal was then converted to a sine wave in a band-pass tracking filter (Vibration Instrument Company, Tracking Analyzer 235 DS). The phase relationship between the converted reference signal and each of the displacement signals (analyzed one at a time) was measured in a phase meter (Model 933A, also made by Vibration Instrument Company.)

Amplitude readout was monitored for proper range adjustments (signal amplification) at the Tracking Analyzer, which provided an output level meter from 0.003 to 10 volts rms full scale, adjustable in seven steps.

Phase angle readout was visually monitored at the digital phase-angle display provided by the phase meter.

The data acquisition system, as described above, is sufficient to conduct flexible rotor balancing. However, depending upon the mechanical charactersitics of the rotor system, it may be important, and at the same time difficult, to obtain amplitude data for all four probes at exactly the same rotational speed. This may be important if either amplitudes or phase angles are sensitive to small changes in speed, as for example, near an undamped shaft critical speed. Particular rotor drive controls, temperature effects, and damping may make it difficult to hold rotor speed constant long enough to take all required readings.

The requirement of nearly simultaneous readings was previously met through use of an available seven channel tape recorder. Five phase-tied channels were used for the four displacement signals and the reference signal, while two direct reading channels were used for data identification (voice and rotational speed). By playing back the magnetic tape four times and switching from one displacement signal to the next, data was obtained at nearly identical rotational speeds.

A different technical approach was pursued during the course of the tests described herein. This approach not only permitted data acquisition from all four probes at the same rotational speed, but also considerably reduced the cost of the data recording system (the need for the tape recorder was removed) and improved the accuracy of the data through elimination of errors inherent in visual readout of data.

The capacitance probe signals were fed into an automatic switch (Scanner, Monsanto Model 508A) which switched them upon command, one at a time, into the tracking analyzer. The outputs of the tracking analyzer and the phase meter were digitized in two digital voltmeters (Monsanto 200A) and printed sequentially from all four probes by a 20-column line printer (Monsato 511A). The printer recorded the paired amplitude and phase angle values at a rate of approximately three lines per second. Print commands were given manually whenever rotor speed was within close limits of the preselected balancing speed. Multiple recordings were thus made for each data point, which were later (if necessary) averaged prior to processing in the computer.

Instrumentation calibration procedures are presented in Appendix B.

General Analysis of the Rotor-Bearing System

A basic understanding of the dynamic response characteristics of a particular rotor to be balanced can be extremely valuable with respect to selection of both balancing planes and measurement stations. Critical speed calculations, and associated undamped mode shapes, will identify the number of criticals within or close to the operating speed range of the rotor, as well as the degree of "flexibility" of the rotor over the speed range. The mode shape plots can greatly assist in the selection of balance planes, both number and location.

As a matter of practical preparation for the balancing process, the locations of the proximity probes along the rotor axis should be at other than the shaft nodal points as they occur in the vicinity of the balancing speeds. Should the probes be at or near the nodal points, the low amplitude readings obtained may be a source of error in the calculation.

Similar comments apply to the locations selected for balancing planes. Highest balancing effectiveness will in general be obtained through the location of the balancing planes at non-nodal positions along the rotor for the rotor speeds of interest (including the effects of damping). This is because unbalances located at such non-nodal positions are most effective in producing large amplitudes. Quite obviously, the closer the balancing planes are to the most important unbalances, the better will be the result of the balancing procedure.

For the flexible rotor balance tests reported herein, two test rotor configurations were used. In its original configuration, the test rotor had a steel end mass overhung from each journal bearing. After modification, one steel end mass (opposite from the drive end) had been replaced by a lightweight aluminum disc. For both test rotor-bearing systems, the following calculations were performed:

1. Journal bearing stiffnesses, both horizontal and vertical, as functions of rotation speed (Curve A, Figure 10 for the three-mass rotor, and Figure 12 for the modified two-mass rotor).

2. Rotor critical speeds as functions of bearing stiffness (Curves B, C, D, Figure 10 for the three-mass rotor and Figure 12 for the two-mass rotor).

3. Rotor undamped mode shapes at the calculated critical speeds for vertical bearing stiffnesses of 10^5 lb/in. (1.75×10^7 n/m) for each bearing (Figure 11 for the three-mass rotor and Figure 13 for the two-mass rotor).

TEST RESULTS

Initial Rotor Condition Prior To All Tests

Prior to a previous test series the test rotor had been dynamically balanced at low speeds in a commercial balancing machine. In the course of subsequent flexible rotor balancing experiments, the same rotor was balanced in-place until it ran with acceptably low vibration orbits over a speed range encompassing the first three critical speeds. Nominally, this was the balance condition of the rotor at the start of the experiments described in this report. In this condition, orbits were generally quite small (less than 0.0002 inch (0.005 mm) peak-to-peak) for operating speeds up to 10,000 rpm. They increased rapidly at the approach to the third critical speed at 10,960 rpm to levels on the order of 0.0035 inch (0.089 mm) peak-to-peak, the limit set for passage through the resonance point. This condition was considered acceptable as a starting point, since previous balancing experiments had indicated that a finer initial rotor unbalance condition (prior to the deliberate addition of unbalance weights) would be of little significance to the interpretation and conduct of such experiments. Having a reasonably good initial level or rotor balance was found, however, to be helpful in determining whether the first set of calculated correction weights was of the correct order of magnitude.

Sequence of Balancing Runs

The sequence of balancing runs followed in the experiments described in this report reflects past experience, and is aimed at the quickest, most effective completion of the balancing effort. This approach was taken in lieu of an extensive exploration of the numerous different avenues provided for balancing by the computerized method. The following details will be noted from examination of the flow charts in Figures (14), (25), (31), (36) and (47):

1. The majority of attempts to utilize four balancing planes in the three-mass rotor were unsuccessful when the Exact Point-Speed balancing procedure was used. Considering all balancing experiments performed to date on this rotor (including those reported in Reference (1), only one in six attempts at four-plane balancing was successful. A case is considered unsuccessful if the calculated correction weights for the end planes of the center disc are 180° apart, very large, and nearly equal in size. While such weights may be expected to produce a balanced rotor, it would be impractical and inefficient to attach such relatively large weights to a rotor if only a very small net weight is required in the center disc and if the required balance moments may be obtained more efficiently by addition of weights to the end masses. The four-plane problem on this rotor was not encountered when the Least-Squares balancing procedure was used with sets of trial weight data taken at two or more rotational speeds. When the amount of input data for the Least-Squares procedure computation was reduced to the same volume as used for the Exact-Point Speed procedure calculation, however, (one speed, four planes, four probes) the calculated correction weights were identical to those calculated earlier (and too large for application to the center disc).

2. The minimum number of probes used was three, with one probe allocated to each large rotor mass. The mode shape of the test rotor at the third critical speed made it advisable to apply correction weights at the overhung masses for most efficient balance improvements. (Reference (1) gives one example where two-plane balancing at two rotational speeds was tried, without much success.)

3. The balancing speed selected for trial weight runs with the Exact Point-Speed balancing procedure was always as high as possible. The upper limit of the balancing speed was determined by the limit established for maximum rotor orbits and the size of the trial weight. After completion of the first balancing run, with correction weights inserted in the rotor, there usually also was an effective lower speed limit below which further trial weight runs could not be conducted. This was because rotor orbits (without the addition of the trial weight) frequently became too small at one or more rotor stations for reliable phase angle measurement. For this particular rotor-bearing system there existed only a relatively narrow speed range within which rotor amplitudes were large enough prior to insertion of trial weights and not too large with trial weights in place after completion of the final balancing run. This was due to the sharp rise in rotor amplitudes at the approach to the third critical speed (first bending critical).

4. The effect that trial weights of different sizes might have had upon balancing effectiveness was not expressly studied in these experiments. It has already been concluded, as indicated in the foregoing discussion on the selection of balancing speed, that trial weight size selection cannot be completely arbitrary for a given rotor-bearing system. Within the limits provided by the Mechanical and Instrumental systems, the trial weight size was kept relatively low for convenience of operation. Generally, no disadvantages arose as a result of size selection, and whenever a larger trial weight was used, such as for the first correction run in the corkscrew unbalance mode, no drastic improvements were noted. For reference, it may be noted that the typical trial weight was on the order of five percent of the total maximum deliberate unbalance weights added to the rotor.

5. All trial weight runs were performed with the trial weight placed first at the zero degree location and then, for a second run, 180° away in the same plane. The purpose behind this procedure is to obtain an improvement in experimental accuracy through vectorial averaging of the measurements. Attempts were not made to fully evaluate the precise need for this procedure with this test setup, or the benefits which have accrued from it. Obviously, the need for this increased effort will decrease with increases in the quality of measurements.

6. For the corkscrew unbalance configuration tests, and later for the conical unbalance configuration, two independent sets of calculations were made; one

was based upon the Exact Point-Speed balancing procedure and the other on the Least-Squares balancing procedure. Both sets of calculations had common starting points, which were the measured vibrations resulting from either the initial corkscrew unbalance configuration or the initial conical unbalance configuration. Upon completion of the balancing by the Exact Point Speed balancing procedure, which was signified by passage through the bending critical speed at 10,960 rpm with acceptable rotor orbits for the corkscrew test and reasonably low amplitudes for the conical test case, all correction weights added in the course of this balancing effort were removed from the rotor. Those weights calculated by the Least-Squares procedure from the initial rotor response data were then added. Figure 14 indicates the sequence of events in the balancing of the rotor with initial corkscrew unbalance by both methods. Figure 47 presents similar results for the conical unbalance test case.

First Test Case: Rotor With Corkscrew Unbalance

The Corkscrew Unbalance Test Case had been designed to be the most challenging test situation which the flexible rotor balancing programs under evaluation might face. Four unbalance weights of different magnitude were placed one in each rotor end disk and one each at the two faces of the center mass. They were angularly 90° apart from each other, progressing in a corkscrew fashion from end to end of the rotor. The resulting unbalance condition consisted of static and dynamic unbalance with a corkscrew-type bending distortion. The arrangement of the weights and their magnitude is shown in the top part of Figure 14. At each overhung end mass, the unbalance weight was attached on the side of the disc facing the journal bearing. Balance correction weights were applied to the outboard side of the end disk, and for some correction runs, at only one of the two sides of the center mass. A realistic situation was thus provided in which balancing planes and unbalance locations did not coincide.

The initial rotor amplitudes for the speed range from 3,000 to 10,000 rpm are recorded as curves 'A' in Figures 15 through 19, which present amplitude data for probe locations 1, 2, 3 and 4 as shown in Figure 7. For rotor stations 1 through 3, only the vertical rotor amplitudes are shown, while for station 4 the vertical and sometimes also the horizontal amplitudes are included as separate plots. No balancing operations were performed using the horizontal vibration measurements. All correction weight calculations were based on vertical rotor amplitude measurements.

Test results for rotor with corkscrew unbalance--Balanced by Exact Point-Speed balancing procedure. The effectiveness of the balancing effort was determined and quantified in terms of rotor orbit reduction. For quick visual inspection of rotor orbit sizes over the full rotor speed range, continous plots were made. These plots were obtained simultaneously for all rotor stations by recordings made on magnetic tape and later individual playback.

Figures 15 through 19 contain the amplitude plots for the test rotor at the four designated rotor stations. The rotor balance improvements achieved by

successive balancing runs follow the previously observed pattern found in Reference 1: A very drastic reduction of rotor unbalance after the first balancing run is followed by much more gradual improvements during successive runs. Occasionally there may even occur an increase in rotor orbit size at some rotor stations over all or part of the speed range previously covered. These shifts in rotor unbalance distribution sometimes seem to be necessary if the rotor is to pass through the third critical speed without excessive bending. An example of worsening of rotor balance at one station coupled with a significant overall improvement of rotor balance may be seen in the results of the third balancing runs (curves D) in Figures 15 through 19. At stations 1, 3 and 4 the vertical amplitudes improved while at station 2 larger amplitudes were observed. However, the overall improvement of rotor balance was sufficient to permit passage through the third critical speed with sufficiently small orbits. At this point, it may be worthwhile to recall the speeds at which the trial weight data were taken (see Figure 14): From curve A to curve B (as designated in Figures 15 through 19): 9,870 rpm, from B to C: 10,670 rpm, and from C to D: 10,830 rpm. There were marked improvements in rotor amplitudes in the speed range to the approach of the third critical speed as the balancing speed moved upward and finally approached the critical speed.

For numerical comparison of rotor amplitudes before and after each successive balancing run, rotor orbits at 6,000, 9,000 and 10,670 rpm have been tabulated, together with a calculation of the percentage improvements obtained. Table I gives a listing of these values for the Corkscrew Unbalance Test Case and balancing by the Exact Point-Speed balancing procedure.

The total combined percent improvement* at 6,000 and 9,000 rpm is only 77.4 percent, which is somewhat lower than previously obtained values when balancing the same rotor under similar conditions, but with different unbalance configurations (Reference 1). However, the improvement at 9,000 rpm was considerably better than at 6,000 rpm (86.3 percent versus 68,5 percent) and the improvement at 10,670 rpm for the last two runs was a respectable 81.1 percent. This emphasis on higher improvements at higher rotor speeds explains why the test rotor successfully passed the third critical speed despite the relatively low 77.4 percent improvement at the 6,000 and 9,000 rpm 'test' points.

Test results for rotor with corkscrew unbalance--Balanced by Least-Squares balancing procedure. Rotor vibration amplitude plots which were obtained during balancing efforts with the test rotor first unbalanced with a corkscrew unbalance arrangement and then balanced by the Least-Squares balancing procedure, are shown in Figures 20 through 24. Curves A, which represent the initial unbalance condition are identical to curves A in Figures 15 through 19, because both cases were begun with the same initial unbalance weight combination. The Least-Squares results, curves B through E in Figures 20 through 24, have a distinctly different appearance than those obtained by the Exact Point-Speed

*Total combined improvement relates to the average improvement for all four measurement stations on the rotor. Values for total combined percent improvement as measured at rotor speeds of either 6,000, 9,000 or 10,670 rpm, or as combined values for all rotor speeds at whirl measurements were taken, are shown in Table VII.

TABLE I

Balance Improvement for First Test Case
Rotor with Corkscrew Unbalance
Balanced by Exact Point-Speed Procedure

PEAK-TO-PEAK ROTOR AMPLITUDES													
ROTOR SPEED	PROBE STATION	ROTOR AMPLITUDE BEFORE BALANCING		AFTER 1ST BALANCING RUN (CALCULATION NO. 2)		% REDUCTION DUE TO 1ST BALANCING RUN	AFTER 2ND BALANCING RUN (CALCULATION NO. 6)		% REDUCTION DUE TO 2ND BALANCING RUN	AFTER 3RD BALANCING RUN (CALCULATION NO. 9)		% REDUCTION DUE TO 3RD BALANCING RUN	TOTAL % REDUCTION
rpm		μ in.	micron	μ in.	micron		μ in.	micron		μ in.	micron		
6,000	1	575	14.6	150	3.81	74	100	2.54	33.3	75	1.9	25	86.7
	2	375	9.52	75	1.9	80	100	2.54	86.7	150	3.81	(50)	60.5
	3	325	8.25	280	7.11	13.9	250	6.35	10.8	210	5.33	16	44
	4	1025	26.03	250	6.35	75.7	175	4.44	30	175	4.44	0	83
9,000	1	1175	29.84	110	2.79	90.7	110	2.79	0	110	2.79	0	91.7
	2	1650	41.91	30	0.76	98.2	125	3.17	(316)[2]	100	2.54	20	93.9
	3	650	16.51	310	7.87	52.4	250	6.35	19.4	225	5.71	10	65.4
	4	2100	53.34	325	8.25	84.6	160	4.06	50.8	125	3.17	21.8	94.2
10,670	1	See Note 1		1125	28.57		200	5.08	82.2	200	5.08	0	
	2	See Note 1		1000	25.4		30	0.76	97	200	5.08	(566)	
	3	See Note 1		800	20.32		310	7.87	61.3	230	5.84	25.8	
	4	See Note 1		1800	45.72		275	6.98	84.7	160	4.06	41.8	

1. 3000 microinches was the maximum amplitude permitted in the test rig. Because of this limitation, the test rig was not actually run up to 10,670 rpm until after the 2nd balancing run.

2. Increase in amplitude.

procedure. The amplitude reductions in the speed range near the critical speed at 10,960 rpm are not as sharp after Least-Squares balancing as those observed after Exact Point-Speed balancing. A relatively gradual and early increase in rotor vibration amplitude is observed at the approach to the critical speed in Figures 20 through 24, which show the results of the first two balancing runs and of the fourth. To avoid cluttering of the graphs a third run which yielded results that fell between those of run C and run E, is not shown. The fourth and last run (E) was, however, based upon its predecessor (D) which is therefore included in the tabulation of results in Table II.

Inspection of the rotor vibration amplitude plots obtained from the balancing runs conducted with the aid of the Least-Squares procedure indicates somewhat less successful performance than obtained through balancing by the Exact Point-Speed procedure. Successful balancing is defined here as overall vibration amplitude reduction including passage through the third critical speed. The precise reason for this result is not immediately clear. However, the Least-Squares procedure is known to be a "compromise" procedure which purposely permits vibration amplitudes at some locations to be larger than those which would have been attained by the Exact Point-Speed procedure as the price for attaining lower vibrations for all measurement locations throughout the speed range. Especially interesting are the relatively small vibration amplitude reductions obtained by the first balancing run. The lesser effectiveness of the subsequent runs could be explained by the very nature of the Least-Squares procedure which is designed to accept trial weight data over the whole speed range of the rotor. If the rotor exhibits very low initial amplitude over a good part of the speed range, as was the case after the final balancing run, it actually becomes disadvantageous to include that part of the speed range in the data taking process. This is because the low amplitudes may be below the sensitivity limits of some of the instruments, and thus introduce errors into the data.

Inspection of the rotor amplitude improvements in Table II, for 6,000 and 9,000 rpm reveals a very respectible improvement of 88.4 percent. The answer to the question as to why the rotor did not pass successfully through the third critical speed can be found in the amplitude improvement at 10,670 rpm, which totals only 64.6 percent. This number may be compared to the 81.1 percent for the amplitude improvement at 10,670 rpm obtained after balancing by the Exact Point-Speed procedure. It must not be compared, however, to the percentage figures given for 6,000 and 9,000 rpm, because the base for the latter two was the initial rotor condition, while the improvement at 10,670 rpm is based upon amplitudes as they existed after the first balancing run. For the first balancing run, amplitude reductions could not be calculated because the rotor was not run up to 10,670 rpm in the initial condition prior to any balancing. This is because with the corkscrew unbalance weights in place, rotor amplitudes at 10,670 rpm would have exceeded safe rotor operating limits.

Second Test Case: Rotor With In-Line, In-Phase Unbalance

The second test case was planned as a sequel to an identical test case (Case II) in Reference 1. There, the test rotor with an in-line, in-phase unbalance configuration was balanced by the Exact Point-Speed balancing procedure. This

TABLE II

Balance Improvement for First Test Case
Rotor with Corkscrew Unbalance
Balanced by the Least Squares Procedure

PEAK-TO-PEAK ROTOR AMPLITUDES																
ROTOR SPEED	PROBE STATION	ROTOR AMPLITUDE BEFORE BALANCING		AFTER 1ST BALANCING RUN (CALCULATION #11)		% REDUCTION DUE TO 1ST BALANCING RUN	AFTER 2ND BALANCING RUN (CALCULATION #13)		% REDUCTION DUE TO 2ND BALANCING RUN	AFTER 3RD BALANCING RUN (CALCULATION #15)		% REDUCTION DUE TO 3RD BALANCING RUN	AFTER 4th BALANCING RUN (CALCULATION #16)		% REDUCTION DUE TO 4TH BALANCING RUN	TOTAL % REDUCTION
rpm		μ in.	micron	μ in.	micron		μ in.	micron		μ in.	micron		μ in.	micron		
6,000	1	575	14.6	125	3.17	78.3	30	0.76	76.0	30	0.76	0	25	0.63	16.7	95.7
	2	375	9.52	230	5.84	38.7	50	1.27	78.3	75	1.90	(50)	50	1.27	33.3	86.7
	3	325	8.25	280	7.11	13.9	255	6.47	9.0	250	6.35	2.0	25	0.63	90.0	92.3
	4	1025	26.03	300	7.62	70.7	325	8.25	(8.3)[2]	350	8.89	(7.6)	200	5.08	42.9	80.5
9,000	1	1175	29.84	375	9.52	68.1	200	5.08	46.7	150	3.81	25.0	75	1.90	50.0	93.6
	2	1650	41.91	200	5.08	87.9	100	2.54	50.0	30	0.76	70.0	285	7.24	(850)	82.8
	3	650	16.51	500	12.7	23.1	400	10.16	20.0	375	9.52	6.3	100	2.54	73.4	84.6
	4	2100	53.34	250	6.35	88.1	300	7.62	(20)	300	7.62	0	175	4.44	41.7	91.7
10,670	1	See Note 1		2375	60.32		1750	44.45	26.3	1375	34.92	21.5	375	9.52	72.8	
	2	See Note 1		2250	57.15		1625	41.27	27.8	1500	38.1	7.7	525	3.33	65.0	
	3	See Note 1		2000	50.80		1325	33.65	33.8	1150	29.21	13.3	250	6.35	78.3	
	4	See Note 1		2500	63.5		1875	47.62	25.0	1625	41.27	13.4	1000	25.4	39.4	

1. 3000 microinches was the maximum amplitude permitted in the test rig. Because of this limitation, the test rig was not actually run up to 10,670 rpm until after the 2nd balancing run.

2. Increase in amplitude.

section describes the balancing of the same rotor, with an identical initial unbalance condition, by the Least-Squares procedure.

Four unbalancing masses of 0.37 oz-in. (26.64 gr-cm) each were added to the rotor after removal of all unbalance and correction weights previously applied for the first test case. The angular position of the unbalance weights was 195°. (See Figure 3 for angular rotor location and Figure 25 for a schematic of the unbalance distribution on the rotor for this test case.)

Rotor amplitudes resulting from this unbalance addition are shown in Figures 26 through 30, curves A. The amplitude curves (together with phase angle measurements which are not shown) indicate the rotor to be orbiting in what is essentially a cylindrical mode (with some rotor bending) in the frequency range between 5,000 and 10,000 rpm. The rotor orbits, as recorded in Figures 26 through 30, are somewhat smaller than those shown in Reference 1 for nearly identical unbalance conditions. The sequence of balancing runs in the Third Test Case is shown in Figure 25.

Test results for rotor in-line, in-phase unbalance--Balanced by Least-Squares procedure. For this test case, balancing by the Least-Squares procedure led to an astonishingly rapid improvement in rotor balance. After only two trial weight runs, rotor amplitudes at 6,000 and 9,000 rpm had decreased by about 94 percent and the rotor passed successfully through the third critical speed. Maximum amplitudes at the third critical speed were below 0.003 inch (0.076 mm). See Figures 26 through 30 for rotor amplitude curves and Table III for numerical amplitude values at the selected speeds of 6,000, 9,000 and 10,670 rpm.

The quick success of the balancing effort utilizing the Least-Squares procedure stands in stark contrast to the successively smaller improvements for each balancing run previously obtained by the Exact Point-Speed procedure (Reference 1).

Third Test Case: Rotor With In-Line, Out-Of-Phase Unbalance

For the third test case investigated, the intentionally-added unbalance weights from the second test case were shifted in both end masses by 180°. All previously added correction weights were removed. The resultant unbalance configuration was thus nearly identical to that of Test Case III in Reference 1. The sequel described here was planned to yield yet another comparison between the balancing effectiveness of the Exact Point-Speed procedure applied in Reference 1 and the Least-Squares procedure used here.

The balancing runs for the Third Test Case were performed in the sequence shown in Figure 31. The second trial weight run (number 10), which was based upon initial rotor amplitudes B in Figures 32 through 35, was conducted at the relatively high and closely-spaced speeds of 10,670 and 10,780 rpm. At the lower rotational speeds, successful data taking was impeded by low amplitudes.

Test results for rotor with in-line, out-of-phase unbalance--Balanced by the Least-Squares procedure. The balancing effort applied to the test rotor with

TABLE III

Balance Improvement For Second Test Case

Rotor With In-Line, In-Phase Unbalance

Balanced By Least-Squares Procedure

PEAK-TO-PEAK ROTOR AMPLITUDES										
ROTOR SPEED	PROBE STATION	ROTOR AMPLITUDE BEFORE BALANCING		AFTER 1ST BALANCING RUN (CALCULATION #56)		% REDUCTION DUE TO 1ST BALANCING RUN	AFTER 2ND BALANCING RUN (CALCULATION #57)		% REDUCTION DUE TO 2ND BALANCING RUN	TOTAL % REDUCTION
rpm		μ in.	micron	μ in.	micron		μ in.	micron		
6,000	1	1325	33.65	310	7.87	76.6	10	0.25	96.8	99.3
	2	1450	36.83	375	9.52	74.2	210	5.33	44.0	85.5
	3	1425	36.19	160	4.06	88.8	110	2.79	31.3	92.3
	4	1350	34.29	70	1.77	94.9	30	0.76	57.2	97.8
9,000	1	1600	40.64	210	5.33	86.9	5	0.12	97.6	99.7
	2	1480	37.59	460	11.68	68.9	200	5.08	56.5	86.5
	3	1475	37.46	175	4.44	88.1	125	3.17	28.6	91.5
	4	1650	41.91	100	2.54	93.9	0	0	100	100
10,670	1	See Note 1		525	13.33		100	2.54	81.0	
	2	See Note 1		1075	27.30		180	4.57	83.3	
	3	See Note 1		375	9.52		160	4.06	57.4	
	4	See Note 1		750	19.05		0	0	100	

Note 1-3000 microinches was the maximum amplitude permitted in the test rig. Because of this limitation, the test rig was not actually run up to 10,670 rpm until after the 2nd balancing run.

in-line, out-of-phase unbalance was very successful. Only two trial weight runs were required to reduce rotor amplitudes to levels low enough for passage through the third critical speed with acceptable (less than 0.003 in. or 0.076 mm) maximum rotor excursions.

Figures 32 through 35 show plots of rotor amplitudes for the in-line, out-of-phase test case. Curves A represent the initial rotor condition before balancing, and curves B and C show the reduced rotor amplitudes resulting from the first and second successive balancing runs, respectively. The first correction run reduced rotor amplitudes at 9,000 rpm rotor speed by nearly 95 percent, while the next run produced another 2.3 percent reduction. This very successful performance of the Least-Squares procedure was better than what previously had been achieved for the same test configuration by the Exact Point-Speed procedure (Reference 1). With the Exact Point-Speed procedure, a total of three correction runs were necessary because the second and third runs reduced rotor amplitudes only by 1.6 and 1.1 percent, respectively, based upon initial rotor amplitudes. While the difference between a 1.6 percent and a 2.3 percent reduction may appear slight, it appears to affect significantly the ability of the rotor to pass through the third critical speed.

Balancing results achieved by the Least-Squares procedure for the in-line, out-of-phase test case are shown in Table IV. There, rotor amplitudes are tabulated for each rotor station, and amplitude reduction percentages are given for each reduction, based upon the results of the previous correction run. Total amplitude reduction percentages, based upon the initial rotor amplitudes are also given.

Fourth Test Case: Two-Mass Rotor with Conical Unbalance

The designation 'Conical Unbalance' is used in this report to describe the test rotor with one steel end mass replaced by a light aluminum disc and unbalance weights added to the remaining end mass and center mass (Figure 36). This purposely creates conical rotor centerline motions. Amplitude and phase angle plots (Figures 37 through 41 and Figures 42 through 46, respectively) indicate that at low speeds the rotor was orbiting in a conical mode with the apex of the cone intersecting the rotor centerline in the vicinity of the journal bearing furthest from the drive motor (that is, closest to the end at which the steel end mass had been replaced by the smaller aluminum disc).

At higher speeds the rotor mode shapes differ considerably from those of the three-mass rotor. At the second critical speed there is practically no rotor damping from the journal bearing adjacent to the overhung mass and appreciably more rotor bending than for the three mass rotor. The third critical occurs now at a higher rotational speed (assuming unchanged bearing stiffness). There is now some bearing damping for the light end of the rotor, and consequently a much more gradual increase in rotor amplitudes may be expected when approaching the third critical speed.

In the conical configuration, the rotor was balanced first by the Exact Point-Speed procedure and subsequently, after removal of all balance correction

TABLE IV

Balance Improvement For Third Test Case

Rotor With In-Line, Out-Of-Phase Unbalance

Balanced By Least-Squares Procedure

PEAK-TO-PEAK ROTOR AMPLITUDES									
ROTOR SPEED	PROBE STATION	ROTOR AMPLITUDE BEFORE BALANCING		AFTER 1ST BALANCING RUN (CALCULATION #50)		% REDUCTION DUE TO 1ST BALANCING RUN	AFTER 2ND BALANCING RUN (CALCULATION #51)		% REDUCTION DUE TO 2ND BALANCING RUN	TOTAL % REDUCTION
rpm		μ in.	micron	μ in.	micron		μ in.	micron		
6,000	1	460	11.68	125	3.17	73.0	50	1.27	60.0	89.2
	2	650	16.51	235	5.97	63.9	150	3.81	36.2	77.0
	3	700	17.78	80	2.03	88.6	40	1.01	50.0	94.3
	4	210	5.33	85	2.16	59.6	35	0.89	58.9	83.4
9,000	1	2925	74.29	150	3.81	94.9	25	0.63	83.4	99.2
	2	2800	71.12	210	5.33	92.5	125	3.17	40.5	94.4
	3	1875	47.62	100	2.54	94.7	75	1.90	25.0	96.0
	4	2700	68.58	60	1.52	97.8	50	1.27	16.7	98.2
10,670	1	See Note 1		1250	31.75		150	3.81	88.0	
	2	See Note 1		1000	25.4		160	4.06	84.0	
	3	See Note 1		525	13.33		175	4.44	66.6	
	4	See Note 1		1075	27.30		150	3.81	86.1	

Note 1 - 3000 microinches was the maximum amplitude permitted in the test rig. Because of this limitation, the test rig was not actually run up to 10,670 rpm until after the 2nd balancing run.

weights, by the Least-Squares procedure. In fact, this case should yield one of the best comparisons between the two balancing methods, because both calculations were made from the same trial weight data. For the Exact Point-Speed procedure, only trial weight data obtained at 9,370 rpm was used, while the Least-Squares procedure utilized additional trial weight data taken at 4,500, 6,290 and 8,290 rpm. Each set of data, comprising four rotational speeds, was obtained in a continuous series.

Based upon earlier experience, correction weights were calculated by the Exact Point-Speed procedure for three rotor planes only. In the interest of a closer comparison between calculation methods, the same three rotor planes were utilized for correction weight calculations by the Least-Squares procedure. However, for the Least-Squares calculations trial weight data from all four probes were used. (Due to the square matrix requirement, the Exact Point-Speed procedure can only accept readings from three probes when three-plane balancing is used).

The unbalance weights were placed on those sides of the end discs that faced the journal bearings. This case, therefore, was the only experimental case in which none of the unbalance planes coincided with any of the balancing planes.

Test results for two-mass rotor with conical unbalance. Rotor vibration amplitudes which resulted from balancing by the Exact Point-Speed and Least-Squares procedures are shown graphically as curves B and C, respectively in Figures 37 through 41. Curves A depict the initial rotor amplitudes produced by the intentionally-added unbalance weights, located as shown in Figure 36. Tables V and VI present numerical values for vibration level improvements at 6,000, 9,000 and 10,670 rpm for the Exact Point-Speed and Least-Squares methods, respectively.

The absence of a sharply defined vibration resonance peak for this rotor configuration is probably the explanation for the excellent balancing results obtained: just one single balancing run was required to bring rotor amplitudes down to levels that are considered acceptable. The results obtained by the Exact Point-Speed procedure are quite comparable to those achieved by the Least-Squares procedure, as may be observed in Figures 37 through 41.

Upon comparison of the calculated percentages of rotor orbit reductions achieved by the Least-Squares procedure (Table VI) with those obtained by the Exact Point-Speed procedure (Table V), it may be noted that slightly better results (larger reductions) were achieved by the latter procedure.

Two-Mass Rotor With Large Out-Of-Roundness At One Probe Location

The first (and major) series of out-of-roundness tests was conducted on the test rotor with one lightweight aluminum disc substituted for one of the heavier steel end masses. This configuration was identical to that used during the conical unbalance test described before, with one exception: the outer diameter of the aluminum disc was intentionally machined out-of-round.

TABLE V

Balance Improvement For Two-Mass Rotor With Conical Unbalance

Balanced By The Exact Point-Speed Procedure

PEAK-TO-PEAK ROTOR AMPLITUDES						
ROTOR SPEED	PROBE STATION	ROTOR AMPLITUDE BEFORE BALANCING		AFTER 1ST BALANCING RUN (CALCULATION No. 59)		% REDUCTION DUE TO 1ST BALANCING RUN
rpm		μ in.	micron	μ in.	micron	
6,000	1	655	16.63	205	5.20	68.8
	2	465	11.81	100	2.54	78.5
	3	1125	28.57	60	1.52	94.7
	4	1775	34.08	50	1.27	97.2
9,000	1	955	24.25	155	3.93	83.8
	2	380	9.65	60	1.52	89.7
	3	1250	31.75	100	2.54	92.0
	4	1925	48.89	0	0.0	100.0
10,670	1	1710	43.43	130	3.30	92.4
	2	1055	26.79	105	2.66	90.1
	3	1475	37.46	30	0.76	98.0
	4	2375	60.32	175	4.44	94.0

TABLE VI

Balance Improvement For Two-Mass Rotor With Conical Unbalance

Balanced By The Least-Squares Procedure

PEAK-TO-PEAK ROTOR AMPLITUDES						
ROTOR SPEED	PROBE STATION	ROTOR AMPLITUDE BEFORE BALANCING		AFTER 1ST BALANCING RUN (CALCULATION No. 60)		% REDUCTION DUE TO 1ST BALANCING RUN
rpm		μ in.	micron	μ in.	micron	
6,000	1	655	16.63	180	4.57	72.6
	2	465	11.81	230	5.84	50.6
	3	1125	28.57	140	3.55	87.6
	4	1775	45.08	120	3.04	93.3
9,000	1	955	24.25	155	3.93	83.8
	2	580	14.73	260	6.60	55.2
	3	1250	31.75	175	4.44	86.0
	4	1925	48.89	0	0.0	100.0
10,670	1	1710	43.43	280	7.11	83.7
	2	1055	26.79	455	11.55	56.9
	3	1475	37.46	275	6.98	81.4
	4	2875	47.62	250	6.35	91.4

The measured out-of-roundness at this location, which corresponded to rotor station (probe location) number 1, was 0.0022 in. (0.056 mm) T.I.R. or double amplitude at an angular location on the disc of -55° (Figure 47). The out-of-roundness was seen on the oscilloscope screen at low rotational speeds (below 1,000 rpm), as a nearly circular orbit 0.0022 in. (0.056 mm) in diameter. As rotor speed increased, vectorial addition of the "actual" rotor orbit (due to unbalance of the initially rigid rotor) generally caused the observed orbit to decrease. At still higher speeds (above 9,000 rpm) rotor bending finally caused the observed orbit to grow beyond the initially observed out-of-roundness. Curve A in Figure 48 depicts the described observation. Rotor amplitudes at the remaining rotor stations (2, 3 and 4) as represented by curves A in Figures 50 through 53 are, of course, nearly identical to those obtained for the conical unbalance test case, Figures 38 through 41.

Test results for two-mass rotor with out-of-roundness at one probe location--conical unbalance configuration. The effect of rotor out-of-roundness upon balancing improvements, or lack thereof, is most suitably demonstrated by comparison of curves B and C in Figures 48 through 53. Curves C were obtained with rotor out-of-roundness data incorporated into the calculations of the balancing correction weights. The computer ignored that part of the dynamic displacement signal at rotor Station 1 which was due to disc eccentricity, making no attempt to reduce the large observed amplitude at Station 1. This can clearly be seen from curve C in Figure 48 where the low speed rotor orbit is equal to the out-of-roundness and changes little with increasing rotor speed. The slight decrease in recorded orbit size is due to vectorial subtraction of rotor out-of-roundness and the effects of residual unbalance. Figures 50 through 53 show good rotor balance improvement, comparable to what had previously been obtained for the test rotor with identical unbalance weights attached.

With rotor out-of-roundness at the measurement probe locations ignored, or not recognized, the balancing process will of course try to reduce the observed dynamic amplitude to zero, even if it means bending the rotor between measurement stations to achieve this. This becomes very clear from inspection of curves B in Figures 48 through 53. Through addition of very heavy "correction" weights, rotor orbits at the out-of-round aluminum disc (rotor station 1, Figure 48) are brought down to zero at the relatively low speed of 6,500 rpm. Even at the remaining measurement stations (Figures 50 through 53), rotor orbits are reasonably low, indicating a considerably improved balance condition for that end of the rotor. However, the true rotor condition is revealed in Figure 49 where rotor orbits have been recorded for a location near the journal bearing adjacent to the out-of-round aluminum disc. Since data from this location was not used for balancing purposes, no restrictions were imposed in the correction weight calculations on rotor amplitudes at this rotor location. Consequently, the rotor was made to bend between stations 1 and 2, to the extent of the out-of-roundness, in the opposite direction.

Three-Mass Rotor With Small Out-Of-Roundness At All Probe Locations

For the three-mass rotor the effect of small out-of-roundness at all measurement probe locations was briefly investigated. For the first part of this investigation available data from the second test case (rotor with in-line, in-phase unbalance) was used. However, no experimental checks on the calculated results were performed, because by the time the calculations were completed, the particular test rig setup upon which they were based had been disturbed. Subsequently, a new trial run was made under nearly identical test conditions and the calculated results were checked out experimentally.

Figure 54 depicts the first part of the investigation (for which the correction weight calculations incorporating the out-of-roundness data at the probe locations were not checked out experimentally). In Figure 54, the three-mass test rotor is shown (drive coupling at right) with identical unbalance weights (A_1 through A_4) from the second test case drawn in their actual locations. Ideally, that is if the rotor had been perfectly balanced prior to the addition of these identical unbalance weights, the correction weight vectors should be equal and opposite. (For convenience of visual comparisons, these equal and 180^o out-of-phase vectors have been drawn as negative vectors and are shown in Figure 54 as A'_1 through A'_4.) For a real rotor, as for example the test rotor, the intentionally-added unbalances and the correction weights will not always be identical, even if the correction weights do balance the rotor very well. Most of the discrepancy is probably due to residual rotor unbalance, with additional contributions from variations in drive coupling positioning and other small factors.

For the rotor shown in Figure 54, two consecutive trial weight runs were made (documented as numbers 7 and 8 in Figure 25) without consideration of rotor out-of-roundness at the probe locations. The resultant correction vectors are shown as B_1 through B_4 for the first correction runs and C_1 through C_4 for the second. For ease of visual inspection, the sums of the A', B and C vectors have been plotted from the c.g. of the rotor. The sums of the B and C vectors do not equal the sum of the A' vectors, even though the rotor was then well-enough balanced to pass through the third critical speed with acceptable orbits.

When the out-of-roundness at the rotor probe locations was incorporated into the correction weight calculations, the first set of correction vectors with shaft out-of-roundness included (plotted in Figure 54 as $\overline{D}$) came very close to matching the sum of both sets of correction weights calculated previously without out-of-roundness data. This result led to a continued investigation of the same test case followed by experimental checks.

Figure 55 shows the three-mass rotor with in-line, in-phase unbalance weights, designated A. The first set of correction weights calculated without consideration of rotor out-of-roundness is shown as $\overline{B}$. (Individual correction weights designated B_1 through B_4 are also shown in their respective locations on the rotor.) Another set of correction weights calculated from the same trial weight data but with individual rotor out-of-roundness values at each probe location incorporated into the calculation is shown as $\overline{C}$. (Individual correction weights C_1 through C_4.) There appears to be little difference

between $\overline{B}$ and $\overline{C}$, and in fact, the correction weights without out-of-roundness data ($\overline{B}$) are even a little closer to $\overline{A}'$, which would appear to indicate a slightly better balanced rotor. However, actual experiment shows that this is not the case.

First, the example in Figure 54 had shown that $\overline{A}'$ is not exactly the sum of all actual unbalances in the test rotor. The balance obtained by $\overline{B}$ is therefore not necessarily better than that obtained from $\overline{C}$. Second, actual experimental measurements demonstrate superiority in rotor balance achieved by those correction weights which were calculated with inclusion of the out-of-roundness data.

Test results for three-mass rotor with out-of-roundness at probe locations. The experimental balancing results are shown in Figures 56 through 60. Curves A represent rotor amplitudes prior to balancing, but with the intentionally-added unbalance weights in place. Curves B and C are rotor amplitudes obtained after addition of calculated correction weights to the rotor. Shaft out-of-roundness was not considered in the calculation of the weights which led to curves B, but was included for those that resulted in curves C. Both sets of trial weights, though independently calculated, were based upon identical experimental trial weight data.

Placement Of Trial Weights At One Or Two Locations

Nearly all flexible rotor balancing experiments conducted on the test rotors described in this report were made with trial weights placed first in one location and then in another angularly 180° away from it. The purpose of this procedure, which in effect doubles the amount of data which has to be acquired for each balancing run, was to obtain increased accuracy in the calculation of the balance correction weights.

Thus far, the claim on improved accuracy is without experimental proof. As a preliminary step to gaining operational experience in evaluating the need for two-location trial weight data, a few computer calculations were made utilizing only half of the trial weight input data originally used for correction weight calculations.

In each of the Figures 61 and 62, a calculated set of correction weights is shown for the rotor with in-line, in-phase unbalance (Second Test Case, Figure 25). In Figure 61, the correction weights were calculated from the trial weight data obtained with the trial weight located in the 0° location in each balancing plane and, correspondingly, in Figure 62 the calculated correction weights are shown for the 180° trial weight location. The correction weight vectors calculated from the combined sets of trial weight data (trial weight location at 0° and 180°) were those shown as $\overline{D}$ in Figure 54.

The differences in vectorial sums between either Figure 61 and 62 and Figure 54 are large. Since the actual rotor responses from correction weight sets similar to $\overline{D}$ in Figure 54, namely $\overline{B}$ and $(\overline{B} + \overline{C})$ in Figure 54 are known to be quite good (Figures 26 through 30, Curves B and C, respectively) it must be

concluded that using only half of the trial weight data would have led to poor improvements in rotor balance in this particular case.

A similar investigation based upon the data from Figure 55 led to nearly identical results. However, when the other cases were examined for the two-mass rotor with a corkscrew unbalance, much less striking differences were noted.

CONCLUSIONS

A previous experimental program had indicated the practical feasibility of computer-assisted flexible rotor balancing (References 1 and 2). In this report systematic extensions of the experimental program are documented to include other rotor configurations, more difficult unbalance conditions in the rotors to be balanced, and more refined and sophisticated methods. The ultimate objective of these efforts is demonstration of the capability to achieve acceptable flexible rotor balance rapidly and with certainty.

Thus far, two procedures have been investigated for flexible rotor balancing: the Exact Point-Speed Influence Coefficient Method and the Least-Squares Influence Coefficient Method. These procedures are closely related (see Reference 3) and their respective selection to help improve the balance condition of a particular rotor may be likened to the choice between a rifle and shotgun: the former will do if applied accurately, and singularly. The latter allows more room for error, and will cover a more erratic movement of the target. The Exact Point-Speed balancing procedure has proven to be capable of utilizing a limited amount of trial weight data for each calculation of correction weights, and as the name indicates, is usually applied at only a few rotor speeds. For the cases investigated, balancing at one speed usually was sufficient to bring rotor amplitudes down over the entire operating speed range. (It is not certain, however, if this will be true if more than one bending critical speed is found in the operating speed range.) The Least-Squares procedure has proven to be capable of utilizing almost any amount of trial weight data for each separate calculation of correction weights. In practice, this permits the recording of trial weight data at several rotational speeds. As the amount of input data increases, the consequences of a single error in the data tend to decrease. However, the number of calculations (computer time) required for the Least-Squares procedure is significantly larger than what is required for the Exact Point-Speed procedure. In spite of this difference, both are quite economical to implement.

The effectiveness of both balancing procedures has been measured and compared for four selected arrangements of rotor unbalance and two rotor configurations. In summary, both procedures were nearly equally successful. The Least-Squares procedure proved superior when used on the three-mass rotor with unbalance configurations that were symmetrical about the rotor center of gravity. The Exact Point-Speed procedure may prove to be less suited to certain symmetrical rotor configurations, such as, for example, the three-mass rotor. In this particular case, the selection of four balancing planes (two for the wide center disc) led to the calculation of very large correction weights to be applied to the center disc, a practical difficulty which was avoided for the test rotor by reduction of the number of balancing planes from four to three.

The three-mass rotor used for some of the balancing experiments received very little bearing damping at the approach to third critical speed (first bending critical) due to the location of the journal bearings near the nodal points of the rotor for that mode. In some cases safe (and slow) operation through the

first flexural critical speed of the rotor was achieved after only two balancing runs, with the first balancing run generally reducing rotor amplitudes by about 80%.

A two-mass rotor with higher bearing damping and reduced flexibility was successfully and sufficiently balanced with only one balancing run.

A summary of rotor amplitudes, as they existed before balancing and after each of the consecutive balancing runs for each test case, is shown in Table VII. Amplitudes have been averaged for all four rotor stations and the percentage reductions shown are the cumulative results of one to four consecutive balancing runs applied to each test case.

The instrumentation system assembled for the experiments was easy to operate and of sufficient accuracy. However, difficulties experienced with gradual instrument drift and from accidental polarity reversals in the interconnecting lines strongly emphasized the need for positive check-out procedures and methods which may be implemented on a regular basis without disturbing the rotor-bearing setup.

TABLE VII

Summary of Balance Improvements

AVERAGE PEAK-TO-PEAK ROTOR AMPLITUDES (FOUR ROTOR STATIONS COMBINED)																
TEST CASE	BALANCING PROCEDURE	ROTOR SPEED (rpm)	BEFORE BALANCING μ in.	BEFORE BALANCING micron	AFTER 1ST BALANCING RUN μ in.	AFTER 1ST BALANCING RUN micron	% REDUCTION DUE TO 1ST BALANCING RUN	AFTER 2ND(a) BALANCING RUN μ in.	AFTER 2ND(a) BALANCING RUN micron	% REDUCTION DUE TO 1ST AND 2ND BALANCING RUNS	AFTER 3RD(a) BALANCING RUN μ in.	AFTER 3RD(a) BALANCING RUN micron	% REDUCTION DUE TO FIRST THREE BALANCING RUNS	AFTER 4TH(a) BALANCING RUN μ in.	AFTER 4TH(a) BALANCING RUN micron	TOTAL % REDUCTION AT EACH SPEED	TOTAL % REDUCTION ALL SPEEDS COMBINED
Corkscrew	Exact Point-Speed	6,000	575	14.6	188	4.77	60.9	156	3.96	66.8	152	3.86	68.5			68.5	
		9,000	1393	35.38	193	4.90	81.4	161	4.09	84.3	140	3.55	86.3			86.3	78.6
		10,670			1181	29.99	(b)	203	5.15	81.3(c)	197	5.0	81.1(d)			81.1(d)	
	Least Squares	6,000	575	14.6	234	5.94	50.4	165	4.19	67.8	176	4.47	65.9	75	1.90	88.8	
		9,000	1393	35.38	331	8.41	66.8	250	6.35	75.3	213	5.41	78.4	158	4.01	88.1	80.5
		10,670			2281	57.94	(b)	1643	41.73	25.7(c)	1412	35.86	38.2(d)	537	3.64	64.6(e)	
In-Line In-Phase	Exact Point-Speed (f)	6,000	1695	43.05	249	6.32	85.3	274	6.95	83.8	229	5.81	86.5			86.5	87.1
		9,000	1865	47.37	254	6.45	86.4	310	7.87	83.4	229	5.81	87.7			87.7	
	Least Squares	6,000	1387	35.22	229	5.81	83.6	90	2.28	93.7						93.7	94.0
		9,000	1551	39.39	236	5.99	84.4	82	2.08	94.4						94.4	
		10,670			681	17.30	(b)	110	2.79	80.4(c)							
In-Line Out-Of-Phase	Exact Point-Speed (f)	6,000	570	14.48	184	4.67	67.8	150	3.81	73.7	120	3.05	78.9			78.9	87.1
		9,000	2645	67.18	163	4.13	93.9	120	3.05	95.5	121	3.08	95.4			95.4	
	Least Squares	6,000	505	12.82	131	3.33	71.2	69	1.75	85.9						85.9	91.5
		9,000	2575	65.4	130	3.30	94.9	69	1.75	97.2						97.2	
		10,670			962	24.43	(b)	159	4.04	81.1(c)							
Conical	Exact Point-Speed	6,000	1005	25.52	103	2.61	84.8									84.8	
		9,000	1177	29.89	78	1.98	91.3									91.3	89.9
		10,670	1778	45.16	110	2.79	93.6									93.6	
	Least Squares	6,000	1005	25.52	167	4.24	76.0									76.0	
		9,000	1177	29.89	147	3.73	81.2									81.2	78.5
		10,670	1778	45.16	315	8.0	78.3									78.3	

(a) Balancing runs 1 through 4 were consecutive for each test case with new balance correction weights added for each new run.

(b) Maximum amplitudes permitted in test rig were 3000 microinches. Because of this limitation, the test rig was not actually run up to 10,670 rpm until after the 2nd balancing run.

(c) Amplitude reduction due to 2nd balancing run only.

(d) Amplitude reduction due to 2nd and 3rd balancing runs only.

(e) Amplitude reduction due to 2nd, 3rd and 4th balancing runs only.

(f) From Reference 1.

REFERENCES

1. Tessarzik, J.M., "Flexible Rotor Balancing By The Exact Point-Speed Influence Coefficient Method," MTI Technical Report No. MTI-70TR59 prepared for NASA-Lewis under Contract No. NAS3-13473, Report No. CR-72774, October 1970.

2. Tessarzik, J.M., Badgley, R.H., and Anderson, W.J., "Flexible Rotor Balancing By The Exact Point-Speed Influence Coefficient Method," ASME Trans., Journal of Engineering for Industry, February 1972, p. 148.

3. Lund, J.W., and Tonnesen, J., "Analysis and Experiments On Multiplane Balancing of Flexible Rotors," ASME Trans., Journal of Engineering for Industry, February 1972, p. 233.

APPENDIX A

BALANCING PROCEDURE

The procedure for conducting a balancing test run is as follows:

1. The unbalanced test rotor is slowly, but continuously run up in speed until rotor deflections reach values which are not to be exceeded for safety or operational reasons. For the test rig, the maximum allowable deflection has been arbitrarily set as 0.0035 to 0.005 in. (0.09 - 0.12 mm) peak-to-peak. At four locations on the rotor, vertical amplitudes and phase angles between the amplitude signal and the reference signal are recorded by an electronic printer. The printout is repeated at four or more different rotor speeds. During subsequent runs trial weight data and improved-rotor data are taken at identical speeds with numbers of recording speeds held to a feasible minimum. Rotor amplitudes are also recorded on magnetic tape for later plotting on an X-Y plotter.

2. Rotor amplitudes as functions of rotor speed are plotted from tape by an X-Y plotter. From these plots, suitable balancing speeds are selected.

3. A suitable trial weight is placed at the reference mark on the rotor in the first balancing plane. The rotor is then run up in speed to the first pre-selected balancing speed. At that speed vertical rotor amplitudes and phase angles are printed on paper tape. The rotor is then brought to the second pre-selected balancing speed and again the vertical rotor amplitudes and phase angles are printed on paper tape.

4. The above process (described in 3) is then repeated with the trial weight placed in each of the remaining balancing planes.

5. Steps (3) and (4) may be repeated with the trial weight placed 180^{o} from the previous locations, but in the same axial planes.

6. The tabulated data is read into the computer for correction weight calculations.

7. The computed weights are vectored for the appropriate hole locations in the rotor discs. In the test rig, steel set screws are filed to match the calculated weights.

8. With the correction weights in place, steps (1) and (2) are repeated. Through comparison of the original and the new rotor amplitudes, either from the printed data or from the plotted curves, the effectiveness of the balancing effort may be determined.

The whole procedure may then be repeated for increased effectiveness.

APPENDIX B

CALIBRATION PROCEDURE

The following probes and instruments were subjected to calibration checks prior to test data acquisition:

a) proximity sensors (4)
b) Wayne-Kerr amplifiers for above sensors (4)
c) Tracking Analyzer (Model 235DS - Vibration Instrument Company)
d) Phase Meter (Model 933A - Vibration Instrument Company)
e) Digital Voltmeter (2) (Model 200A - Monsanto)
f) X-Y plotter

The proximity sensors were calibrated in a bench fixture consisting of a probe hold-down clamp and a flat steel disc mounted on a micrometer stem. Beginning with an initial position where the sensor tip is in close contact with the steel disc, the micrometer was used to move the disc away from the probe. The incremental changes in output voltage indicated by a Wayne-Kerr amplifier connected to the sensor were recorded as a function of micrometer travel. The relationship of distance between sensor tip and steel surface versus output voltage was plotted and a "best-fit" straight line drawn through the data points. Typically, a capacitance - type sensor with a range of 0.010 in. (0.25 mm) (1 volt output for a probe-to-surface distance of 0.010 in. (0.25 mm) may have maximum deviation of approximately two percent from the linear straight line near the ends of the specified distance range.

The linearized voltage-distance relationship was determined for each probe and subsequently utilized as input constants for the Exact Point-Speed Balancing Computer Program.

The following four calibration values were determined for the probes:

Probe No.	Calibration Constant mils/Vrms	(mm/Vrms)
1	30.2	(0.767)
2	29.7	(0.754)
3	30.7	(0.780)
4	31.4	(0.798)

The Wayne-Kerr amplifiers were calibrated prior to the experiments by the manfacturers representative (MTI). A daily check of these meters required only a bias adjustment to reset the meter output to one volt.

The Tracking Analyzer (235 DS) was received as a new and calibrated piece of equipment just prior to the balancing tests (NASA Contract 3-13473) and has been adjusted by the manufacturer just prior to the tests described herein. Daily bias adjustments were made for the amplitude readout and for the phase angle between the two channels. The phase adjustment was accomplished by feeding a common oscillator signal to both channels and comparing the phase angle of the output signals in the phase meter. The bias was adjusted, as required, to bring the phase difference to zero.

The Phase Meter (933 A) was repaired and adjusted by the manufacturer prior to the tests described herein. The meter was daily adjusted for zero phase distortion between reference input and signal input with the same signal fed into both inputs. The adjustment of the phase meter preceded, of course, the phase adjustment of the Tracking Analyzer.

A valuable check on the proper interpretation of the polarity and magnitude of the phase angle indicated by the phase meter was obtained by displaying the appropriate output signals from the Tracking Analyzer on an oscilloscope screen. In this manner phase angles may be determined for checking purposes within five degrees of the values indicated by the phase meter.

The digital voltmeters were checked with a laboratory standard prior to the tests. (One new instrument had to be returned to the manufacturer for replacement.) Daily checks included zero and calibration adjustments.

The X-Y plotter was calibrated in frequency for all amplitudes by using an oscillator to drive the tracking analyzer. During regular data plotting operations, amplitudes were continually spot-checked by readings and corresponding hand notations from the analyzer amplitude meter.

No estimate is available on the overall dynamic accuracy of the instrumentation system used in this experiment. However, certain limitations in the instrumentation were recognized. For instance, the phase meter has a stated minimum signal input requirement of 2.5 millivolts rms. This corresponds to approximately 0.000075-in. (0.002 mm) peak-to-peak rotor amplitude, when measured with capacitance probes having a 0.010-in. (0.25 mm) linear range. If rotors with less initial amplitude due to unbalance are to be balanced, either shorter range probes or pre-amplifiers would have to be used.

APPENDIX C

TYPICAL BALANCING DATA FOR A SELECTED CASE

Date of Test: 11-15-71

Trial Weight Run: No. 3, Third Test Case (In-Line, Out-Of-Phase Unbalance)

Rotor Balancing Speed: 8840 rpm

Measuring Station	Rotor Amplitude (mV rms)	Phase Angle	Trial Weight oz-in.	Trial Weight gm-cm	Trial Weight Location
1	91	111	None	None	
2	88	− 72	None	None	
3	64	− 77	None	None	
4	84	113	None	None	
1	93	106	.0833	6	
2	97	− 72	.0833	6	Plane 1
3	67	− 77	.0833	6	at 0°
4	94	113	.0833	6	
1	91	116	.0833	6	
2	80	− 72	.0833	6	Plane 1
3	61	− 77	.0833	6	at 180°
4	74	114	.0833	6	
1	85	111	.0833	6	
2	86	− 70	.0833	6	Plane 2
3	63	− 75	.0833	6	at 0°
4	77	114	.0833	6	
1	101	111	.0833	6	
2	92	− 74	.0833	6	Plane 2
3	65	− 79	.0833	6	at 180°
4	91	112	.0833	6	
1	86	112	.0833	6	
2	96	− 70	.0833	6	Plane 3
3	64	− 75	.0833	6	at 0°
4	76	114	.0833	6	
1	99	111	.0833	6	
2	92	− 75	.0833	6	Plane 3
3	65	− 80	.0833	6	at 180°
4	92	112	.0833	6	

Measuring Station	Rotor Amplitude (mV rms)	Phase Angle	Trial Weight oz-in.	Trial Weight gm-cm	Trial Weight Location
1	103	111	.0833	6	
2	98	− 73	.0833	6	Plane 4
3	74.3	− 76	.0833	6	at 0°
4	83.5	108	.0833	6	
1	83	111	.0833	6	
2	80	− 72	.0833	6	Plane 4
3	55	− 79	.0833	6	at 180°
4	86	118	.0833	6	

The data listed above was typically averaged from two or three readings taken at the same rotor speed. A typical, original data printout sheet is reproduced below:

Data for 8840 rpm, with trial weight in Plane 4 at 0°:

Measuring Station	Scanner Channel	Phase Angle	Amplitude (m v x 10^{-2})	
1	4 0 0 0 0 0 0 0	0 1 1 1.3 0°	0 1.0 2 9 m v	3. Data Cycle
2	3 0 0 0 0 0 0 0	− 0 7 2.9 0°	0 0.9 7 3 m v	
3	2 0 0 0 0 0 0 0	− 0 7 5.9 0°	0 0.7 3 7 m v	
4	1 0 0 0 0 0 0 0	0 1 0 7.8 0°	0 0.8 3 0 m v	
1	4 0 0 0 0 0 0 0	0 1 1 1.3 0°	0 1.0 2 7 m v	2. Data Cycle
2	3 0 0 0 0 0 0 0	− 0 7 2.9 0°	0 0.9 8 0 m v	
3	2 0 0 0 0 0 0 0	− 0 7 5.9 0°	0 0.7 4 3 m v	
4	1 0 0 0 0 0 0 0	0 1 0 7.8 0°	0 0.8 4 0 m v	
1	4 0 0 0 0 0 0 0	0 1 1 1.2 0°	0 1.0 3 7 m v	1. Data Cycle
2	3 0 0 0 0 0 0 0	− 0 7 2.8 0°	0 0.9 8 5 m v	
3	2 0 0 0 0 0 0 0	− 0 7 5.8 0°	0 0.7 4 3 m v	
4	1 0 0 0 0 0 0 0	0 1 0 8.0 0°	0 0.8 3 7 m v	

APPENDIX D

CALCULATED CORRECTION WEIGHTS FOR TEST BALANCING RUNS

Test Case	Calculation Number	Balancing Plane	Correction Weight oz-in.	Correction Weight gm-cm	Correction Weight Angle (Degrees)
Corkscrew Unbalance Exact Point-Speed Influence Coefficient Method	2	1	.16524	11.92	− 77.9
		2	.28565	20.61	166.2
		4	.28094	20.27	− 2.1
	6	1	.07738	5.58	226.4
		2	.00666	0.48	40.7
		4	.02435	1.75	71.6
	9	1	.01416	1.02	222.5
		2	.02753	1.98	117.8
		4	.00840	0.61	69.0
Corkscrew Unbalance Least Squares Method	11	1	.17122	12.35	− 84.7
		2	.32798	23.66	165.4
		3	.06702	4.83	64.3
		4	.26246	18.93	6.9
	13	1	.030	2.16	− 115.0
		2	.007	0.51	− 95.0
		3	.023	1.66	7.8
		4	.094	6.78	179.0
	15	1	.0101	0.73	169.3
		2	.0137	0.99	− 152.0
		3	.0200	1.44	6.2
		4	.0758	5.47	− 179.1
	16	1	.0154	1.11	165.8
		2	.070	5.05	97.3
		3	.0202	1.46	− 81.5
		4	.0756	5.46	153.9
In-Line In-Phase Unbalance Least Squares Method	56	1	.20415	14.73	18.0
		2	.54222	39.12	34.4
		3	.23658	17.07	25.6
		4	.28045	20.23	21.2
	57	1	.08117	5.85	1.5
		2	.16178	11.67	97.8
		3	.18098	13.05	− 51.9
		4	.02343	1.69	49.1

Test Case	Calculation Number	Balancing Plane	Correction oz-in.	Weight gm-cm	Correction Weight Angle (Degrees)
In-Line Out-of-Phase Unbalance Least Squares Method	50	1	.27749	20.02	− 165.6
		2	.26507	19.12	29.8
		3	.33657	24.28	34.8
		4	.31308	22.59	− 175.0
	53	1	.01952	1.41	175.7
		2	.08590	6.20	175.8
		3	.06509	4.69	32.3
		4	.01509	1.08	− 130.8
Conical Unbalance Exact Point-Speed Influence Coefficient Method	59	1	.08979	6.47	10.2
		2	.19464	14.04	243.0
		4	.41538	29.97	219.8
Conical Unbalance Least Squares Method	60	1	.08426	6.08	26.4
		2	.16964	12.24	− 137.0
		4	.42677	30.79	− 142.4
Conical Unbalance Least Squares Method Without out-of-round data	75	1	.4834	34.88	− 172.0
		2	.7578	54.68	− 110.2
		4	.3699	26.69	− 160.5
Conical Unbalance Least Squares Method With out-of-round data	79	1	.0427	3.08	154.7
		2	.3232	23.32	− 125.9
		4	.4123	29.75	− 145.3

FIGURES

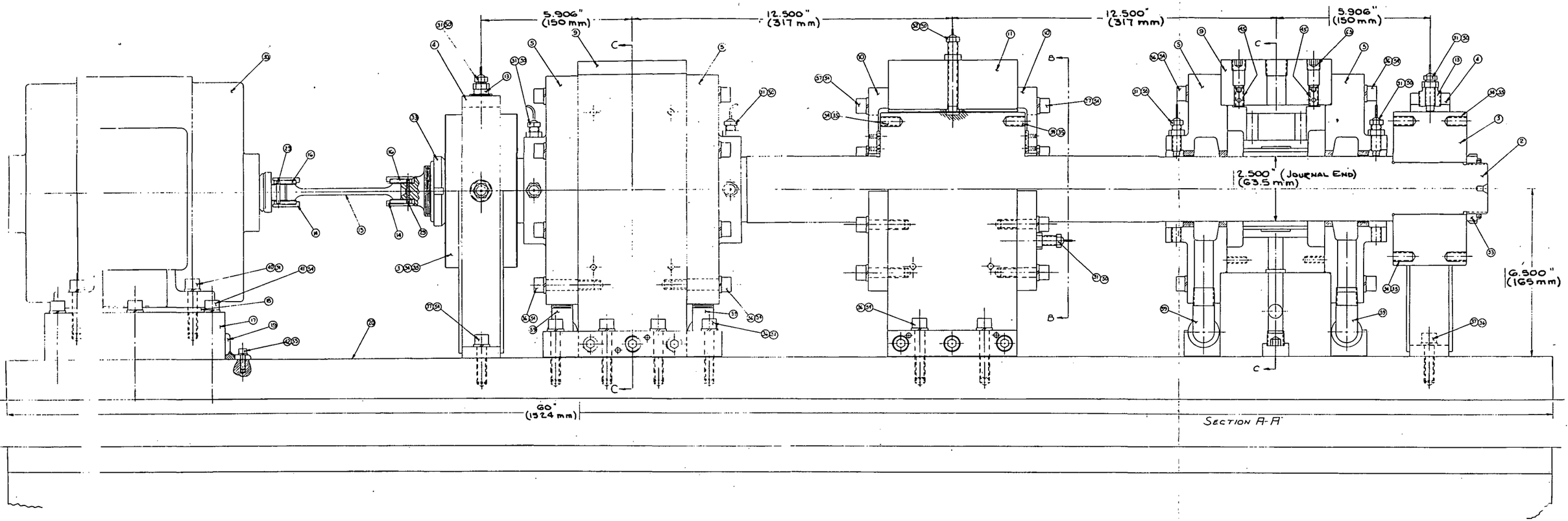

(a) Three-Mass Rotor Configuration with Steel End Mass

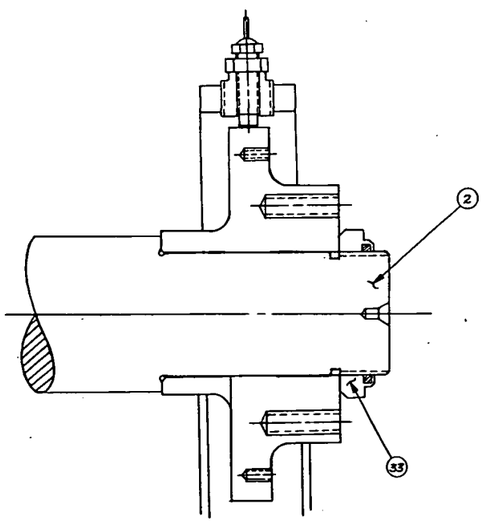

(b) Aluminum End Mass for the Two-Mass Rotor Configuration

Fig. 1 Assembly Drawing of the Flexible-Rotor Test Rig

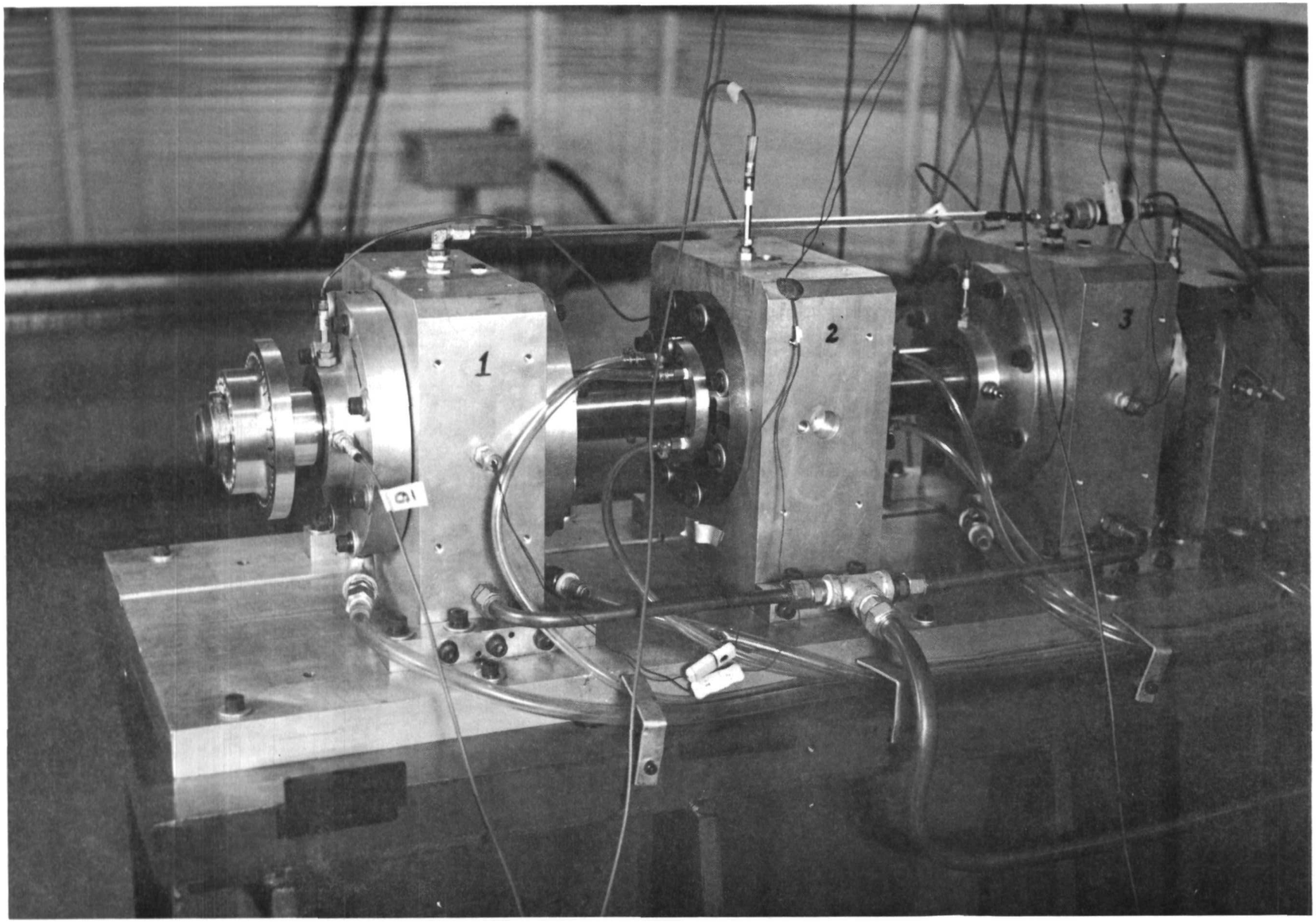

Fig. 2 Photograph of Aluminum End Disk (Two-Mass Rotor)

MTI-13237

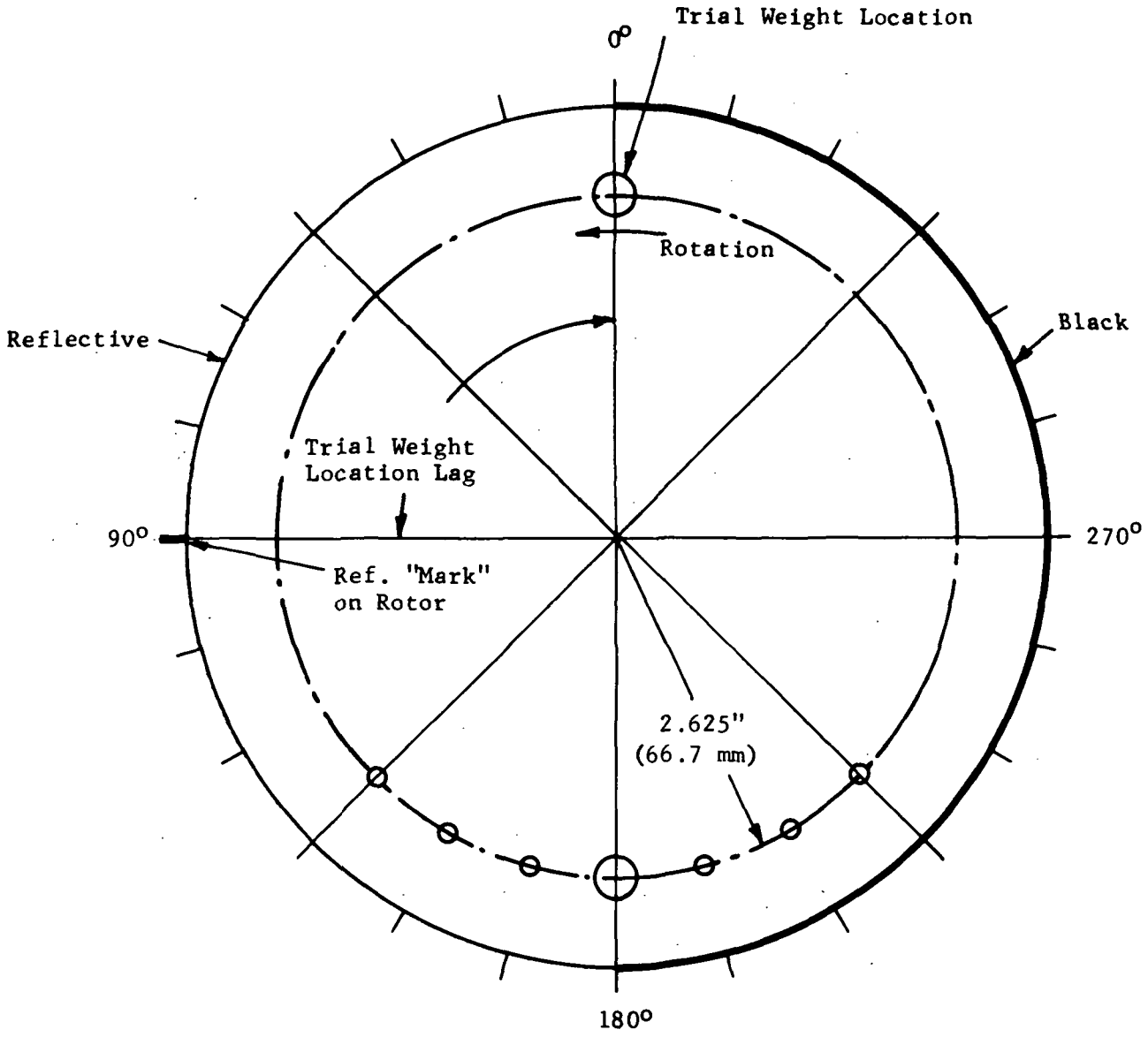

Fig. 3 End View of Rotor End Mass (Opposite Drive End) With Reference Mark and Typical Holes for Balancing Weights

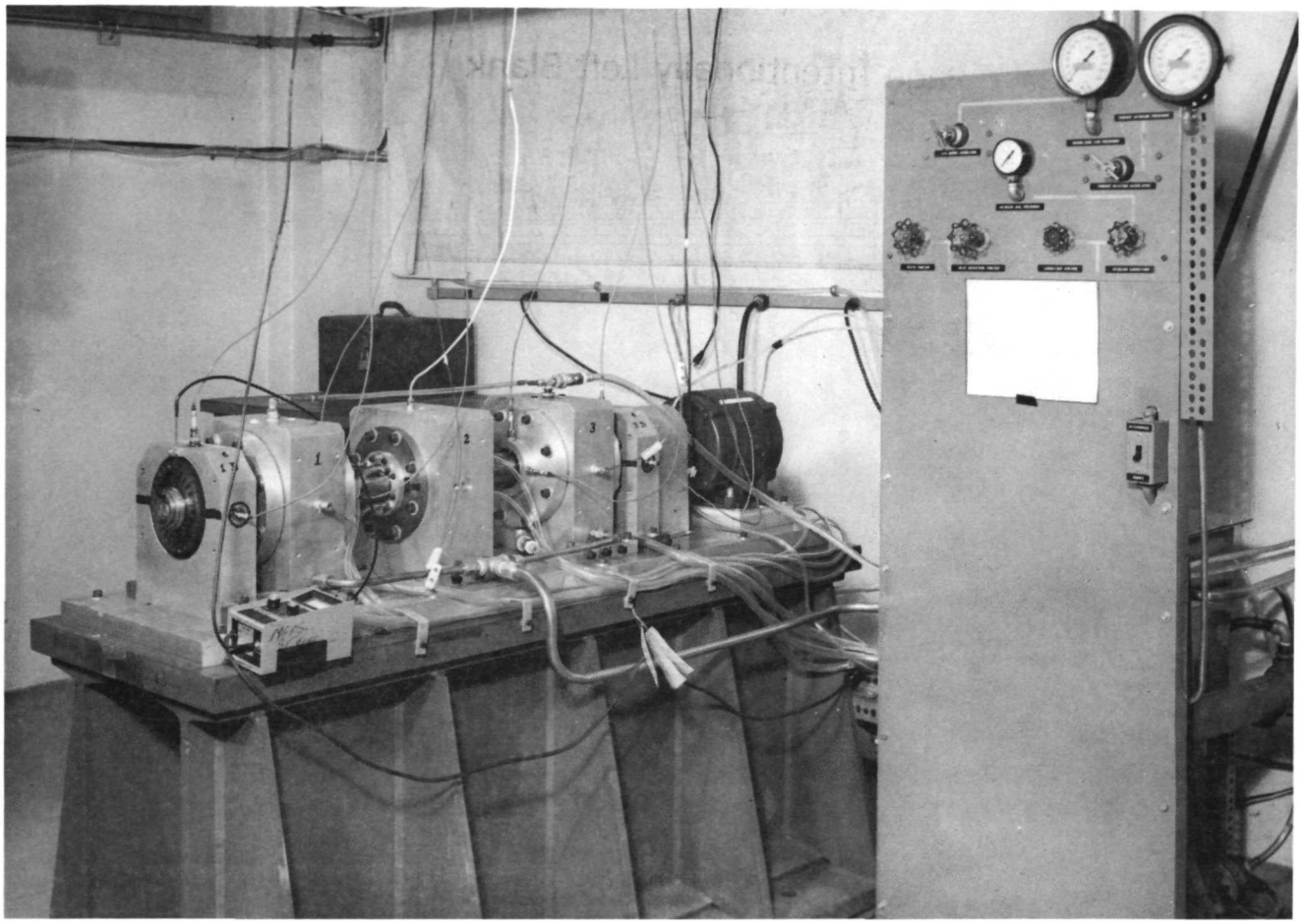

Fig. 4 View of Flexible-Rotor Test Rig

Page Intentionally Left Blank

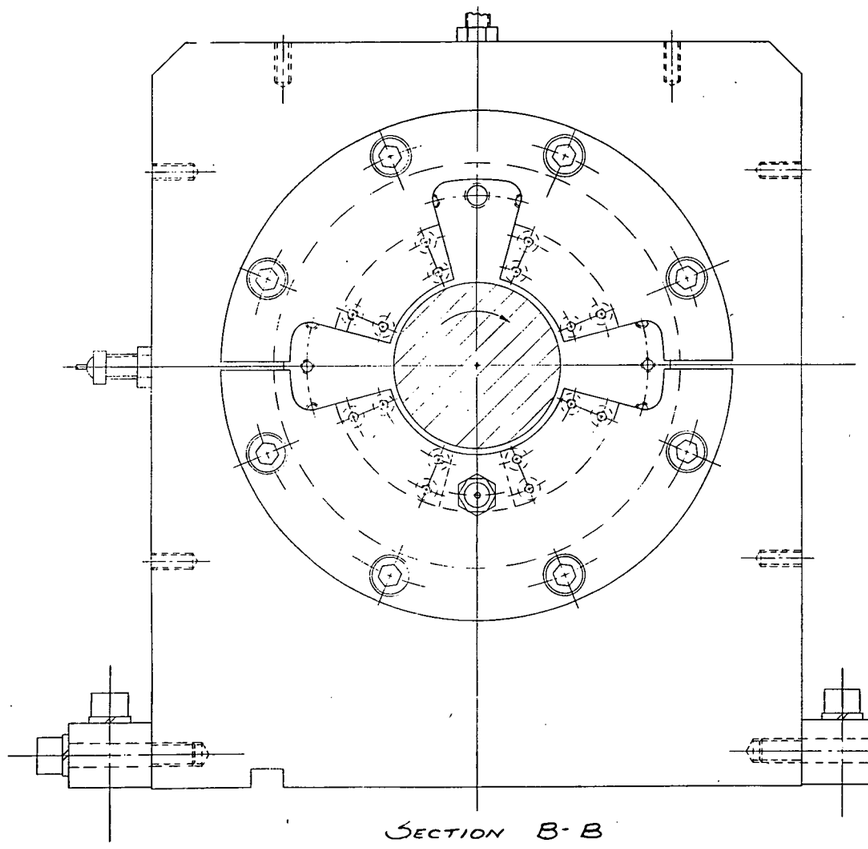

(See Figure 1)

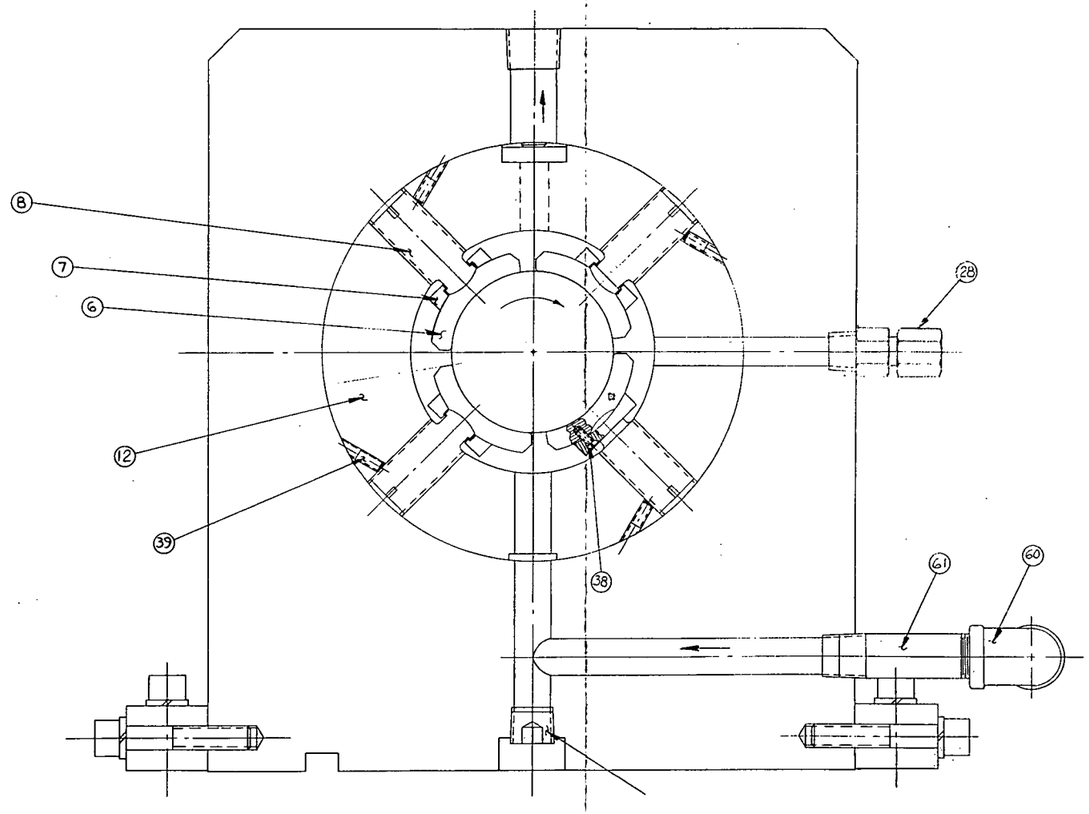

(See Figure 1)

Fig. 5 Bearing Assembly Drawing of Flexible-Rotor Test Rig

Page Intentionally Left Blank

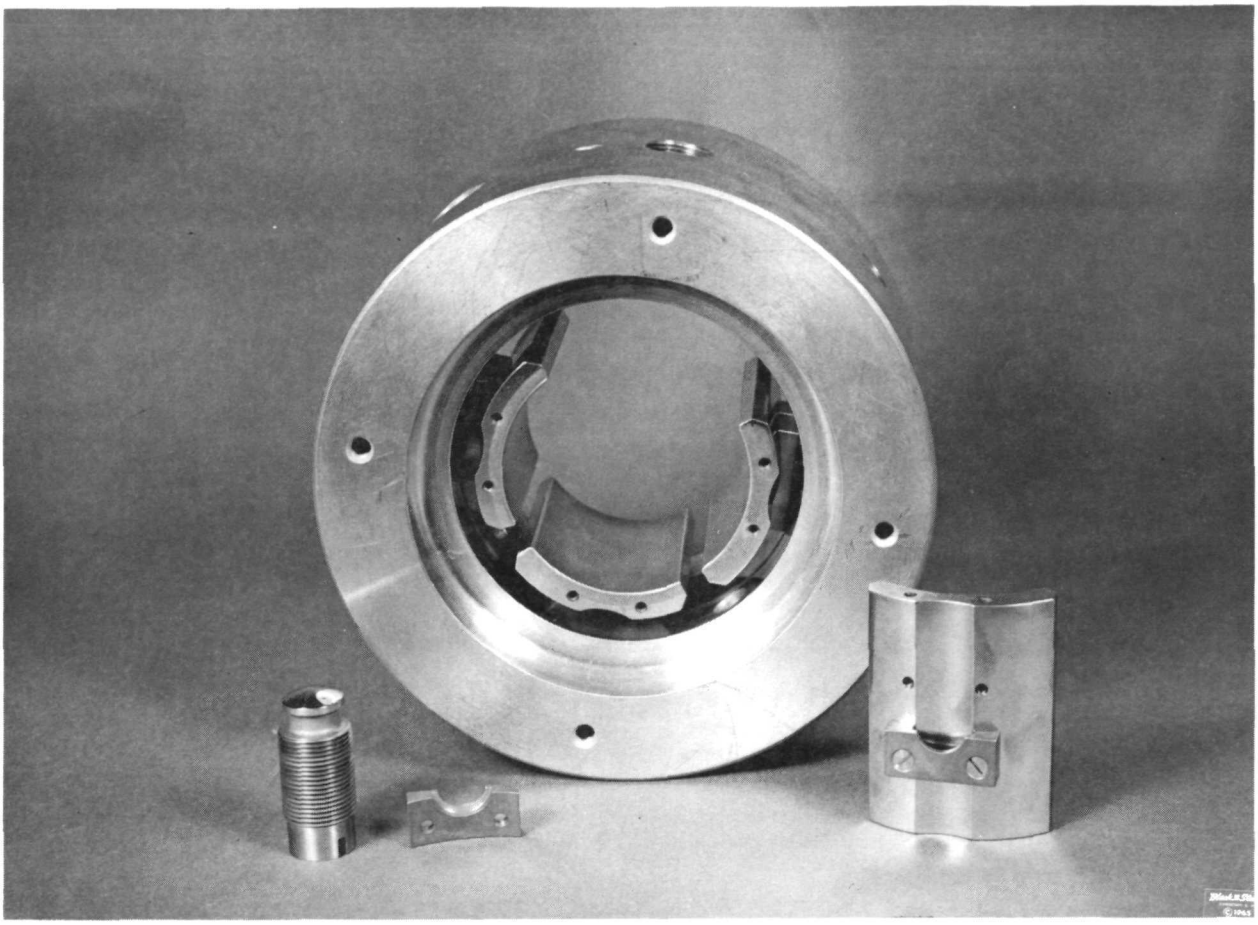

Fig. 6 Tilting-Pad Journal Bearing for Test Rig Rotor

Page Intentionally Left Blank

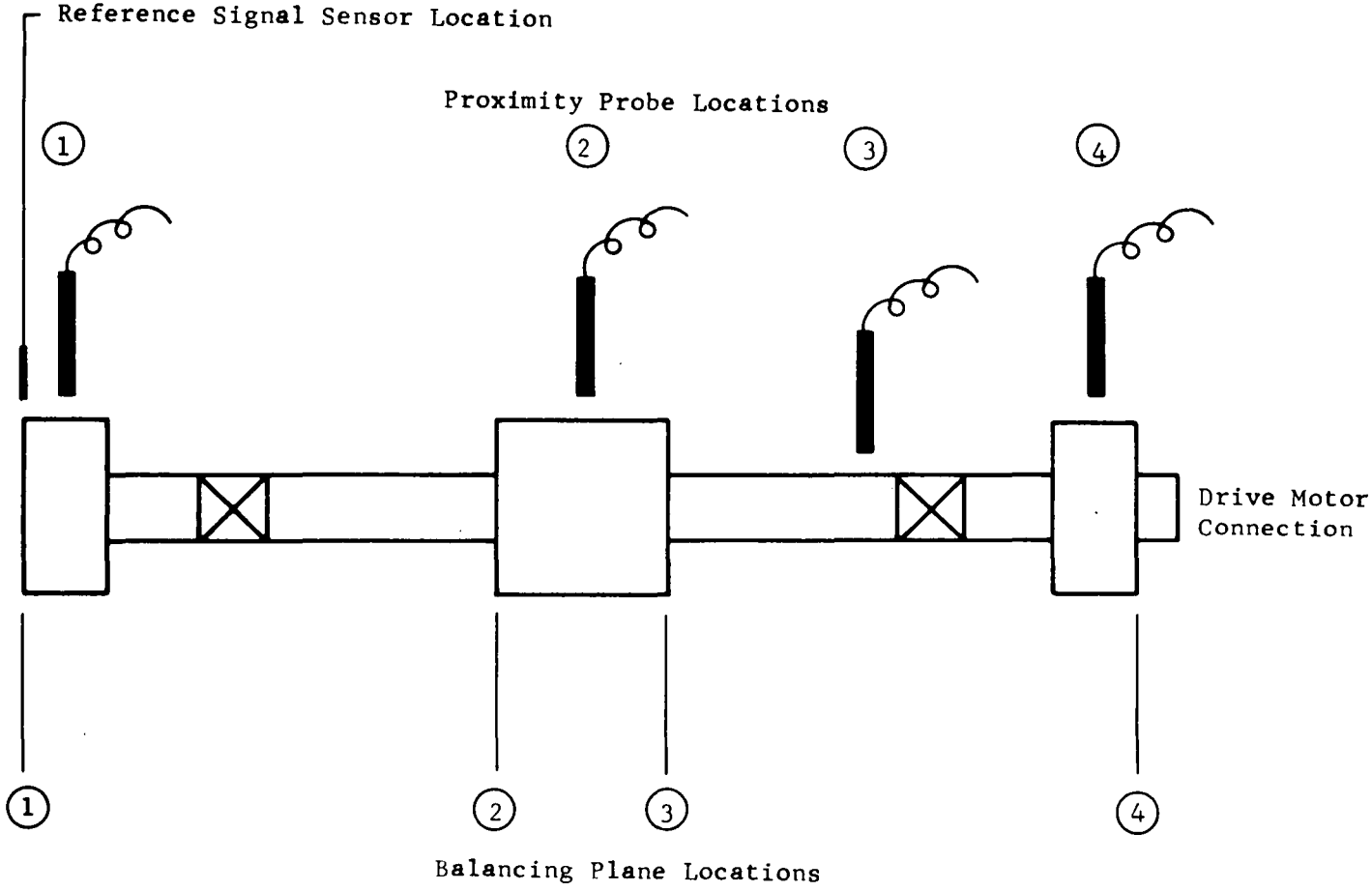

Fig. 7 Probe and Balancing Plane Locations Along Test Rotor (Three-Mass Rotor)

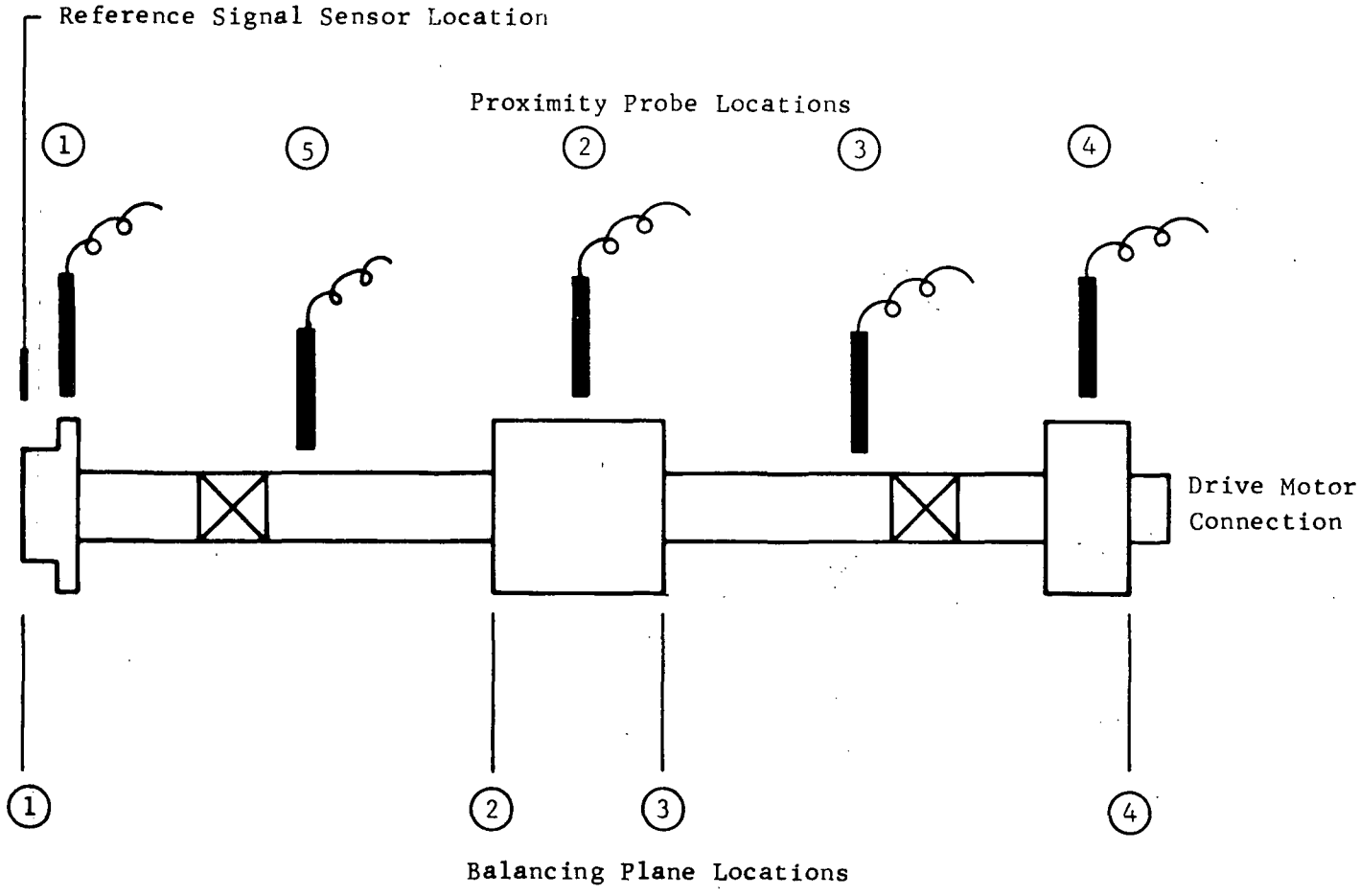

Fig. 8 Probe and Balancing Plane Locations Along Test Rotor (Two-Mass Rotor)

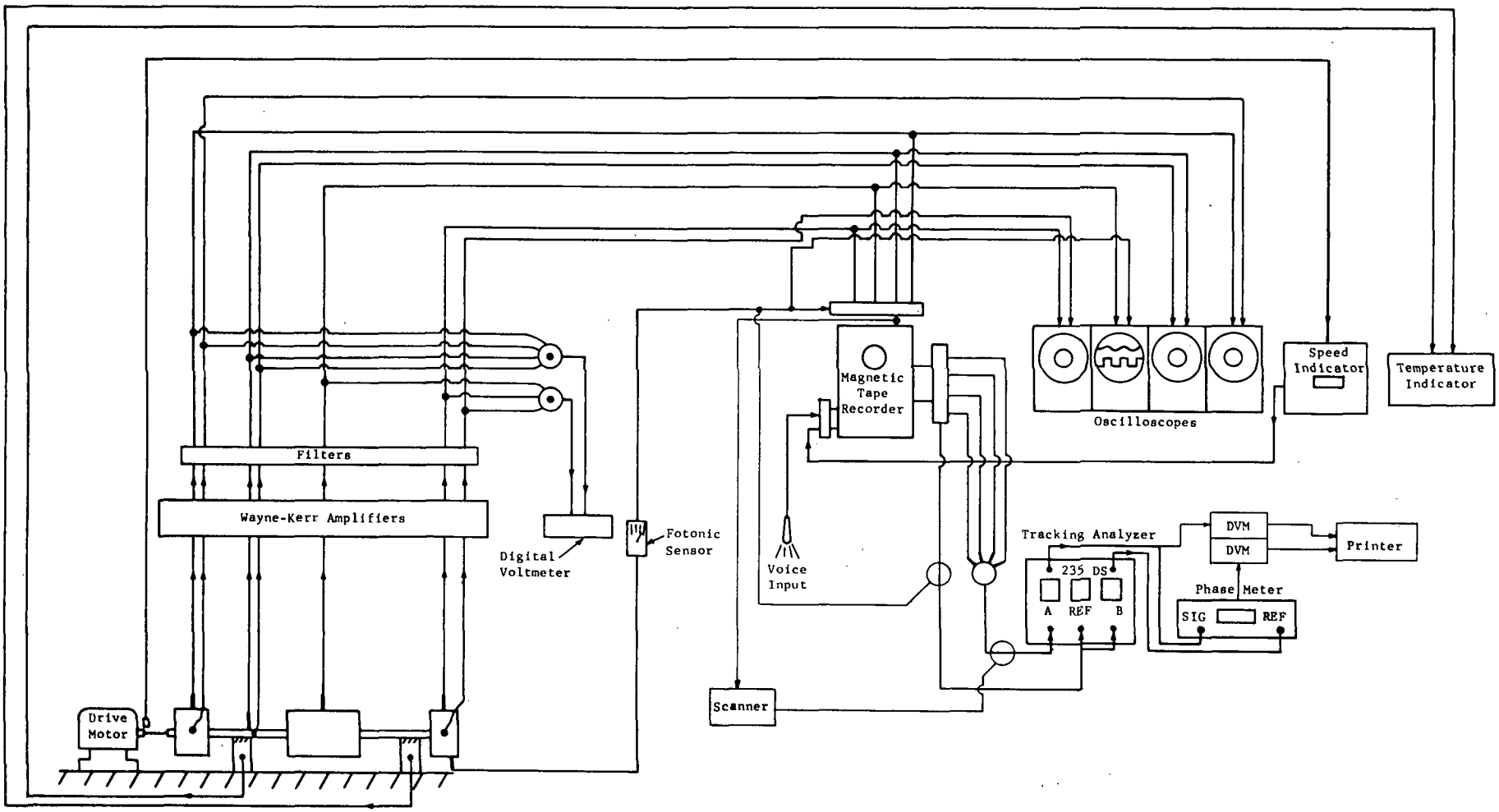

Fig. 9 Schematic of Flexible Rotor Balancing Instrumentation With Scanner and Printer

MTI-13236

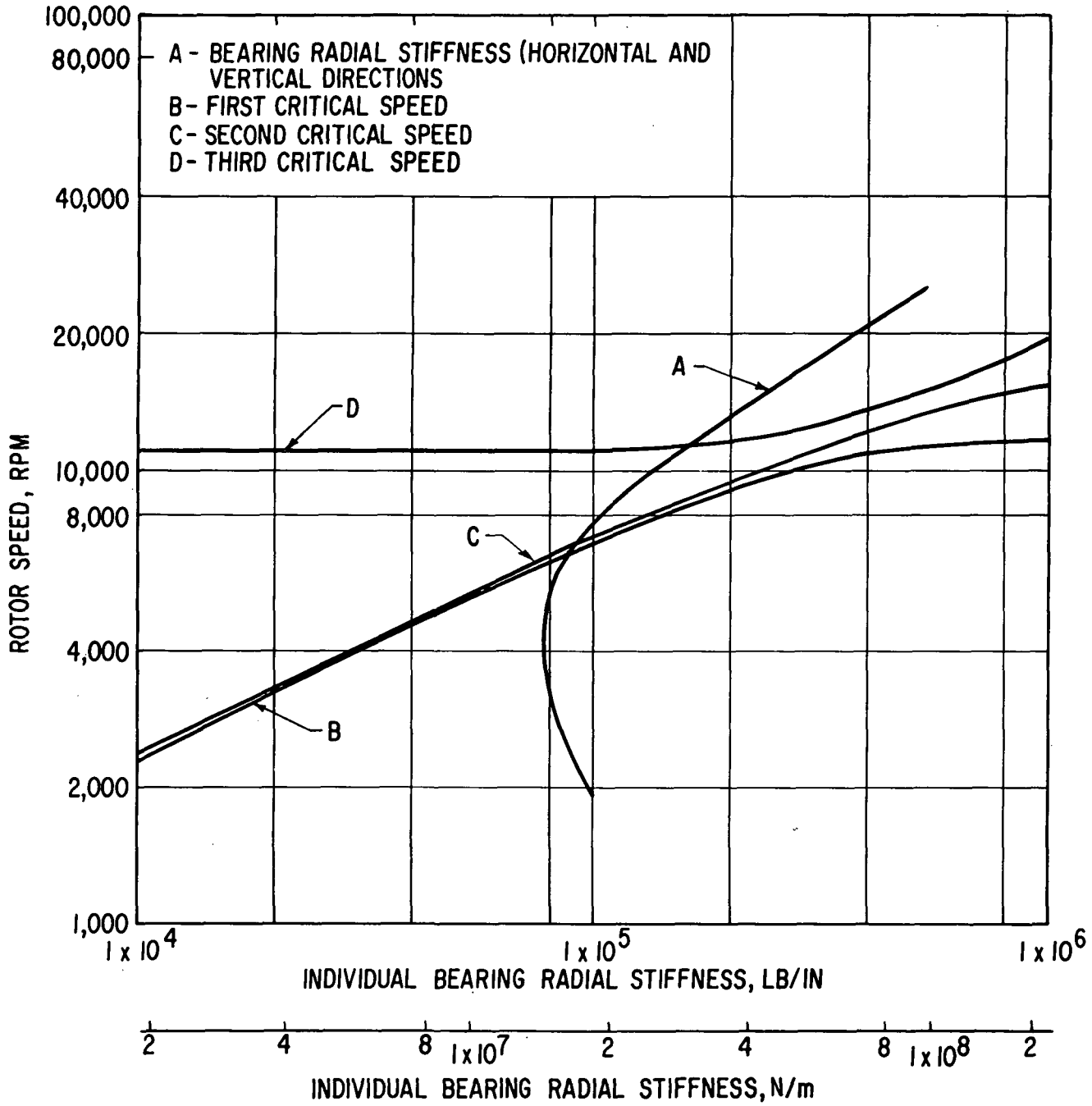

Fig. 10 Critical Speed Map for Flexible-Rotor Test Rig (Three-Mass Rotor)

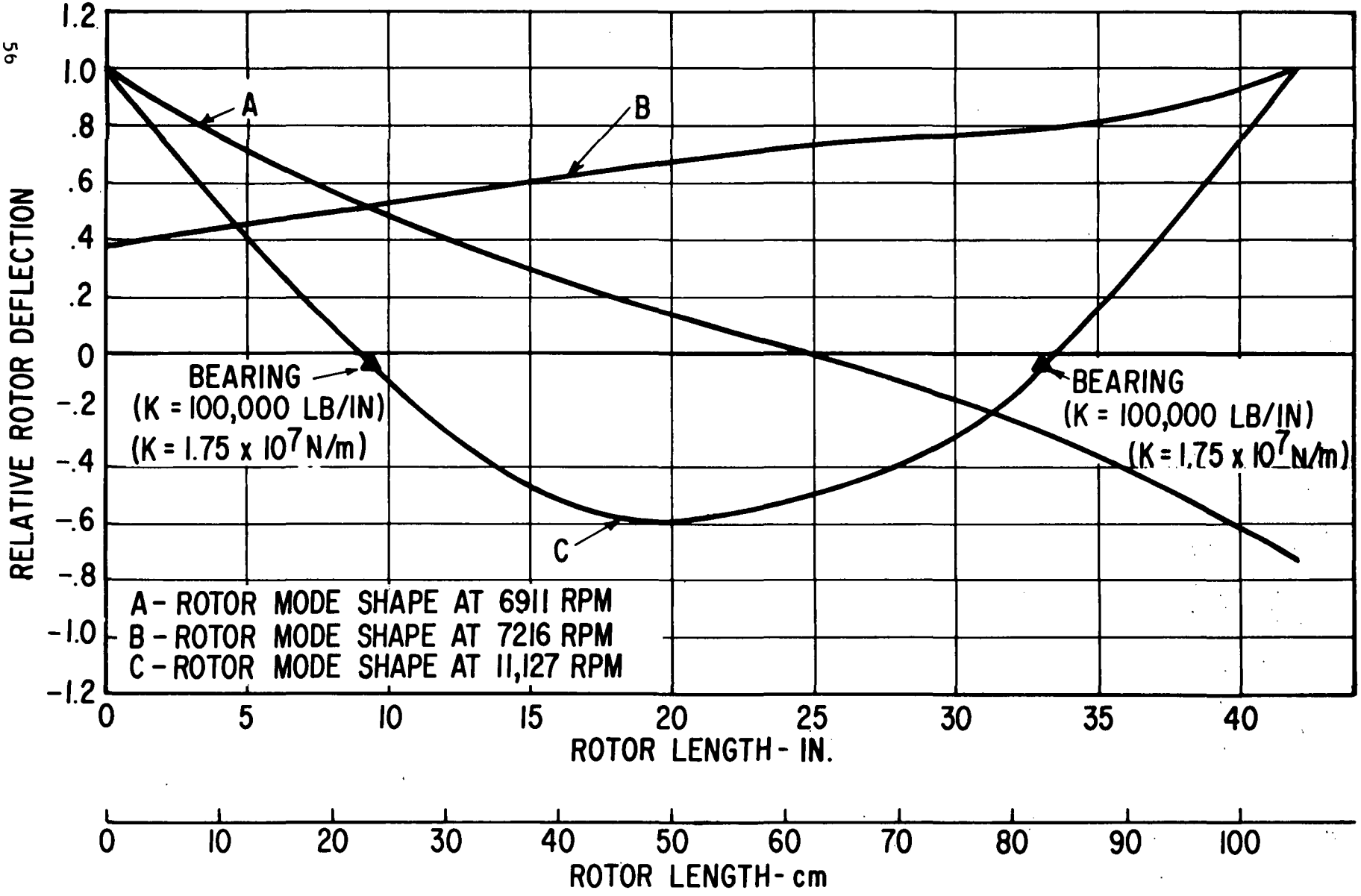

Fig. 11 Undamped Critical Speed Mode Shapes for Flexible-Rotor Test Rig (Three-Mass Rotor)

MTI-9501

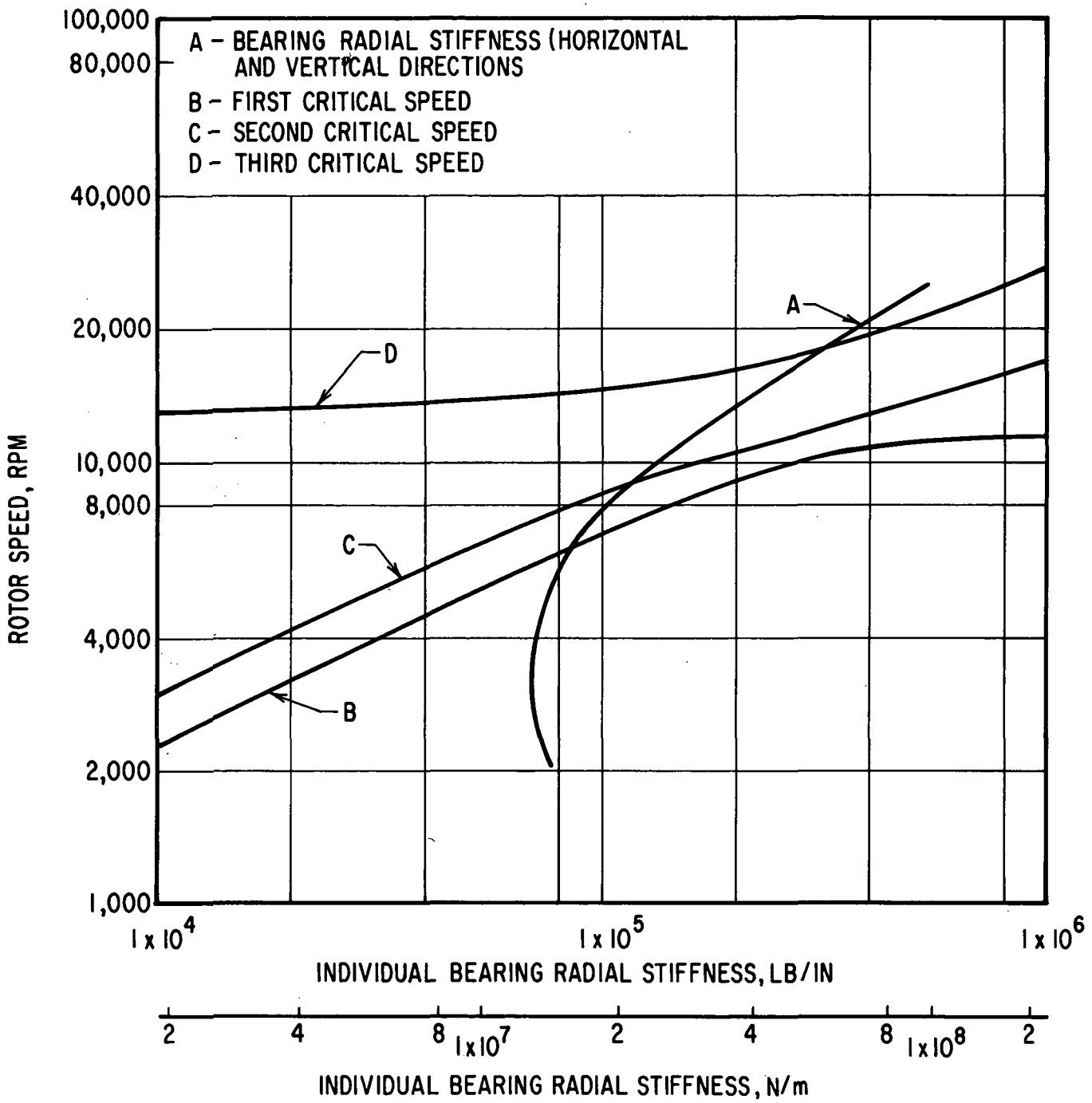

Fig. 12 Critical-Speed Map for Flexible-Rotor Test Rig (Two-Mass Rotor)

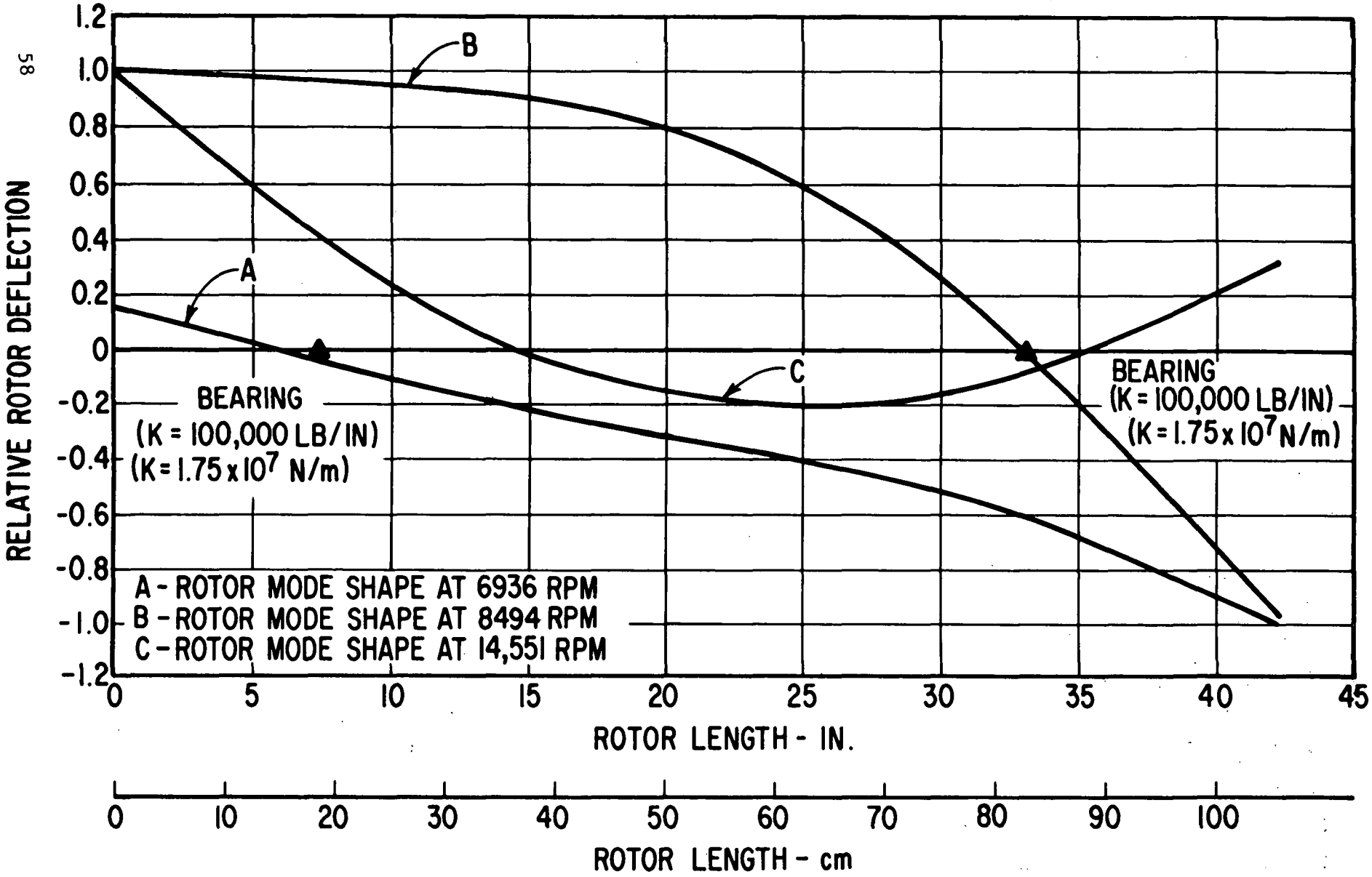

Fig. 13 Undamped Critical Speed Mode Shapes for Flexible-Rotor Test Rig (Two-Mass Rotor)

MTI-13234

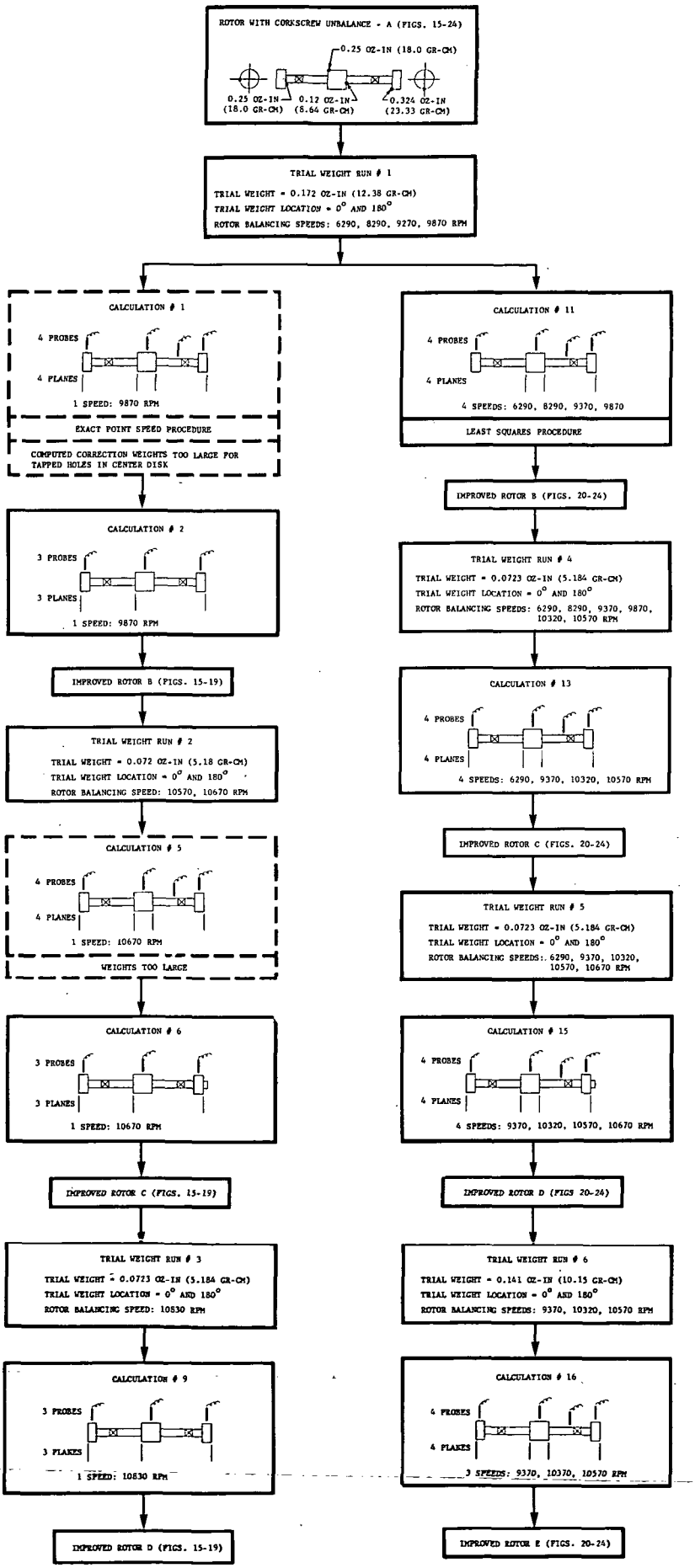

Fig. 14 First Test Case: Rotor With Corkscrew Unbalance

MTI-13275

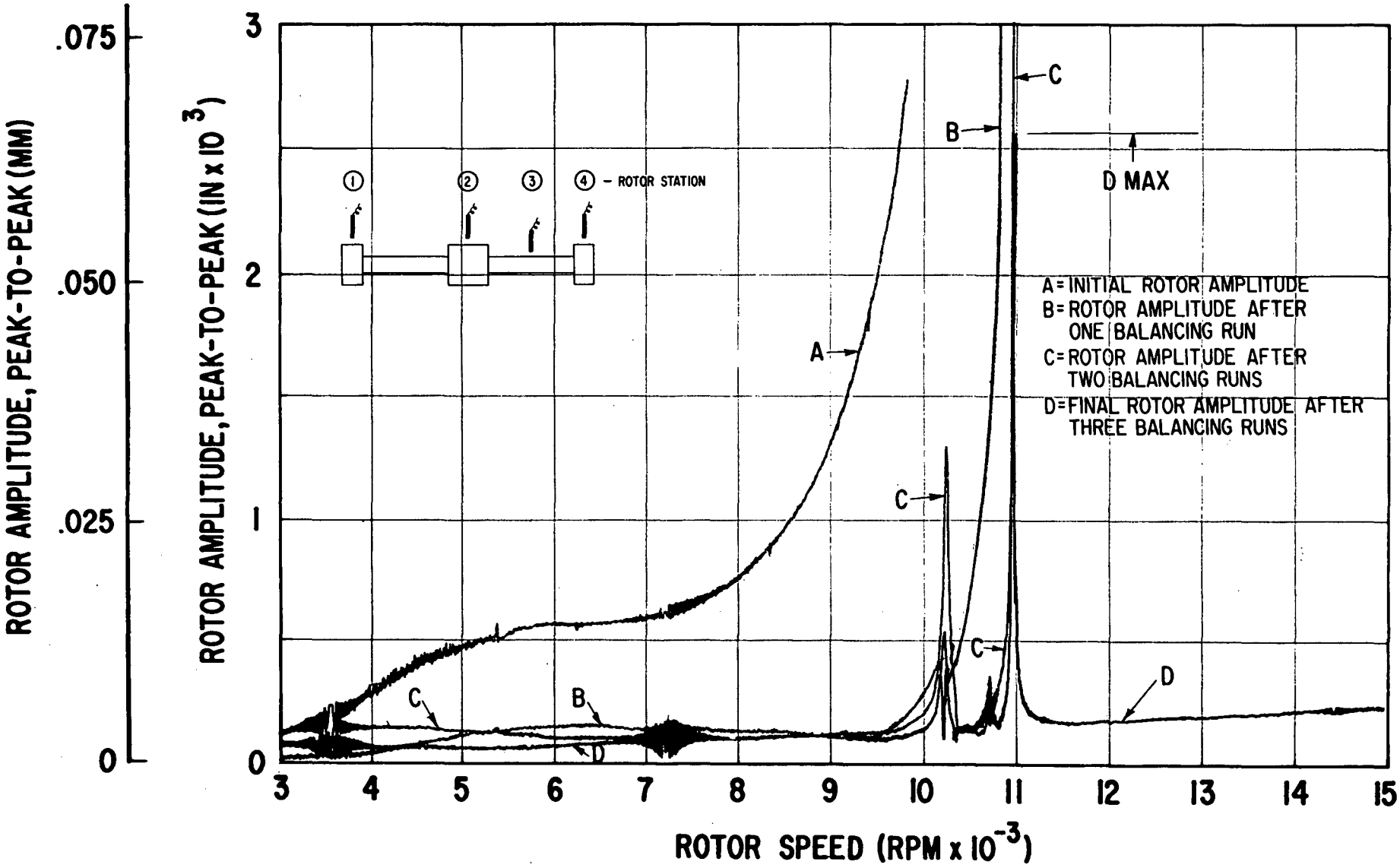

Fig. 15 Vertical Rotor Amplitudes at Station 1 – Initial Condition (Corkscrew Unbalance) and After Three Consecutive Balancing Runs by the Exact Point-Speed Procedure

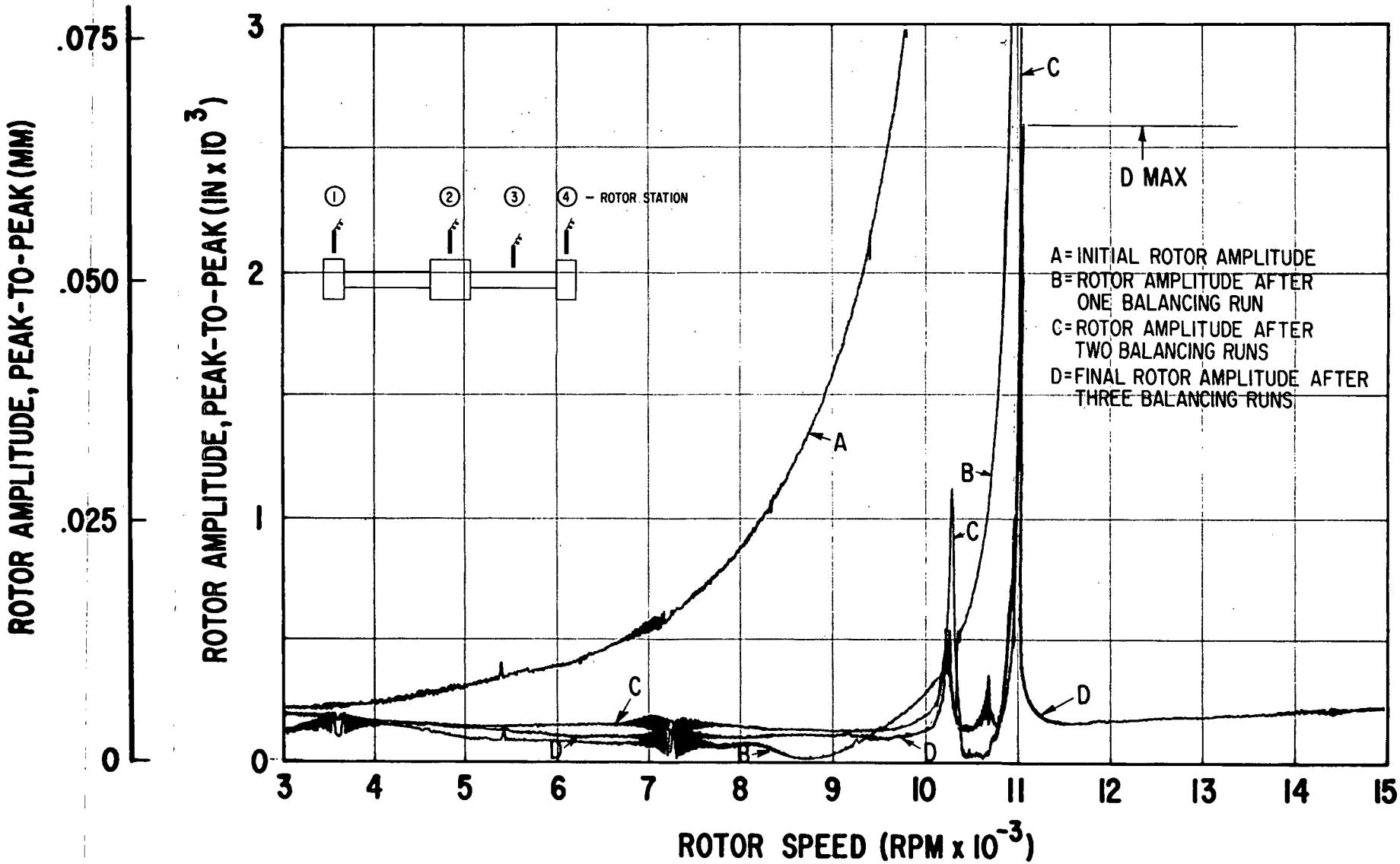

Fig. 16 Vertical Rotor Amplitudes at Station 2 — Initial Condition (Corkscrew Unbalance) and After Three Consecutive Balancing Runs by the Exact Point-Speed Procedure

MTI-13143

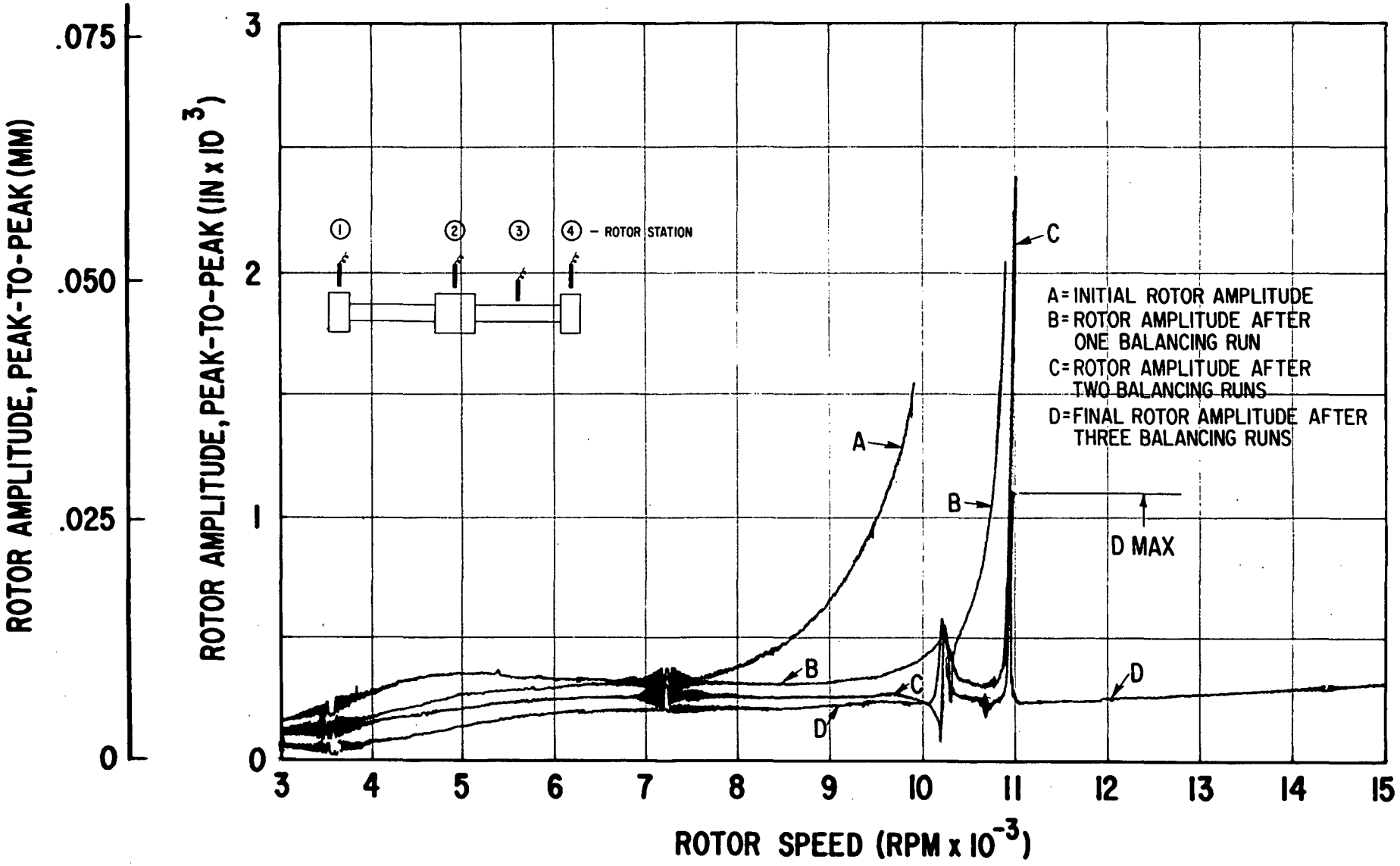

Fig. 17 Vertical Rotor Amplitudes at Station 3 – Initial Condition (Corkscrew Unbalance) and After Three Consecutive Balancing Runs by the Exact Point-Speed Procedure

MTI-13144

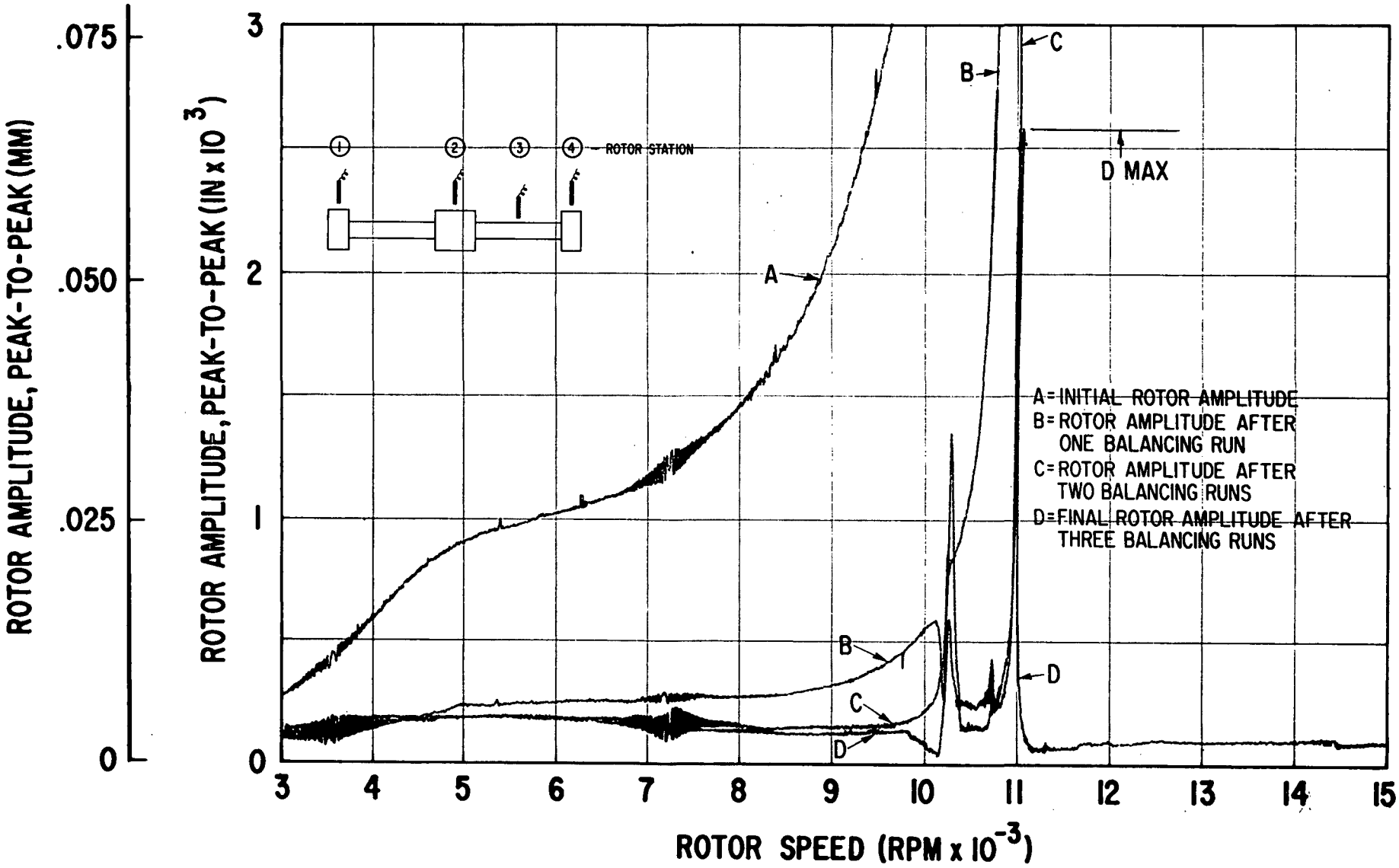

Fig. 18 Vertical Rotor Amplitudes at Station 4 — Initial Condition (Corkscrew Unbalance) and After Three Consecutive Balancing Runs by the Exact Point-Speed Procedure

MTI-13145

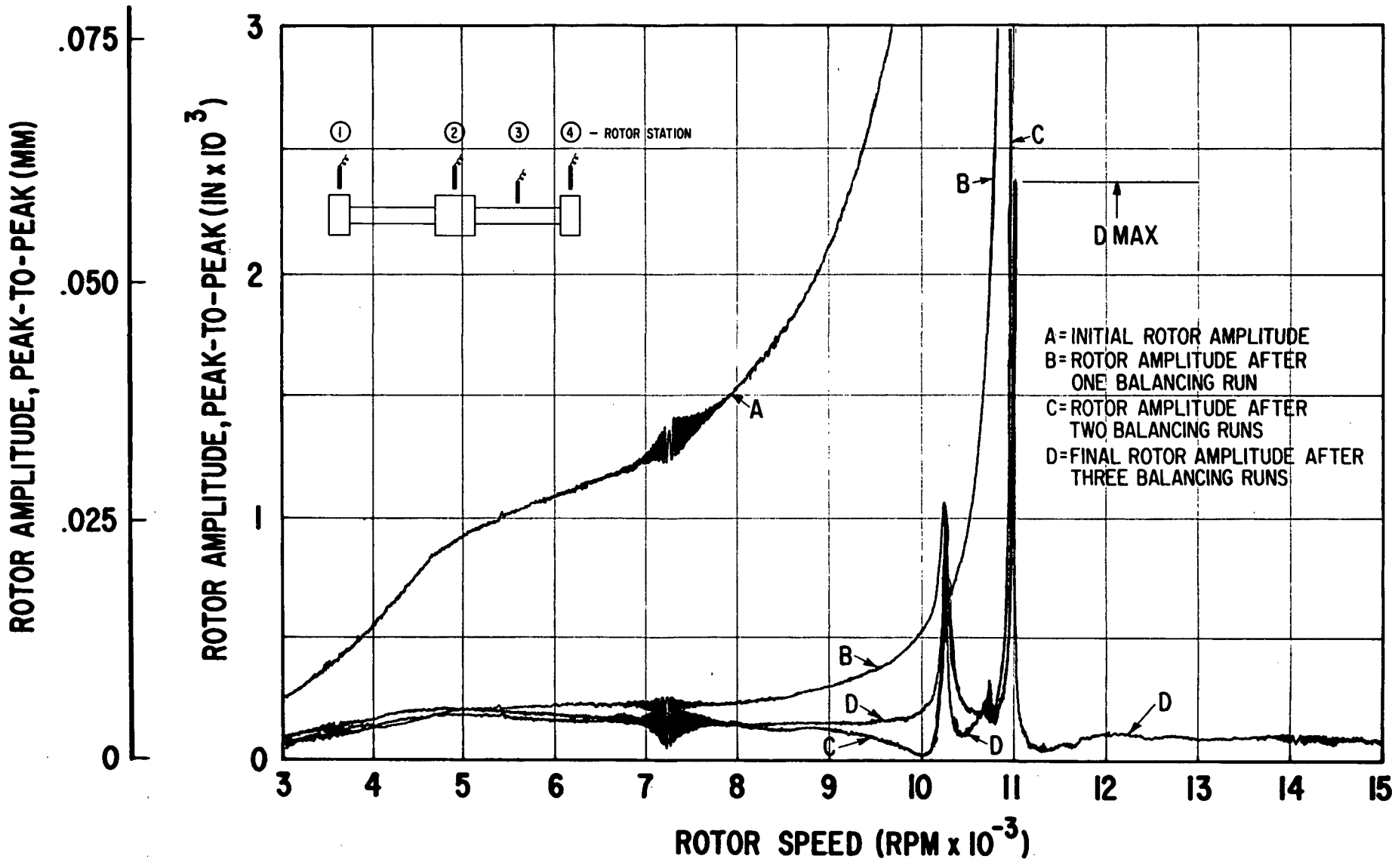

Fig. 19 Horizontal Rotor Amplitudes at Station 4 — Initial Condition (Corkscrew Unbalance) and After Three Consecutive Balancing Runs by the Exact Point-Speed Procedure

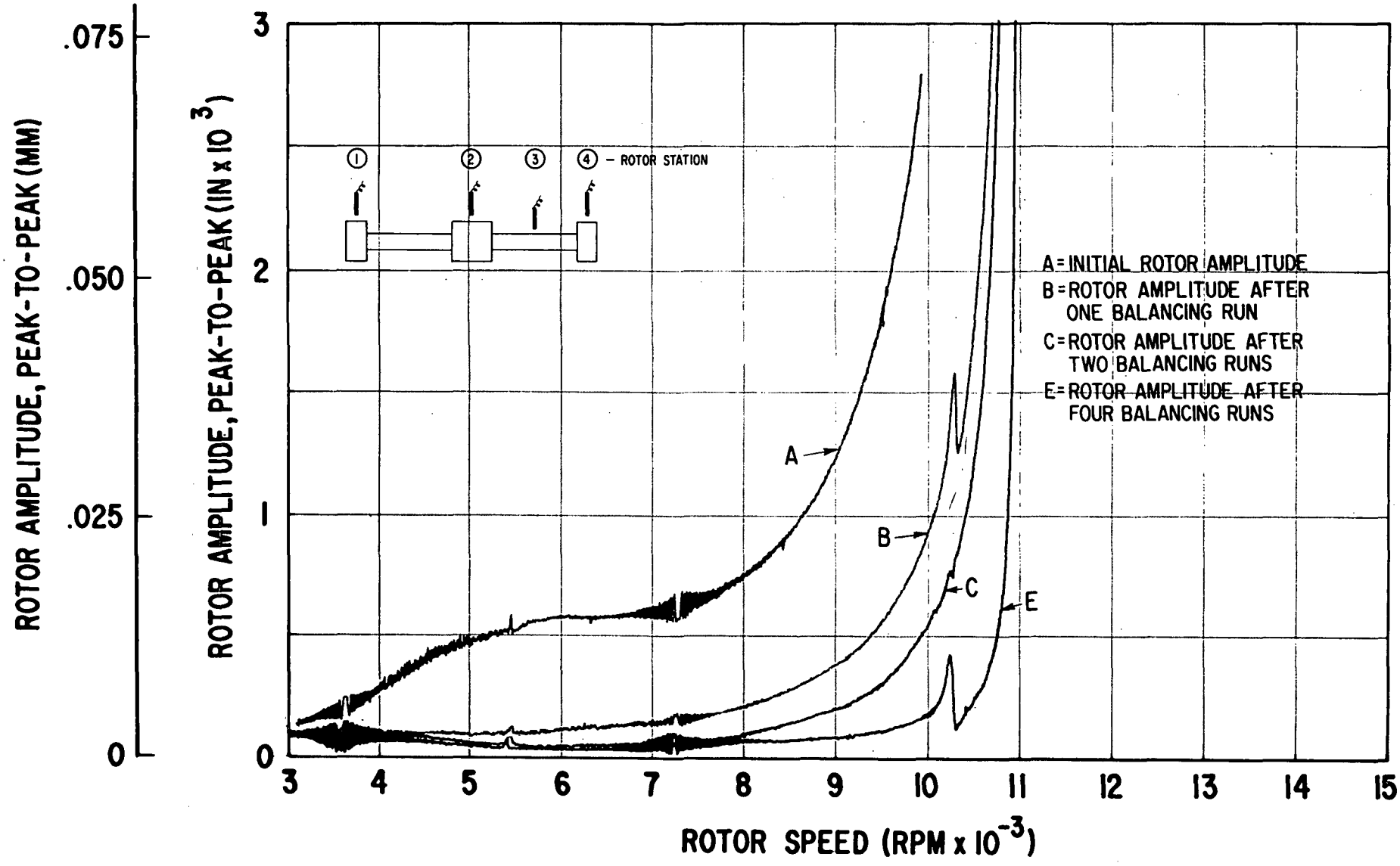

Fig. 20 Vertical Rotor Amplitudes at Station 1 – Initial Condition (Corkscrew Unbalance) and After Four Consecutive Balancing Runs by the Least Squares Procedure

MTI-13147

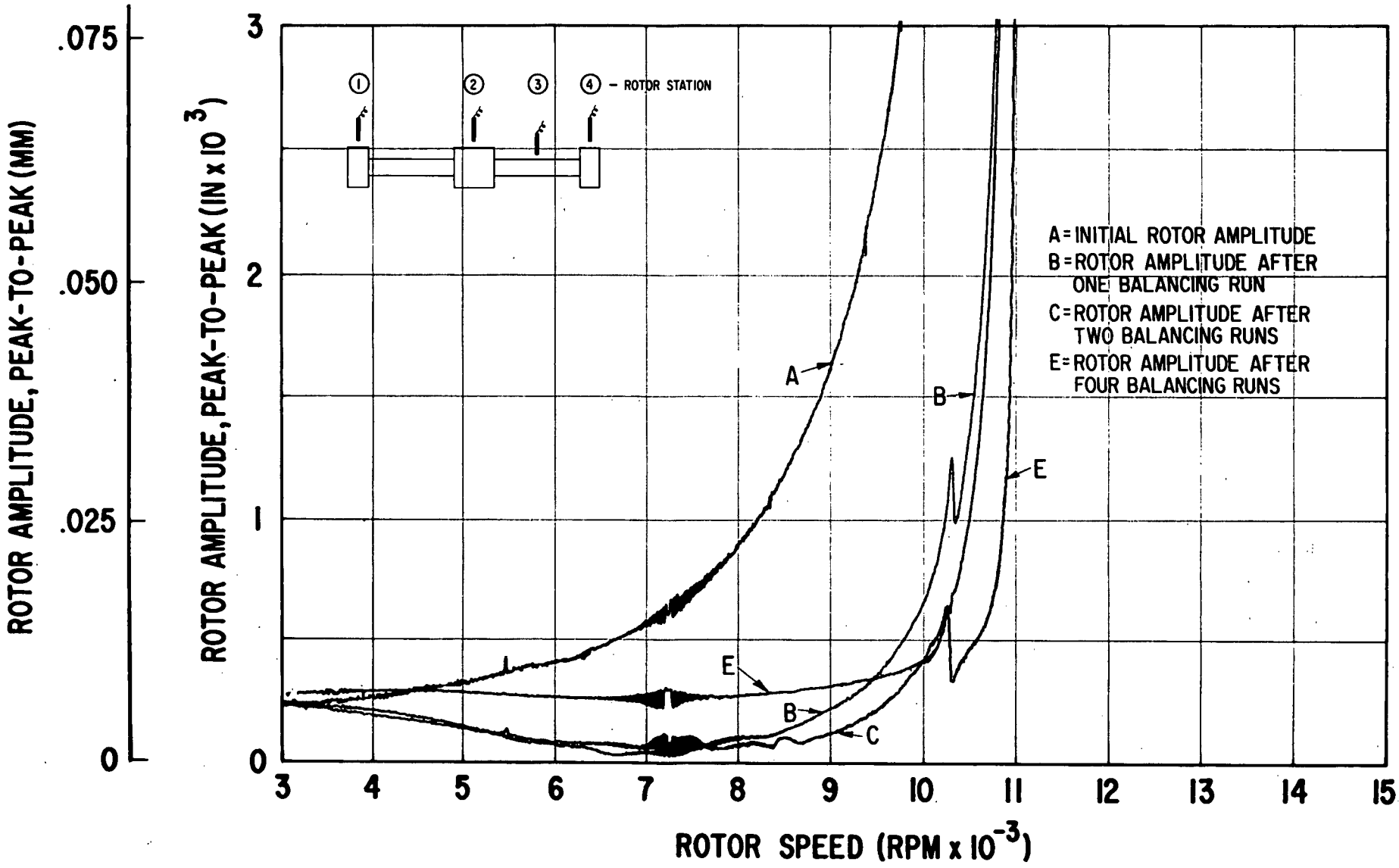

Fig. 21 Vertical Rotor Amplitudes at Station 2 – Initial Condition (Corkscrew Unbalance) and After Four Consecutive Balancing Runs by the Least Squares Procedure

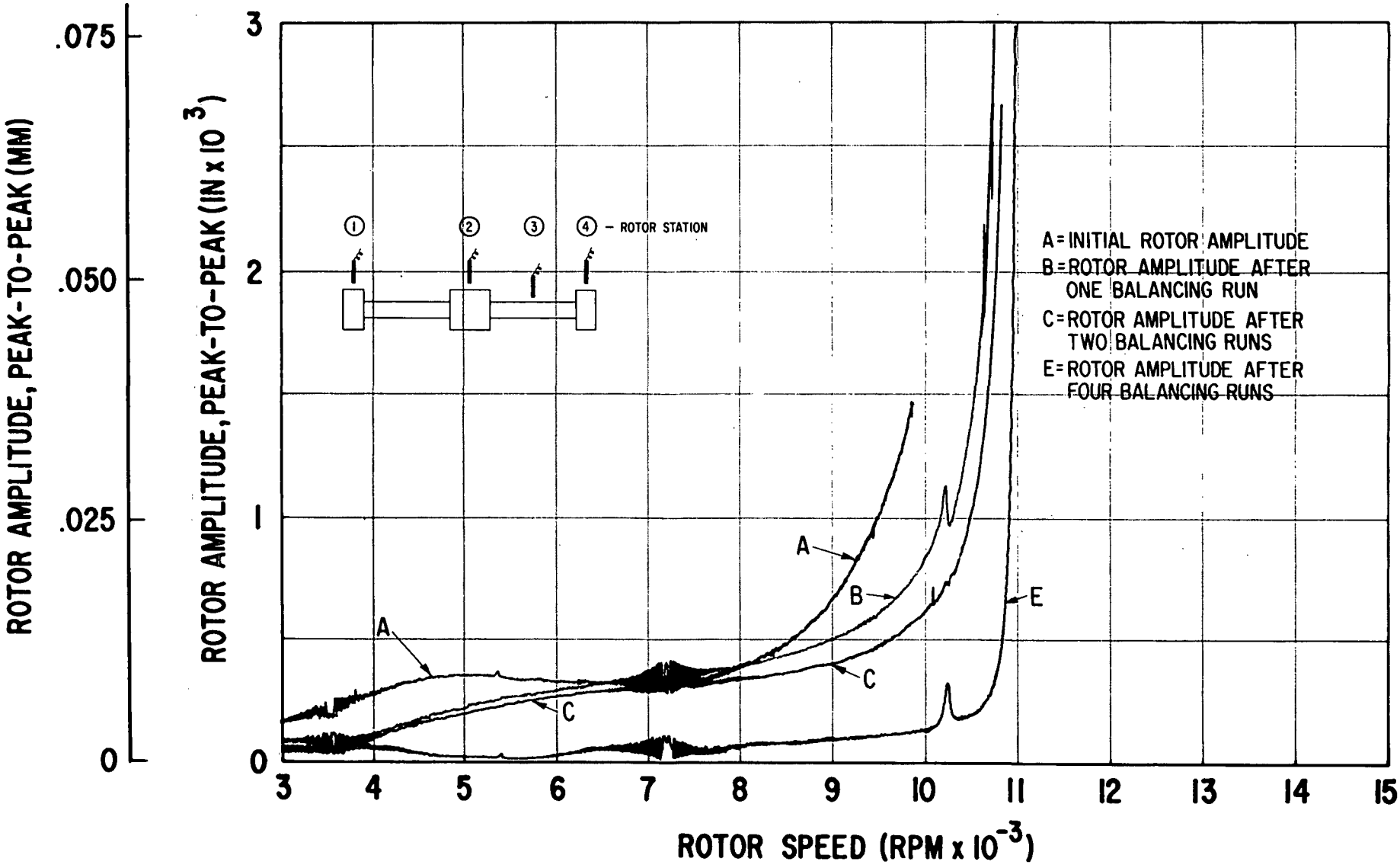

Fig. 22 Vertical Rotor Amplitudes at Station 3 – Initial Condition (Corkscrew Unbalance) and After Four Consecutive Balancing Runs by the Least Squares Procedure

MTI-13149

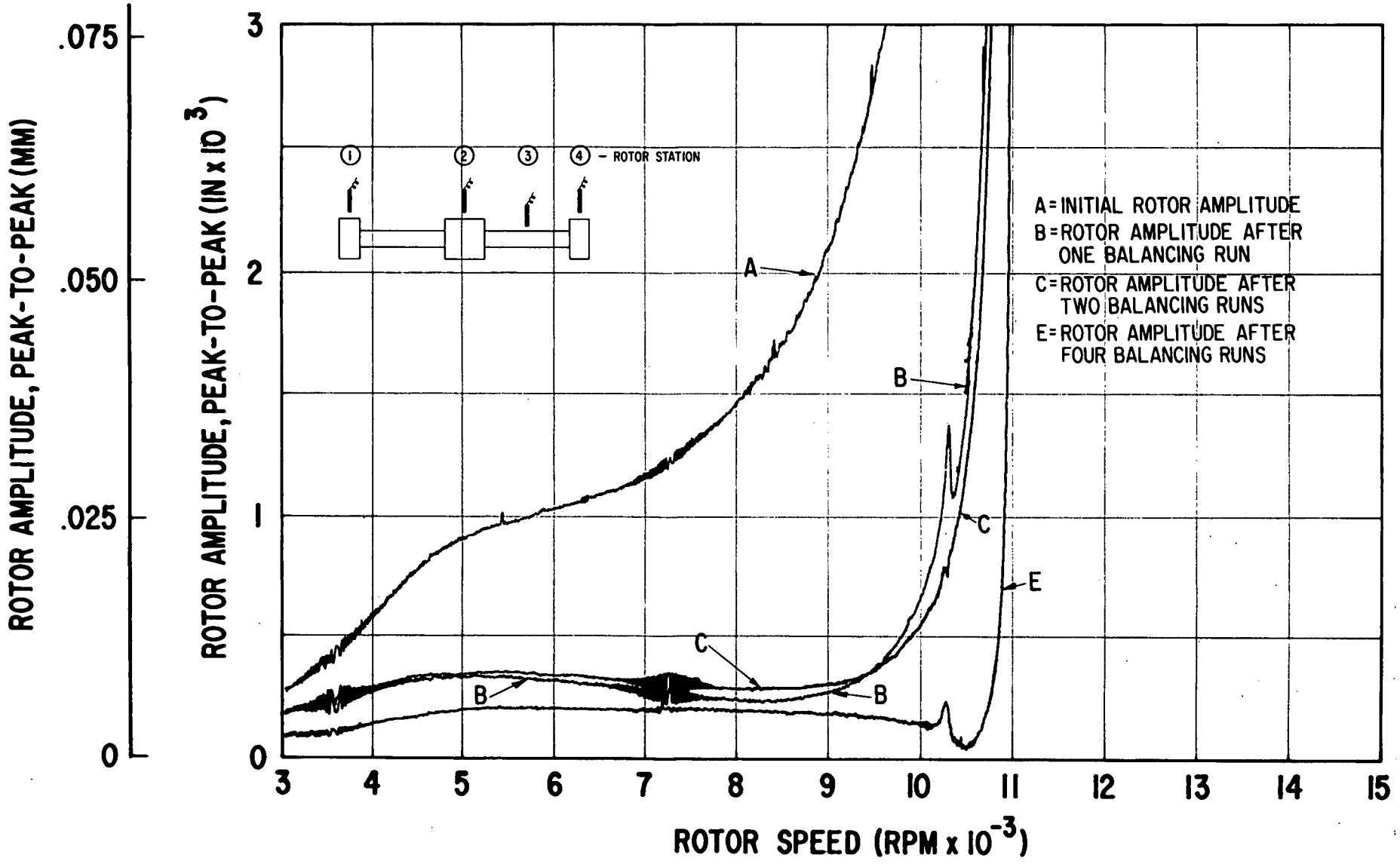

Fig. 23 Vertical Rotor Amplitudes at Station 4 – Initial Condition (Corkscrew Unbalance) and After Four Consecutive Balancing Runs by the Least Squares Procedure

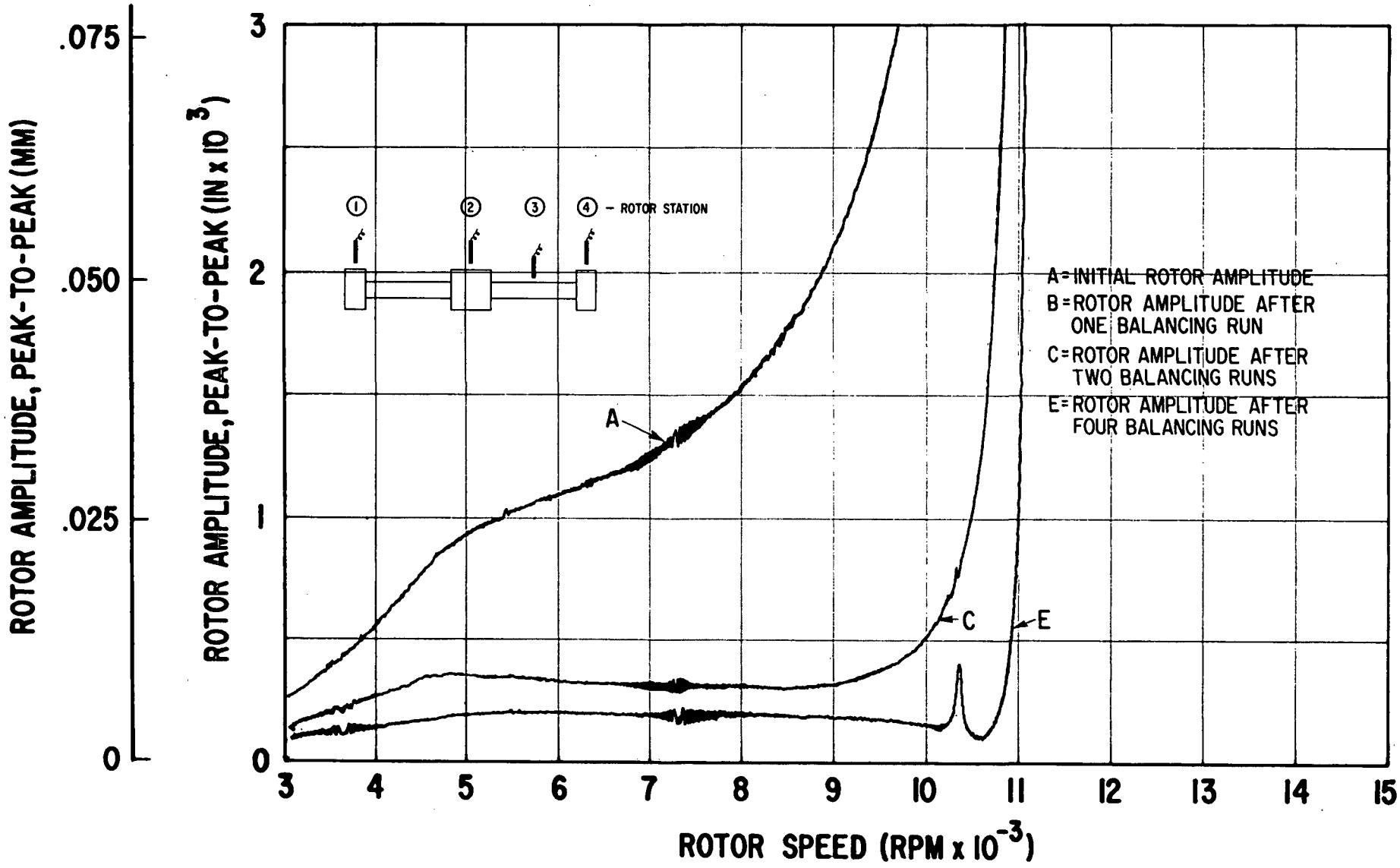

Fig. 24 Horizontal Rotor Amplitudes at Station 4 — Initial Condition (Corkscrew Unbalance) and After Four Consecutive Balancing Runs by the Least Squares Procedure

MTI-13151

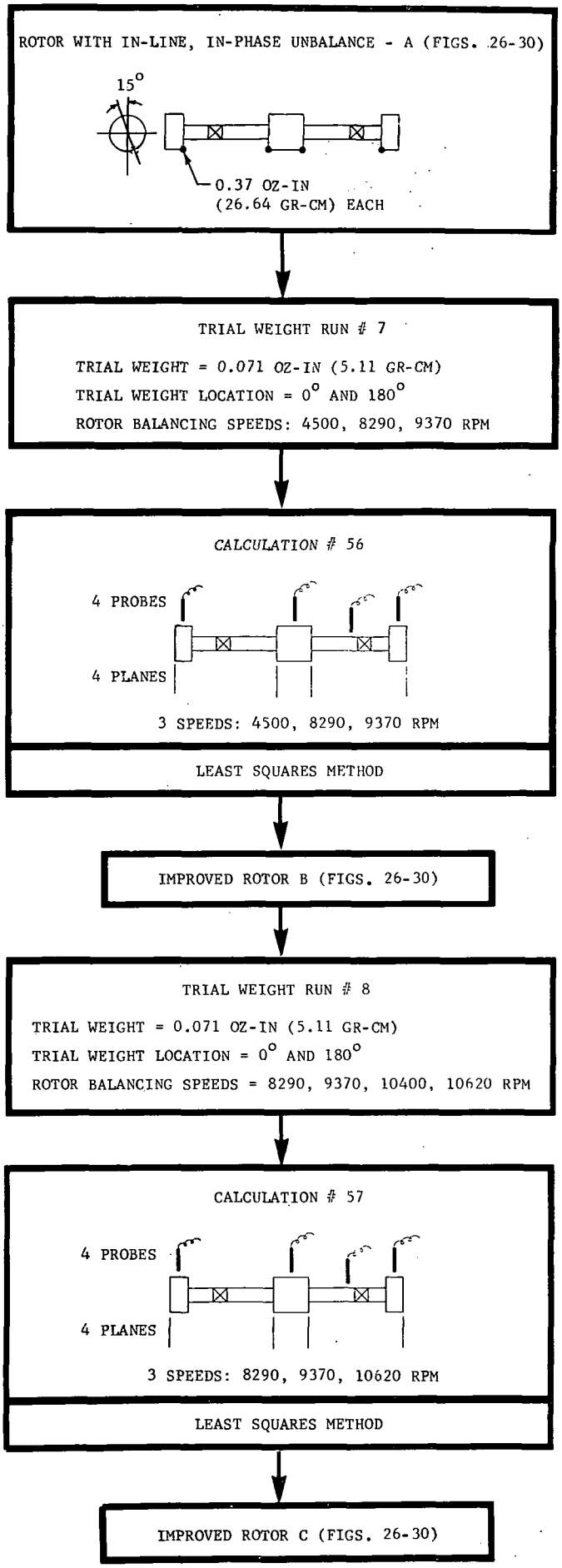

Fig. 25 Second Test Case: Rotor With In-Line, In-Phase Unbalance

MTI-13276

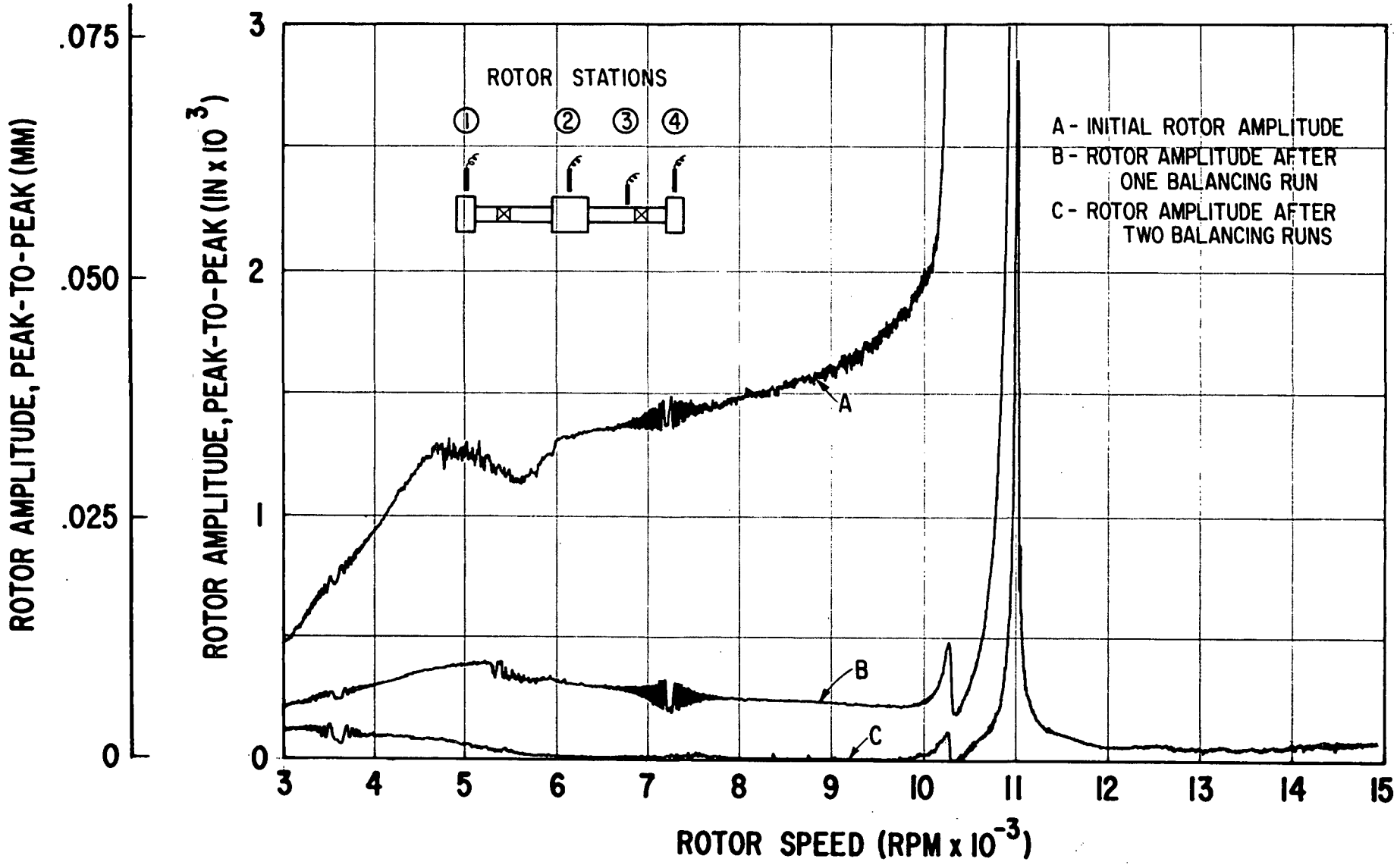

Fig. 26 Vertical Rotor Amplitudes at Station 1 – Initial Condition (In-Line, In-Phase Unbalance) and After Two Consecutive Balancing Runs by the Least Squares Procedure

MTI-13157

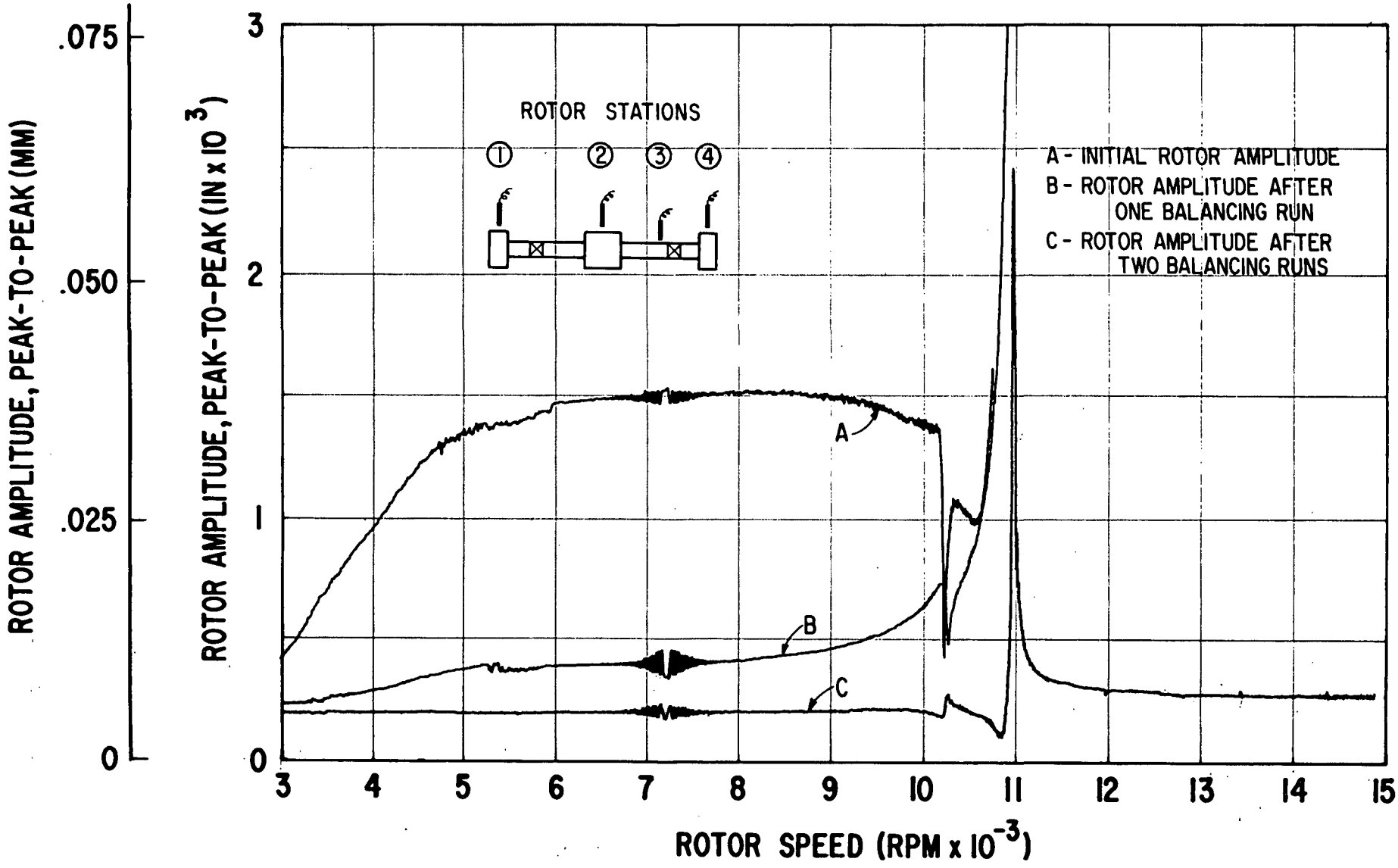

Fig. 27 Vertical Rotor Amplitudes at Station 2 – Initial Condition (In-Line, In-Phase Unbalance) and After Two Consecutive Balancing Runs by the Least Squares Procedure

MTI-13158

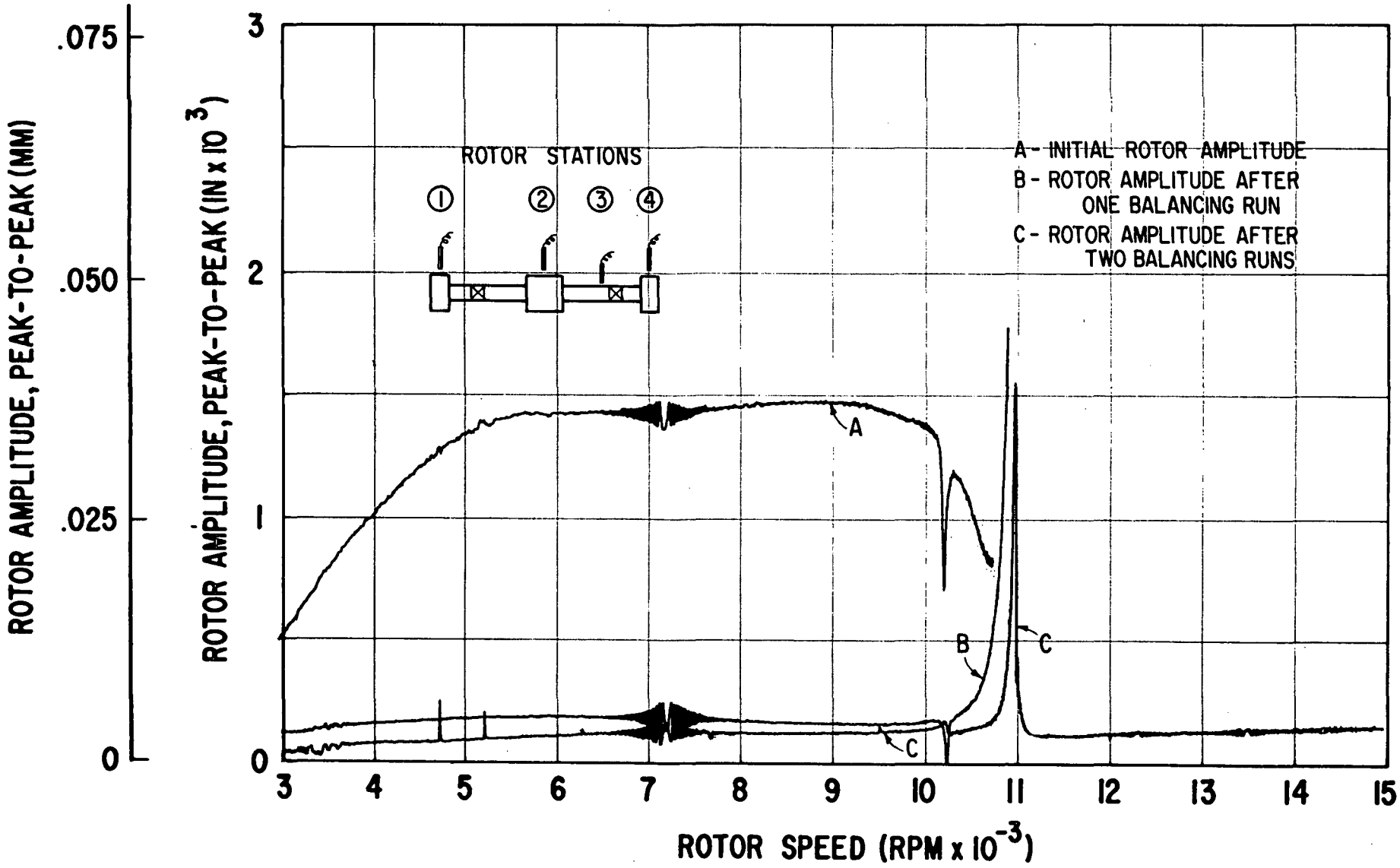

Fig. 28 Vertical Rotor Amplitudes at Station 3 — Initial Condition (In-Line, In-Phase Unbalance) and After Two Consecutive Balancing Runs by the Least Squares Procedure

MTI-13159

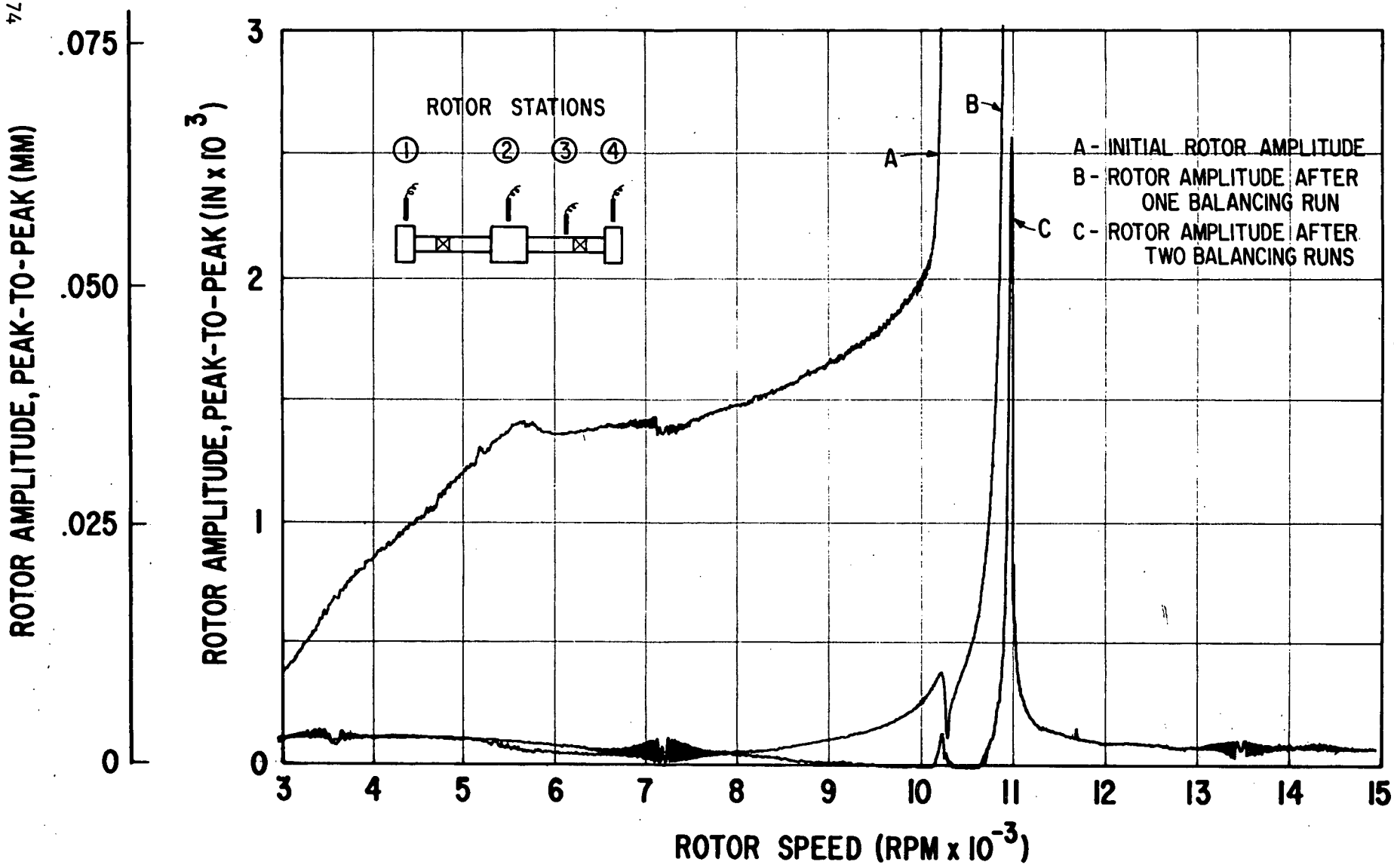

Fig. 29 Vertical Rotor Amplitudes at Station 4 — Initial Condition (In-Line, In-Phase Unbalance) and After Two Consecutive Balancing Runs by the Least Squares Procedure

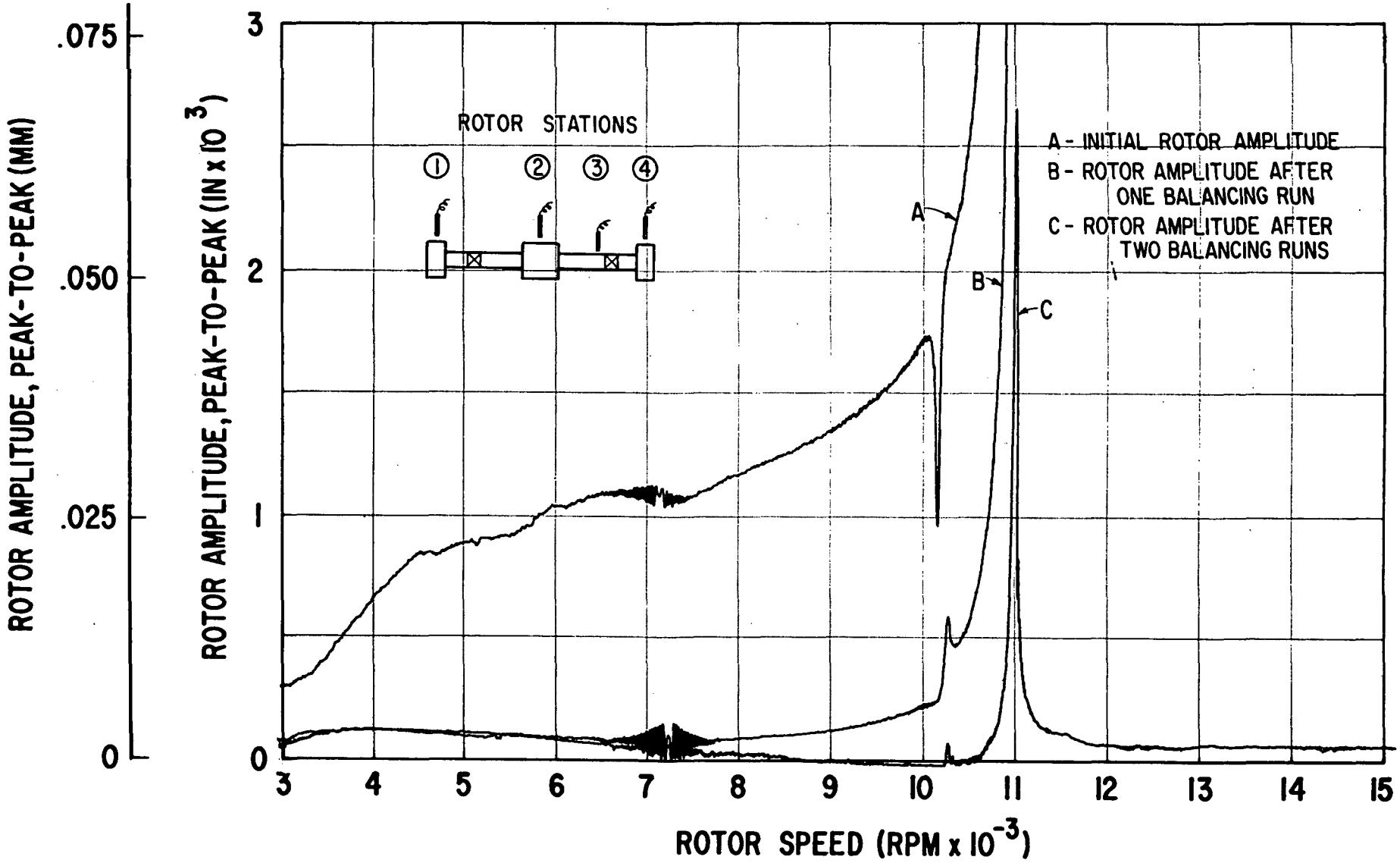

Fig. 30 Horizontal Rotor Amplitudes at Station 4 — Initial Condition (In-Line, In-Phase Unbalance) and After Two Consecutive Balancing Runs by the Least Squares Procedure

MTI-13131

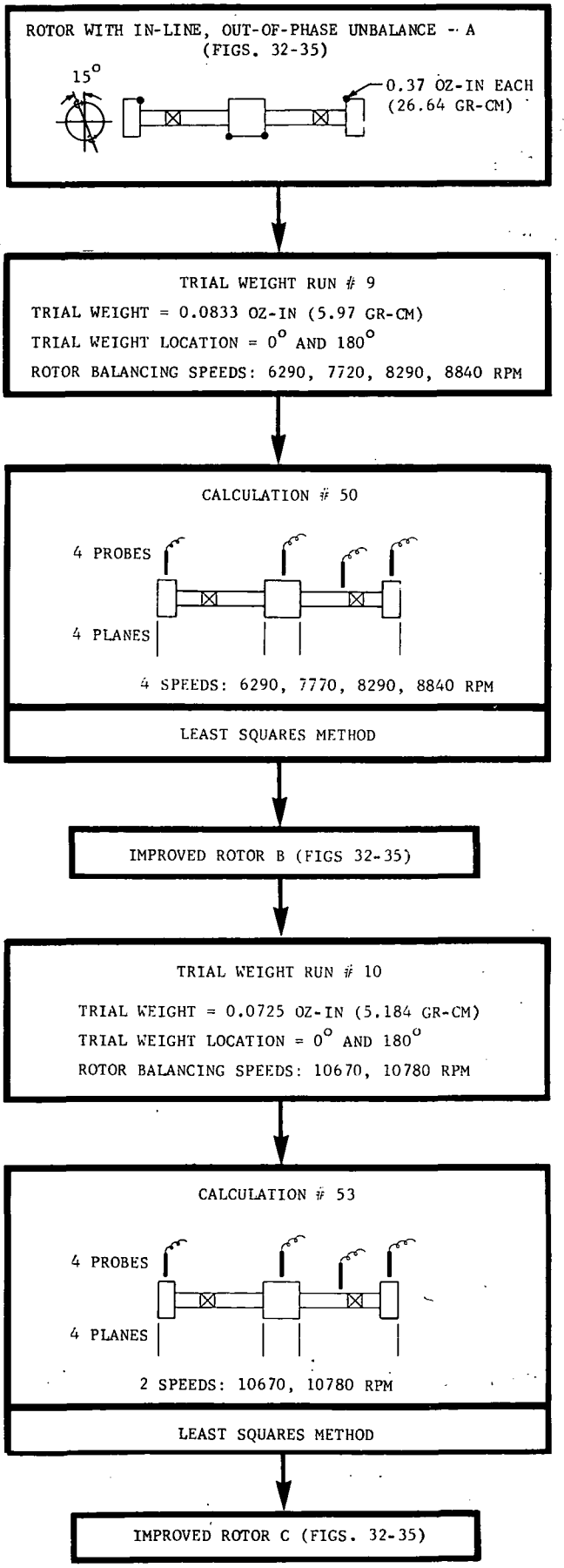

Fig. 31 Third Test Case: Rotor With In-Line, Out-Of-Phase Unbalance

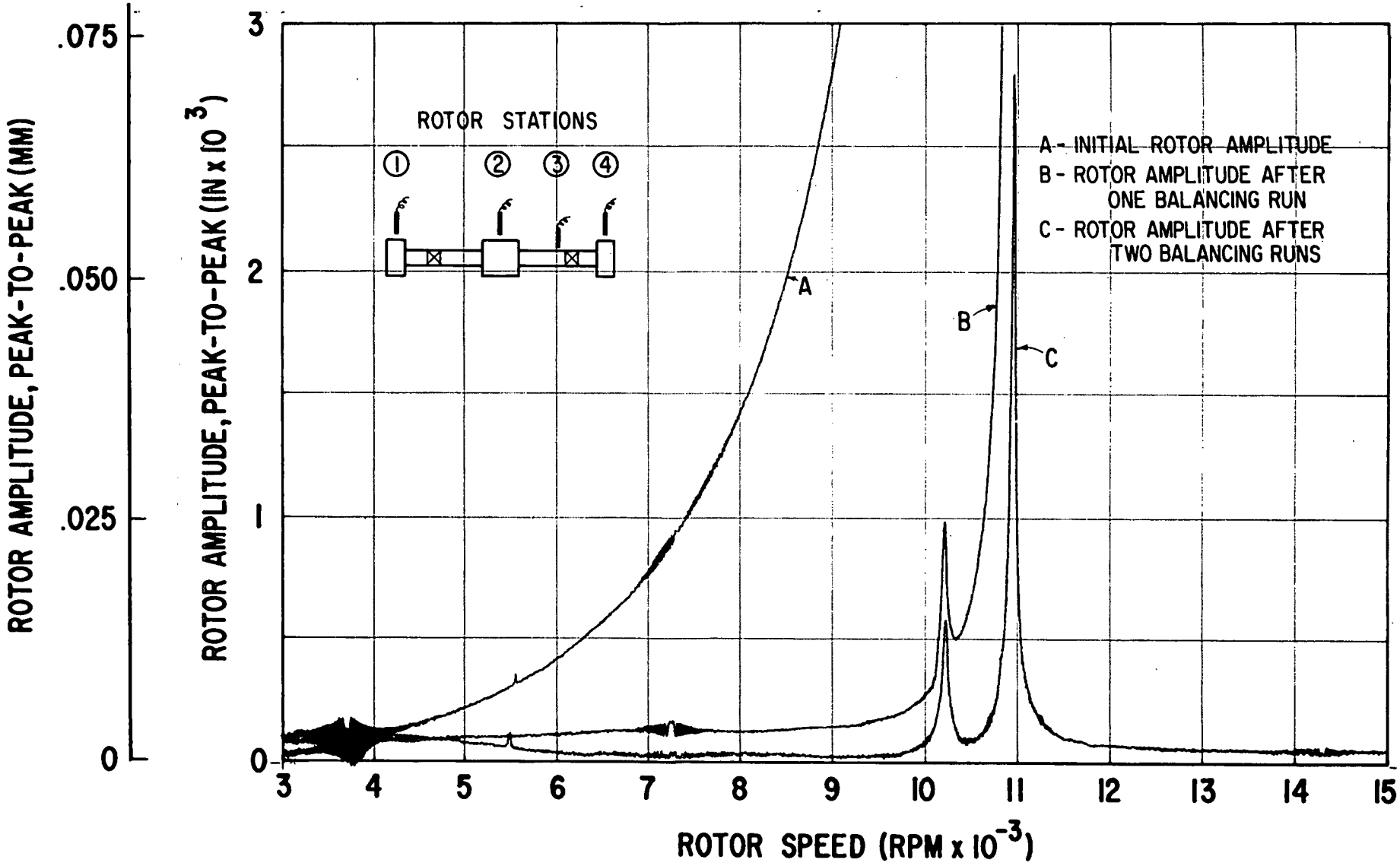

Fig. 32 Vertical Rotor Amplitude at Station 1 — Initial Condition (In-Line, Out-Of-Phase Unbalance) and After Two Consecutive Balancing Runs by the Least Squares Procedure

MTI-13202

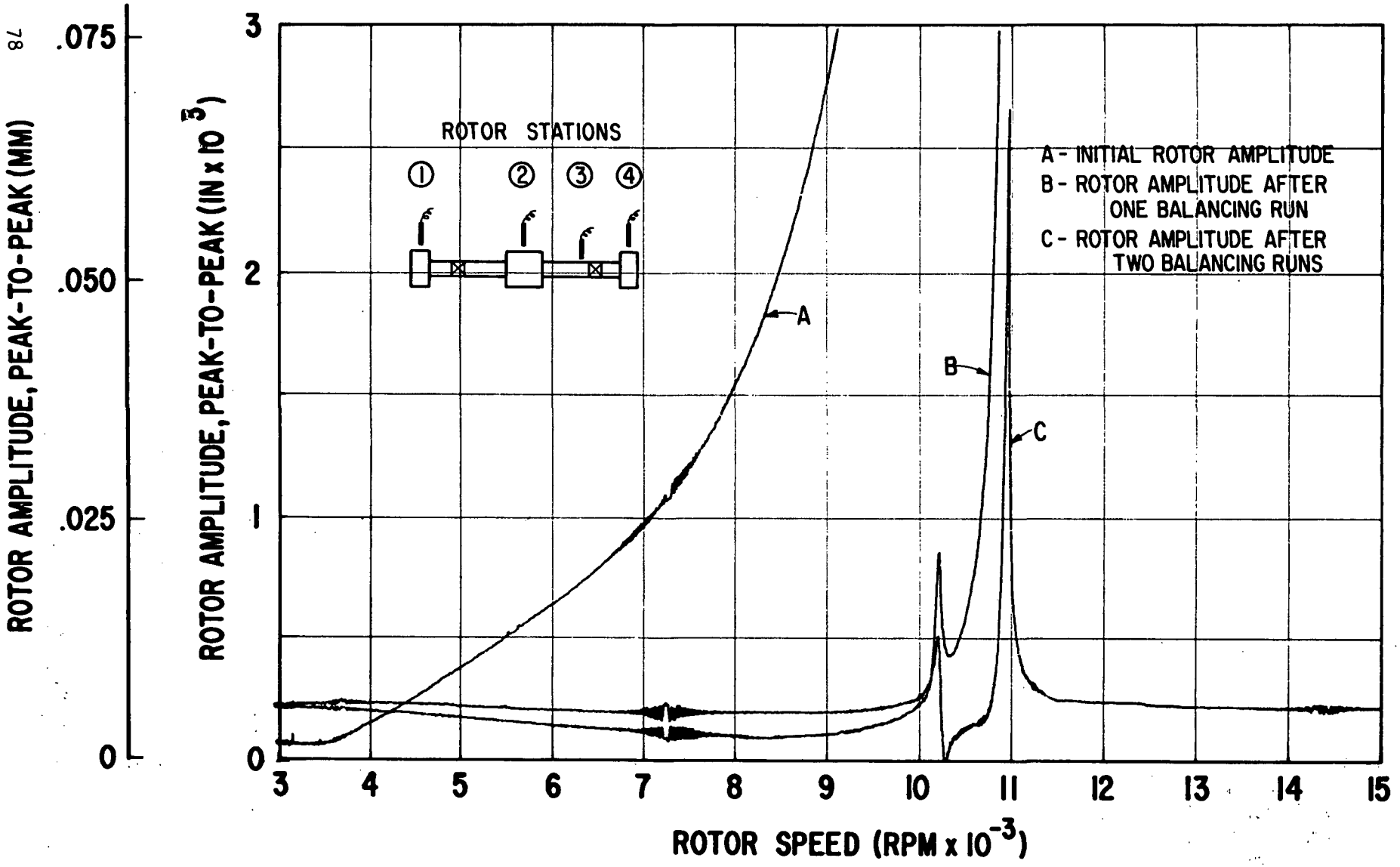

Fig. 33 Vertical Rotor Amplitude at Station 2 — Initial Condition (In-Line, Out-Of-Phase Unbalance) and After Two Consecutive Balancing Runs by the Least Squares Procedure

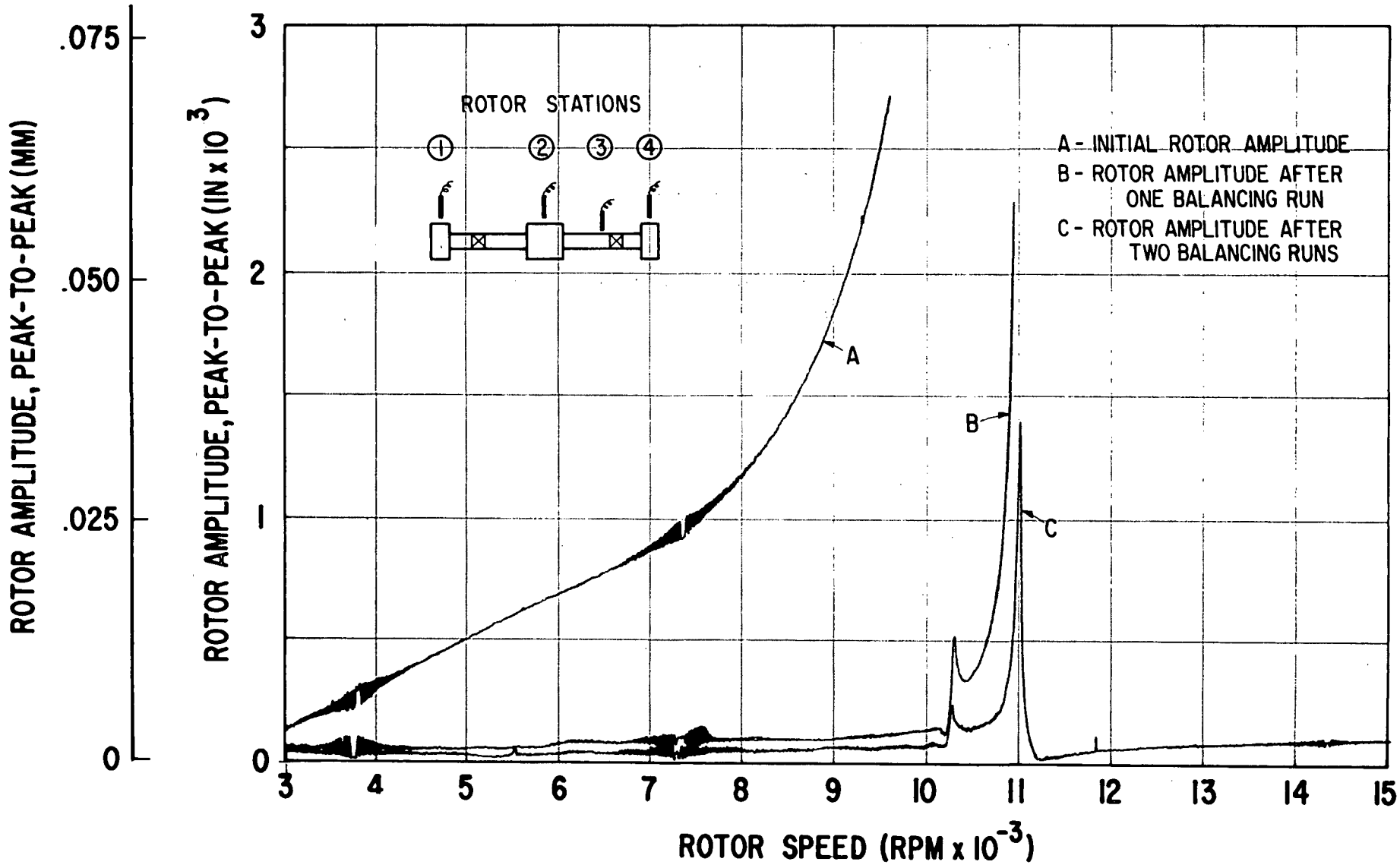

Fig. 34 Vertical Rotor Amplitude at Station 3 — Initial Condition (In-Line, Out-Of-Phase Unbalance) and After Two Consecutive Balancing Runs by the Least Squares Procedure

MTI-13204

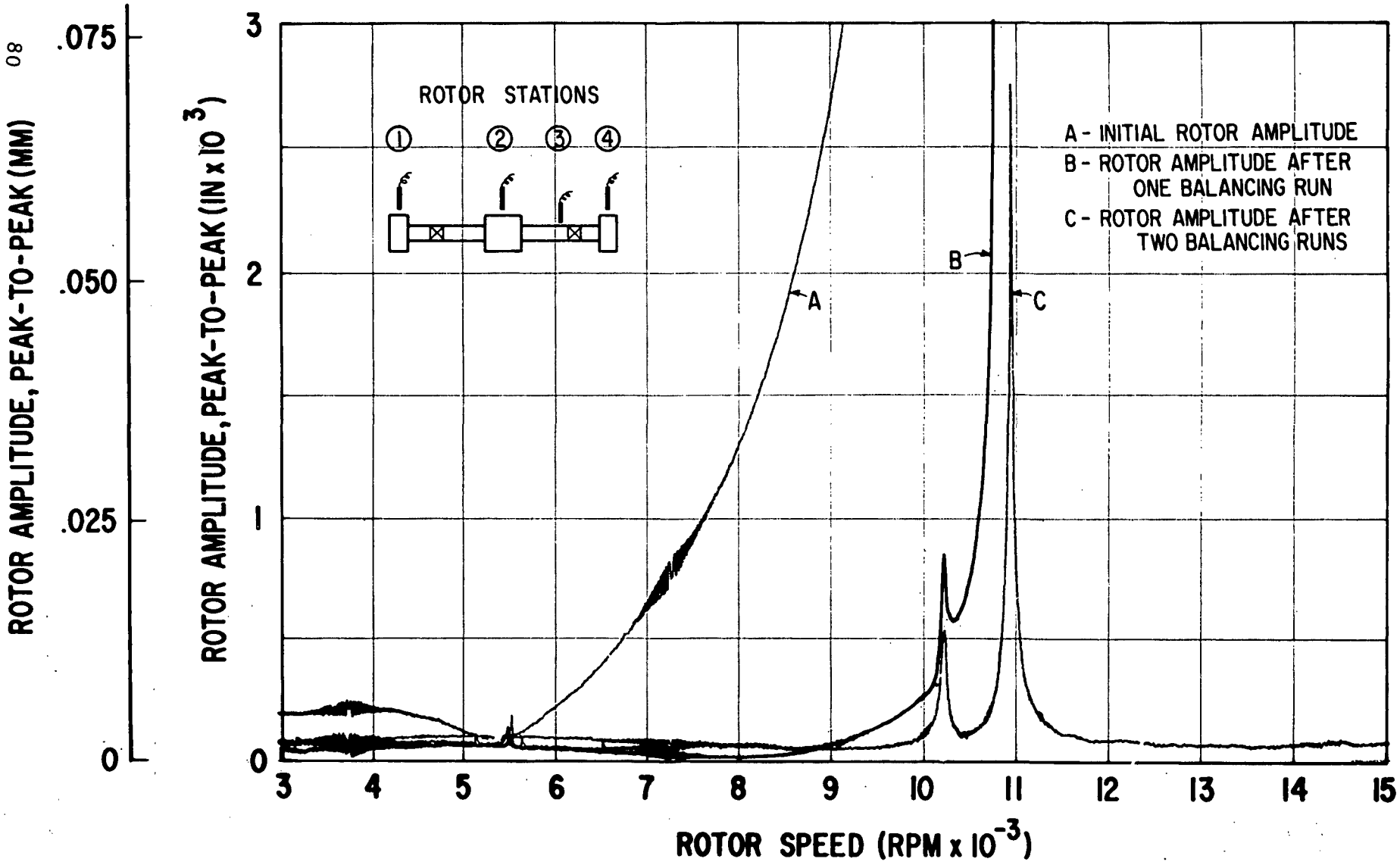

Fig. 35 Vertical Rotor Amplitude at Station 4 — Initial Condition (In-Line, Out-Of-Phase Unbalance) and After Two Consecutive Balancing Runs by the Least Squares Procedure

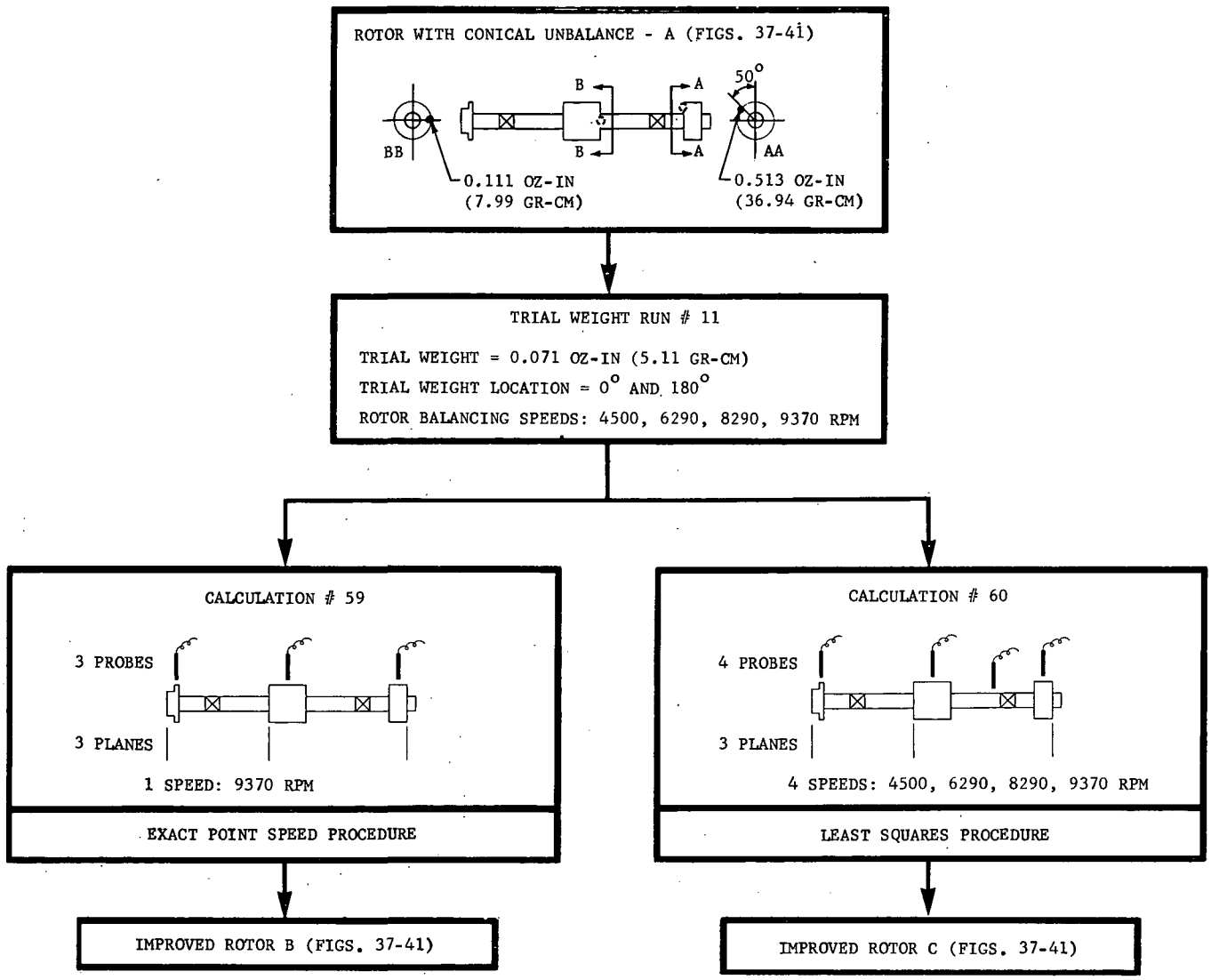

Fig. 36 Fourth Test Case: Two-Mass Rotor With Conical Unbalance

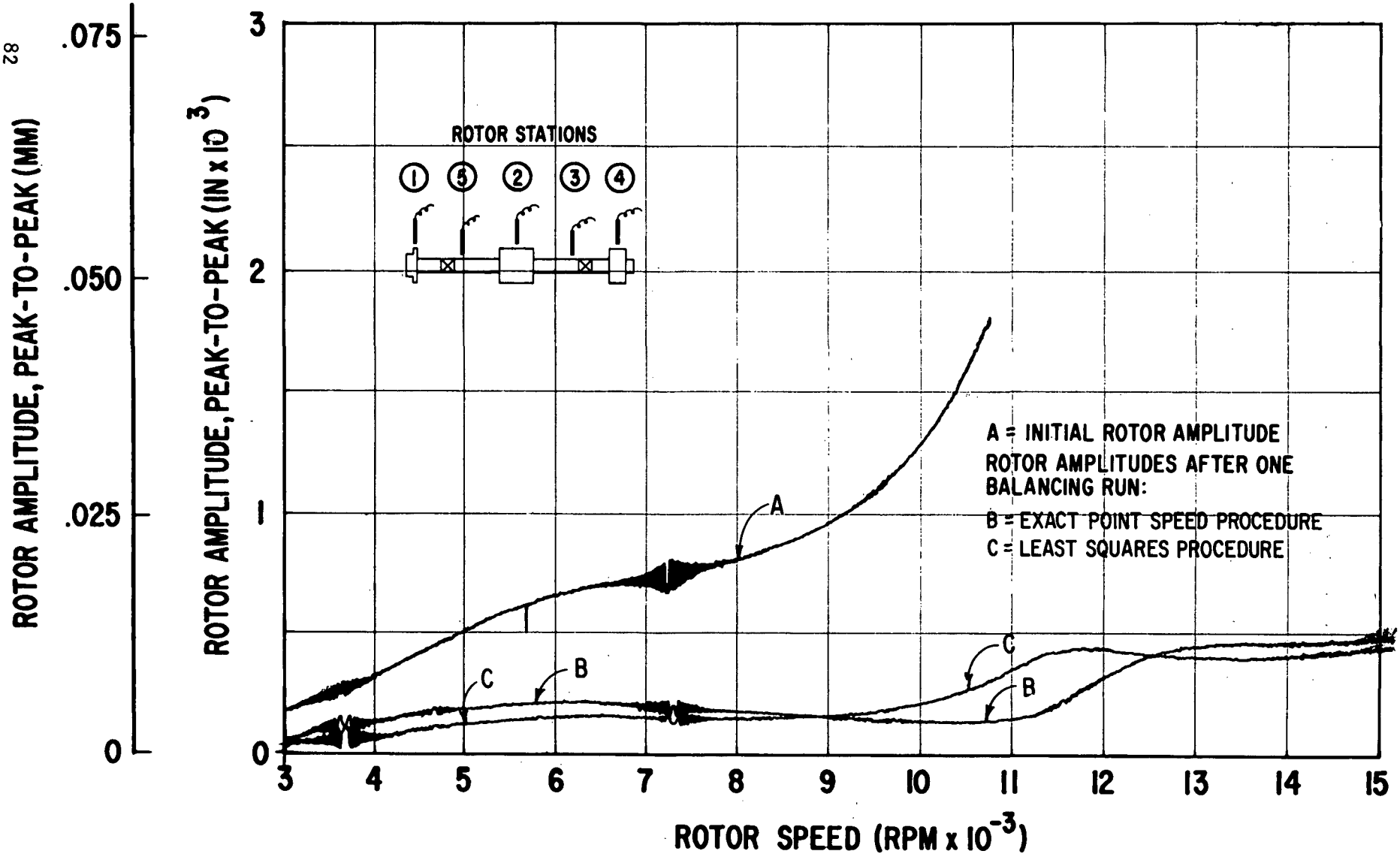

Fig. 37 Vertical Rotor Amplitudes at Station 1 — Initial Condition of Two-Mass Rotor (Conical Unbalance) and After One Balancing Run Each by the Exact Point-Speed and the Least Squares Procedures

MTI-13649

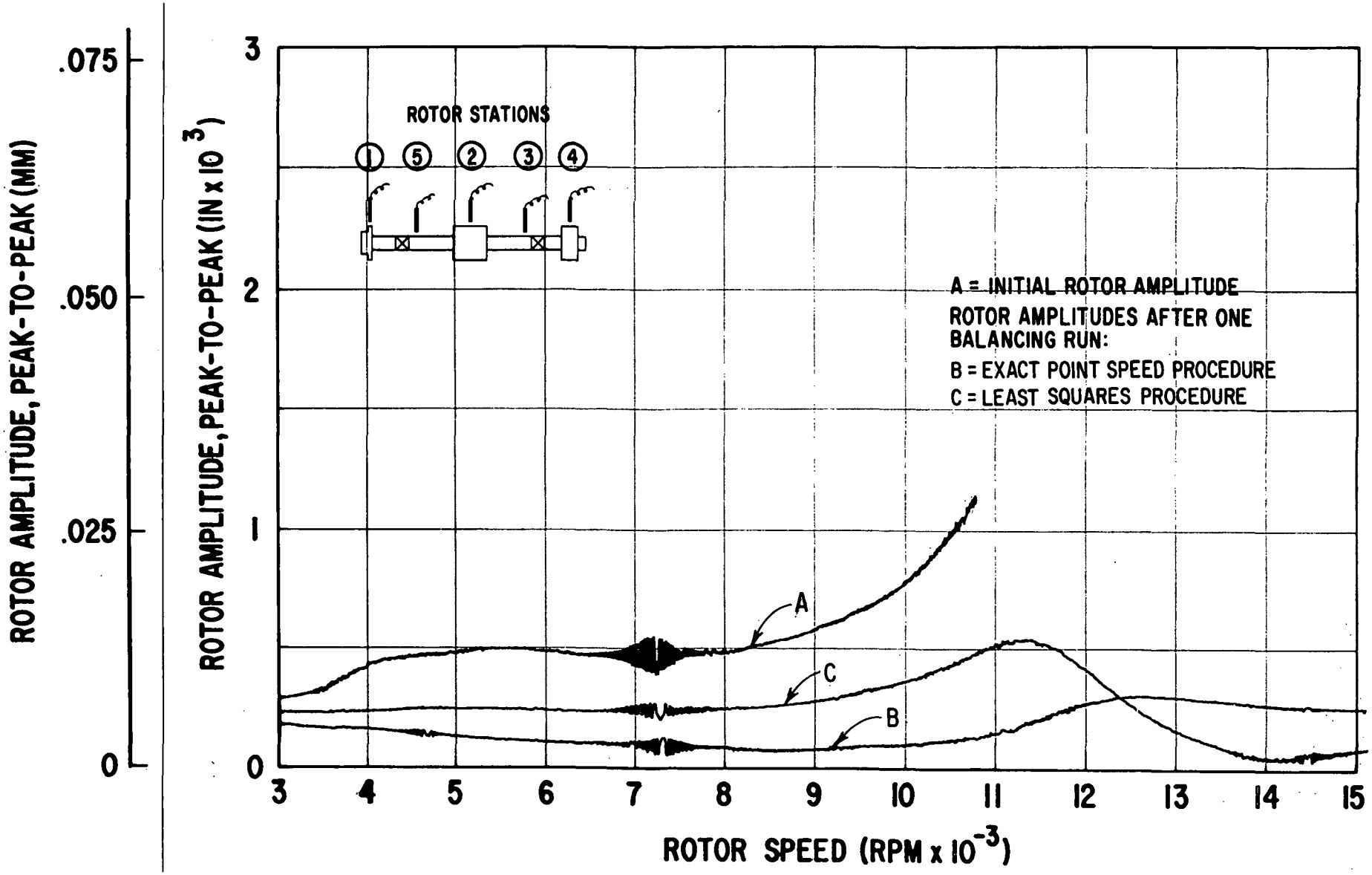

Fig. 38 Vertical Rotor Amplitudes at Station 2 — Initial Condition of Two-Mass Rotor (Conical Unbalance) and After One Balancing Run Each by the Exact Point Speed and the Least Squares Procedures

MTI-13650

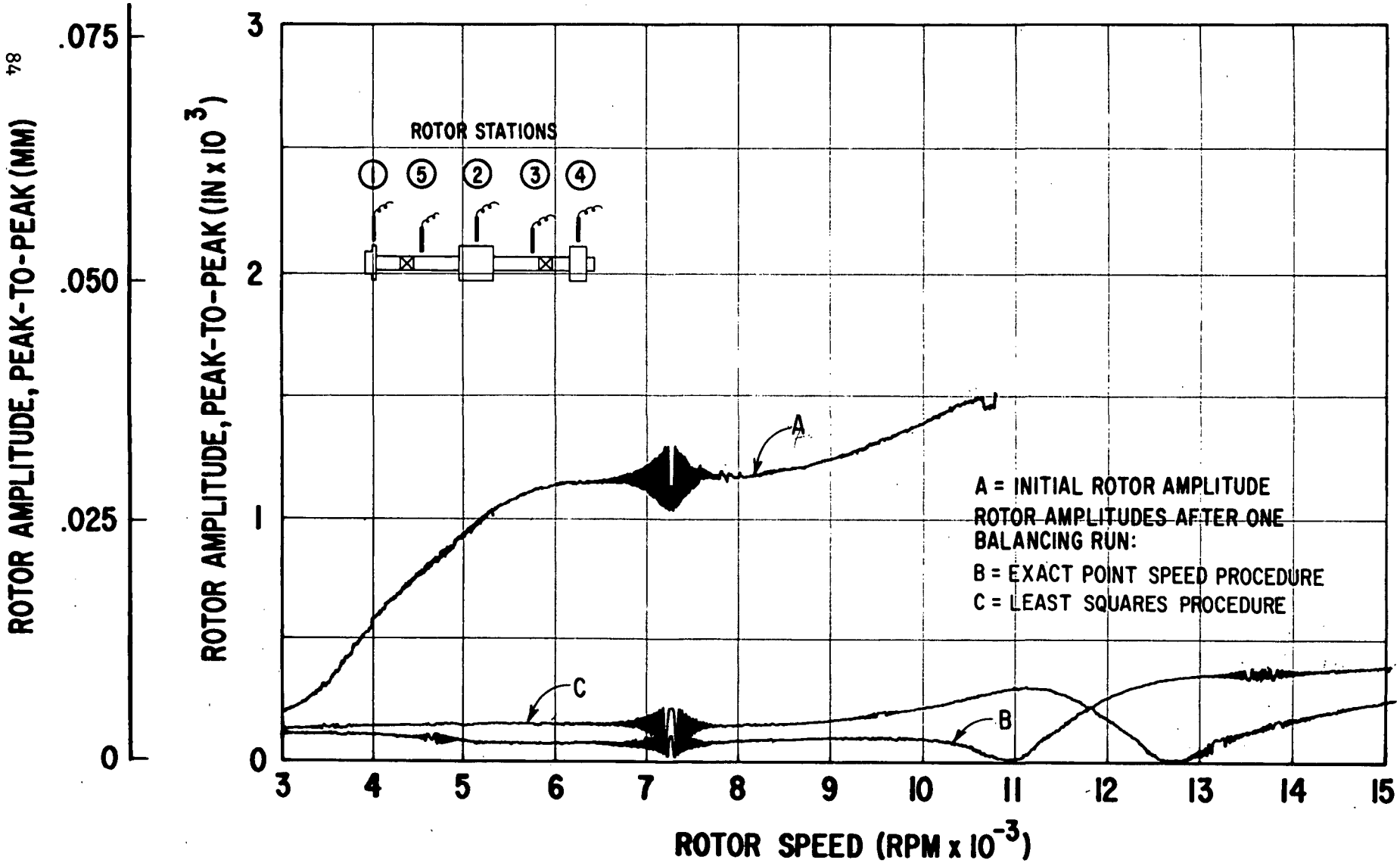

Fig. 39 Vertical Rotor Amplitudes at Station 3 — Initial Condition of Two-Mass Rotor (Conical Unbalance) and After One Balancing Run Each by the Exact Point-Speed and the Least Squares Procedures

MTI-13645

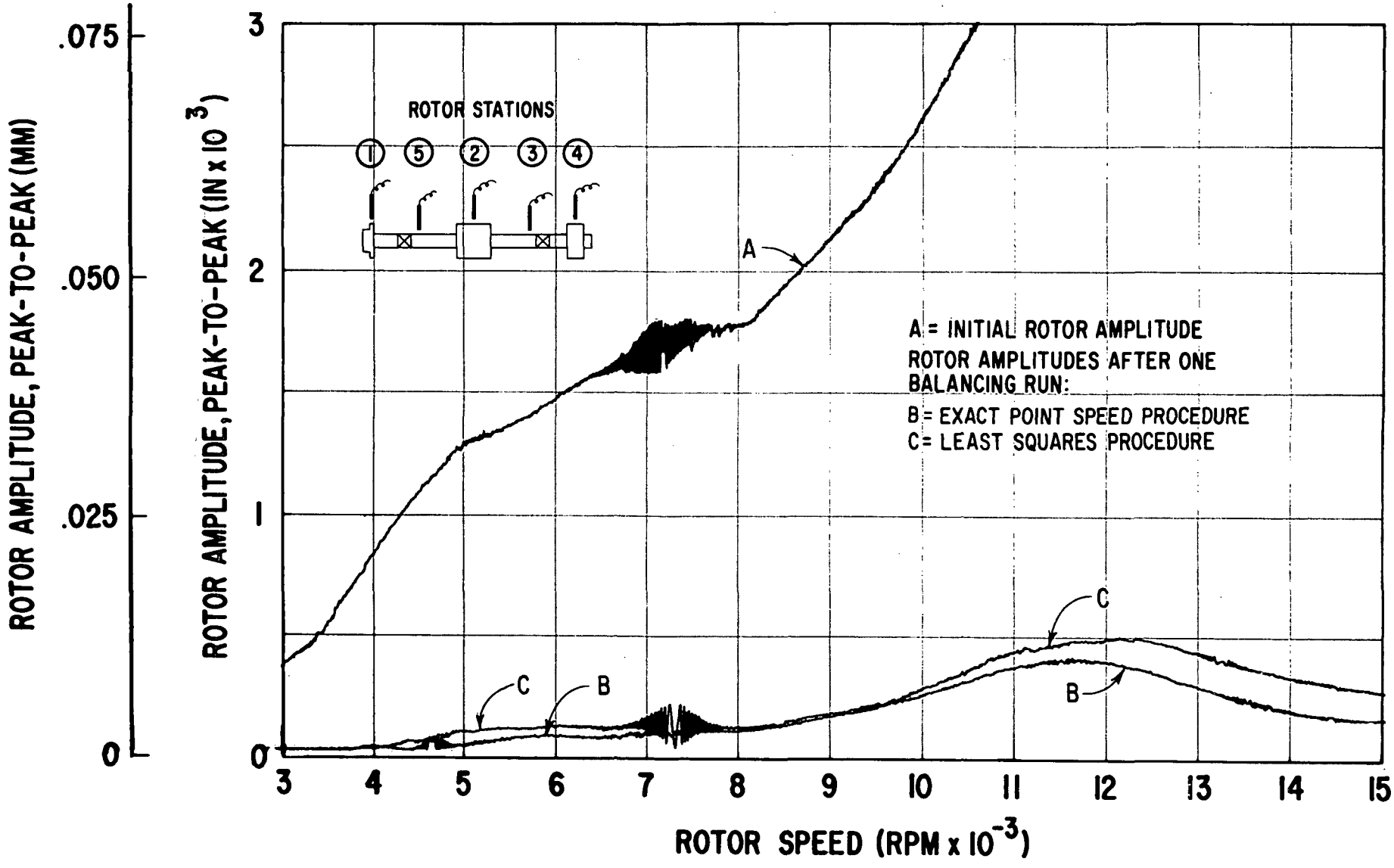

Fig. 40 Vertical Rotor Amplitudes at Station 4 — Initial Condition of Two-Mass Rotor (Conical Unbalance) and After One Balancing Run Each by the Exact Point-Speed and the Least Squares Procedures

MTI-13651

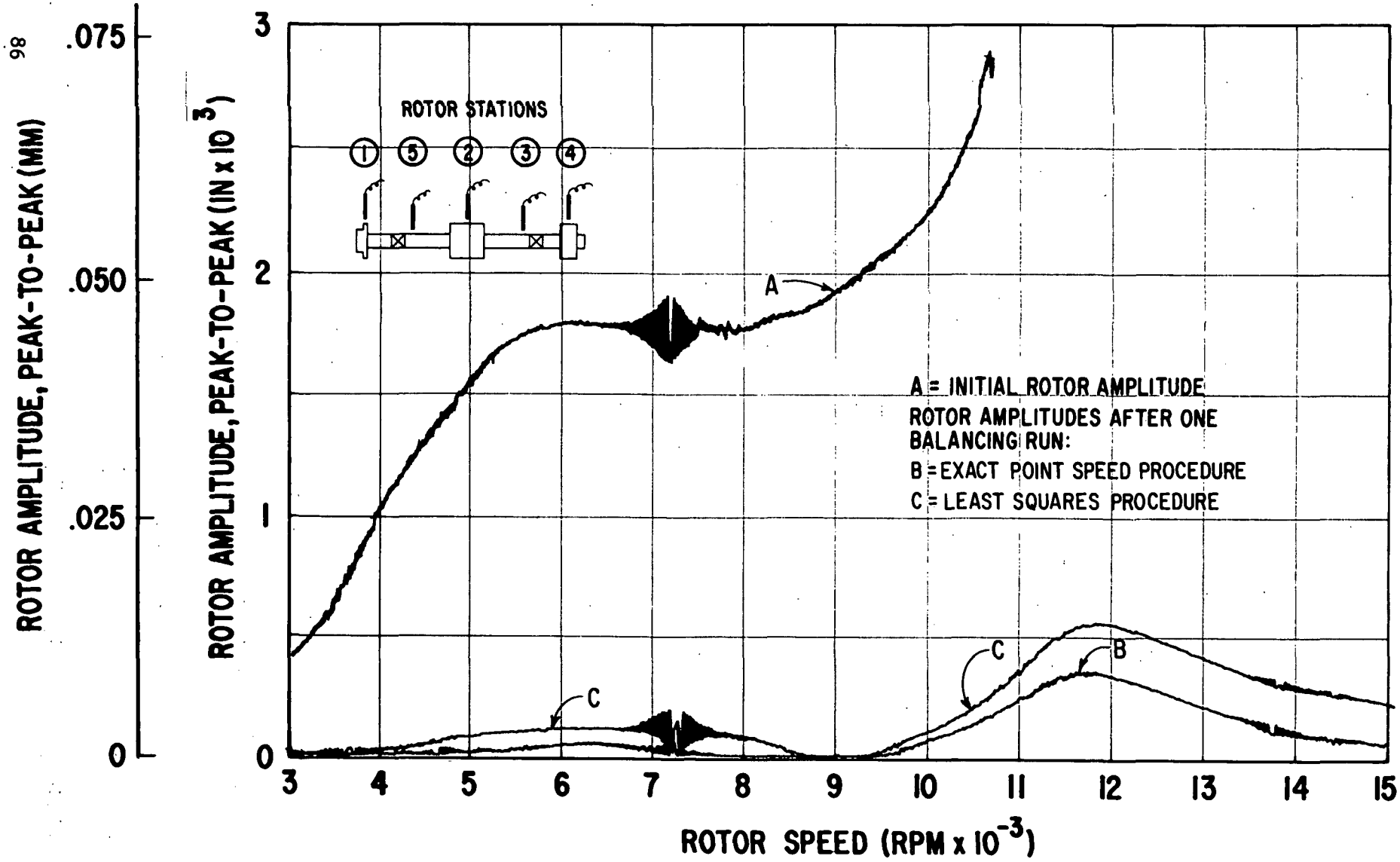

Fig. 41 Horizontal Rotor Amplitudes at Station 4 — Initial Condition of Two-Mass Rotor (Conical Unbalance) and After One Balancing Run Each by the Exact Point-Speed and the Least Squares Procedures

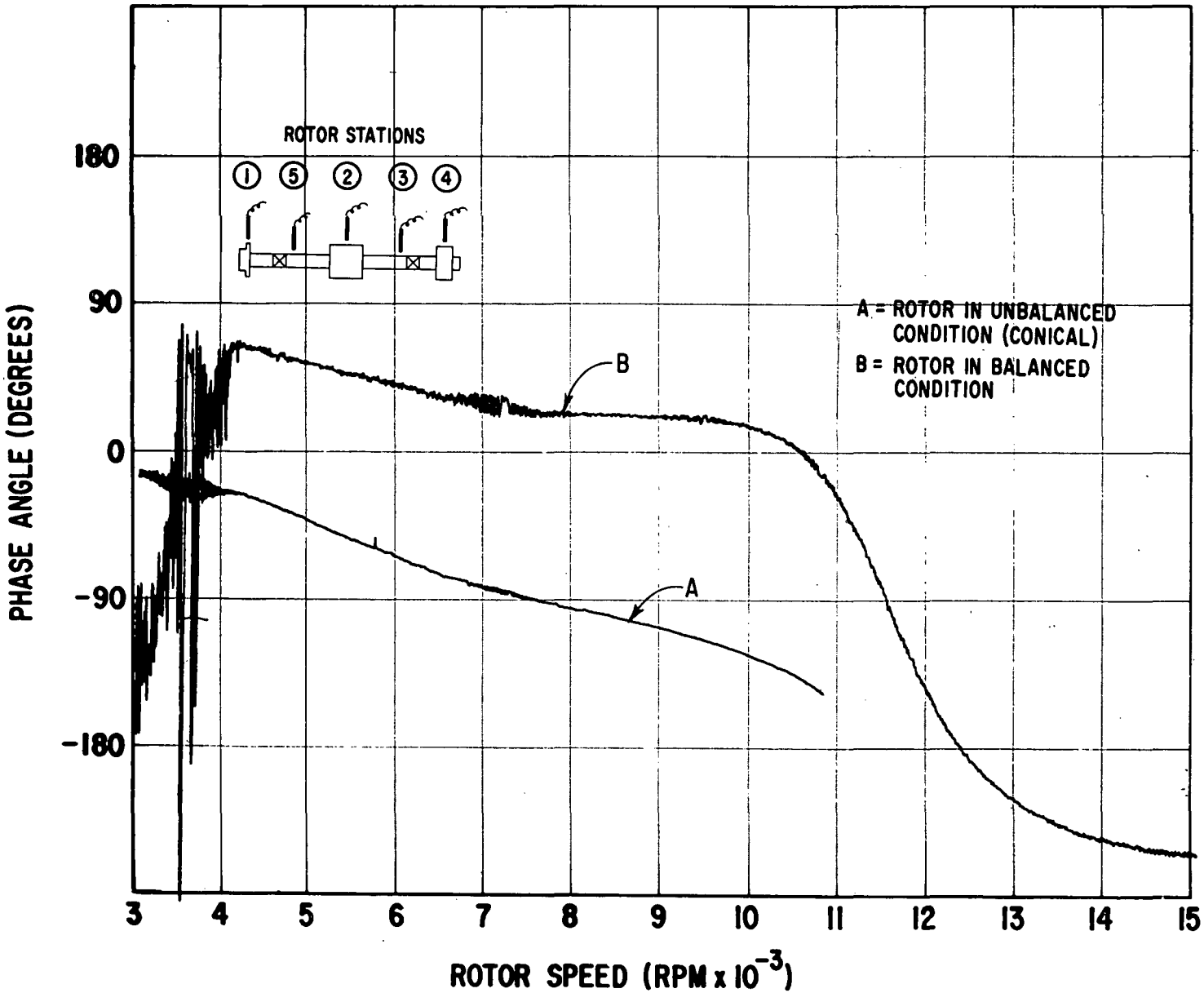

Fig. 42 Phase Angle Between Reference Signal and Vertical Maximum Dynamic Displacement for Two-Mass Rotor at Station 1

MTI-13190

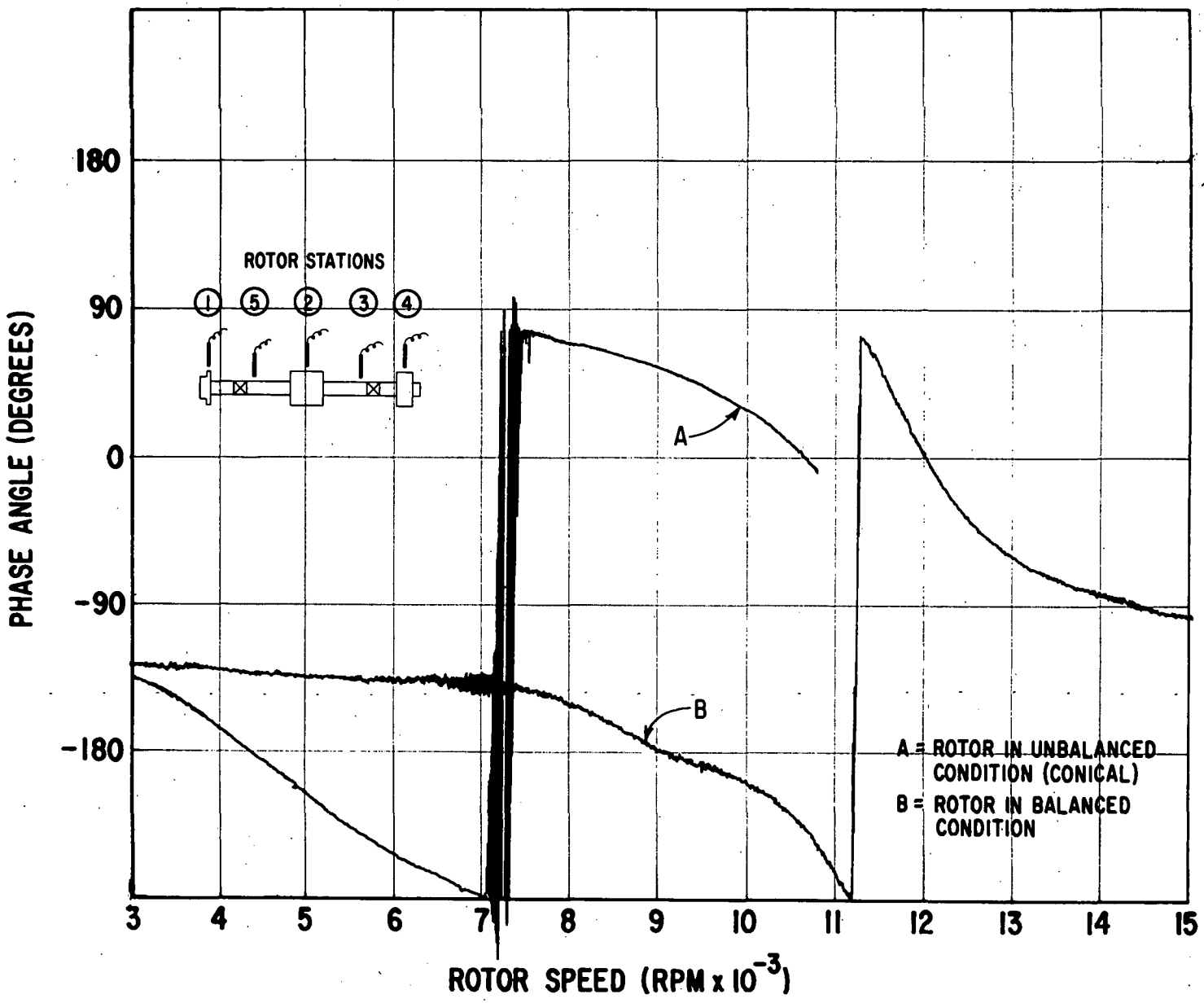

Fig. 43 Phase Angle Between Reference Signal and Vertical Maximum Dynamic Displacement for Two-Mass Rotor at Station 2

MTI-13191

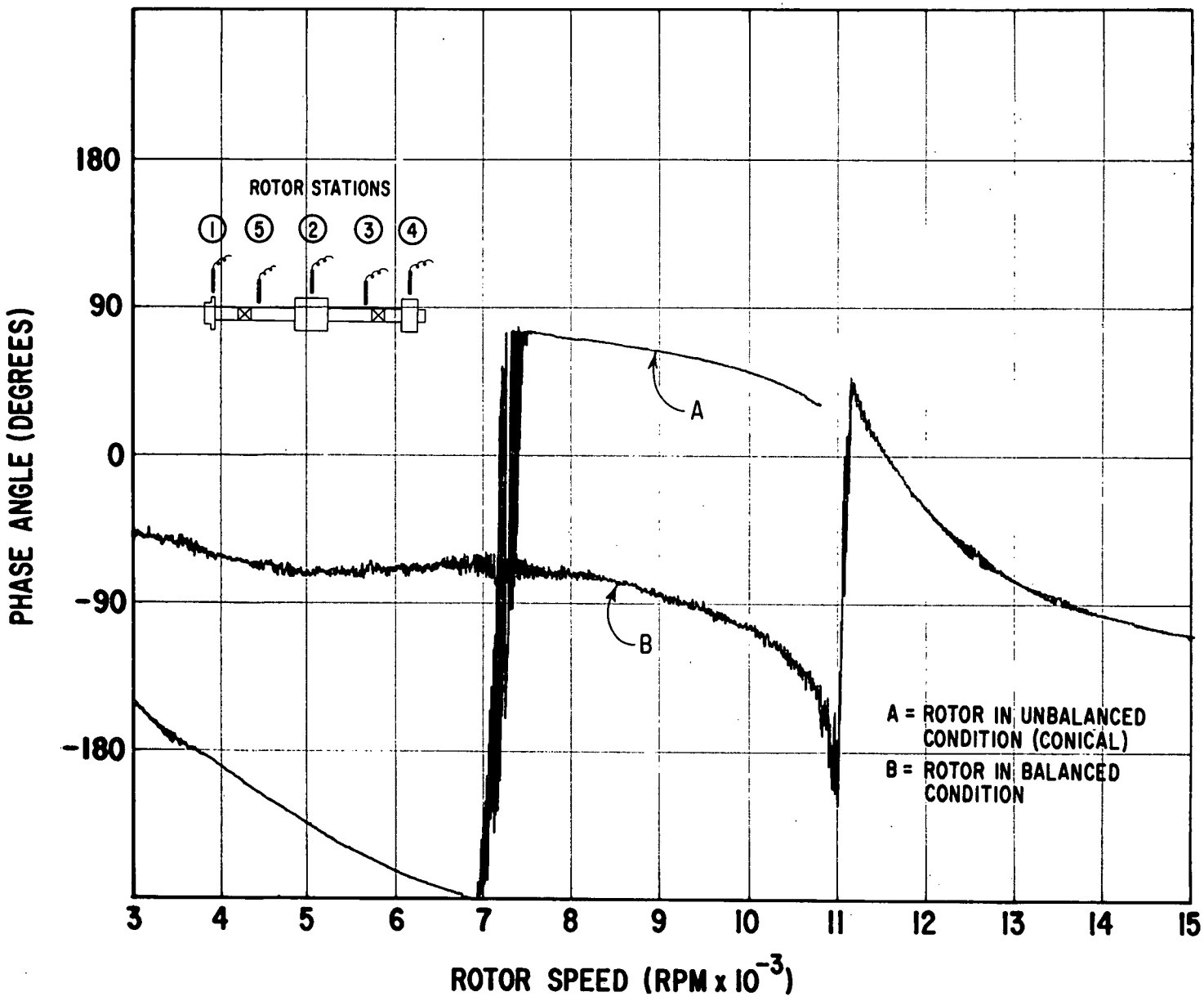

Fig. 44 Phase Angle Between Reference Signal and Vertical Maximum Dynamic Displacement for Two-Mass Rotor at Station 3

MTI-13192.

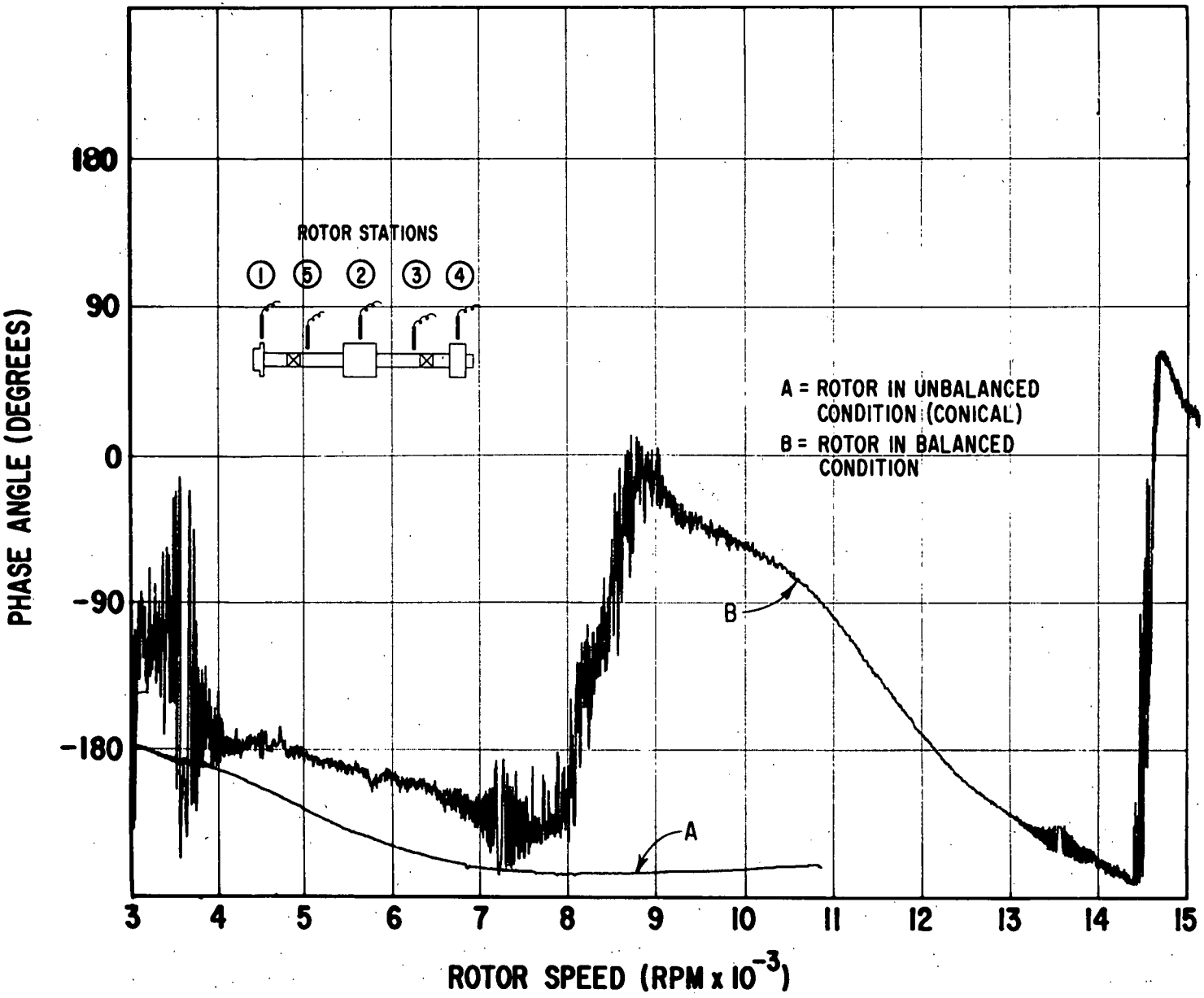

Fig. 45 Phase Angle Between Reference Signal and Vertical Maximum Dynamic Displacement for Two-Mass Rotor at Station 4

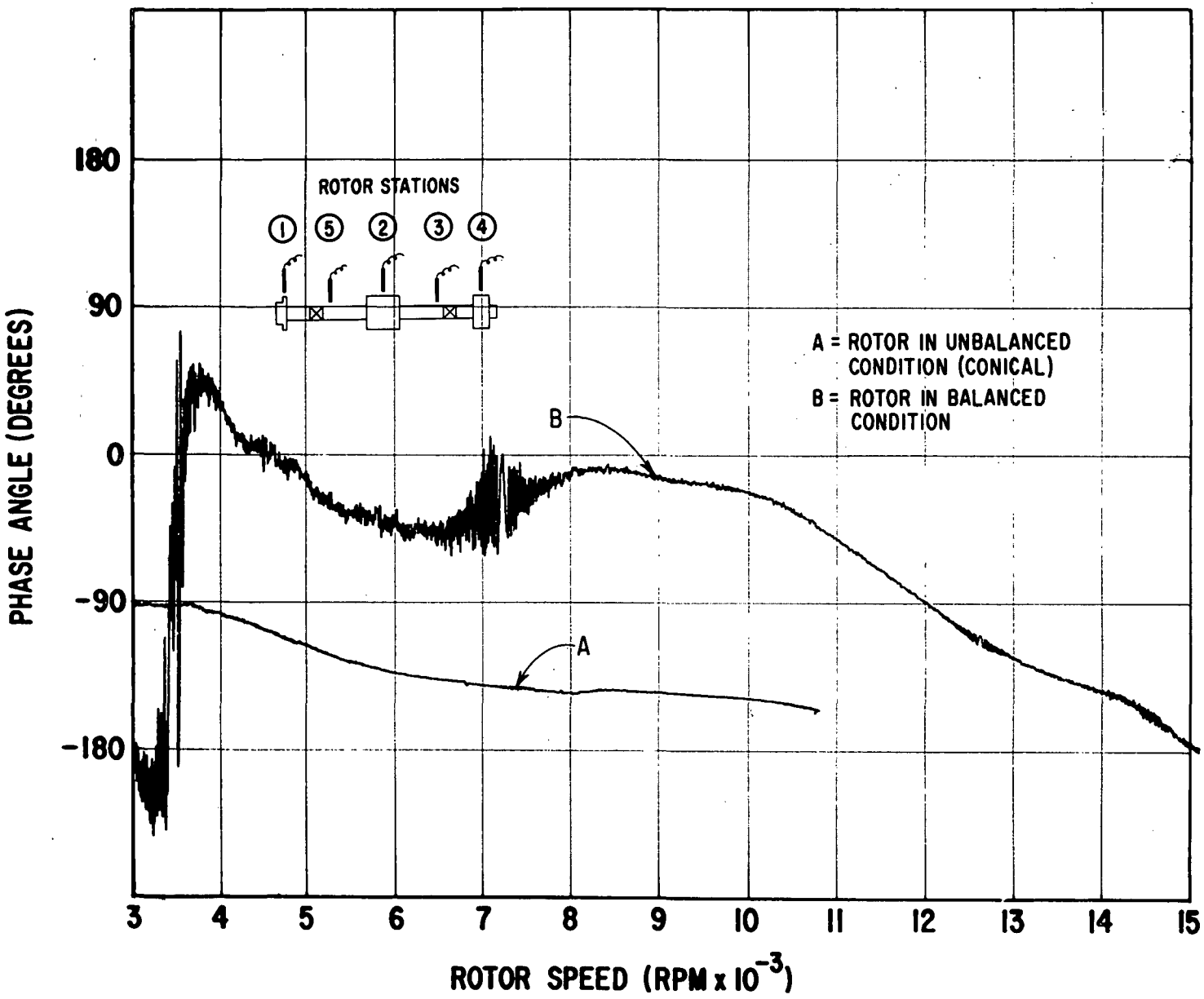

Fig. 46 Phase Angle Between Reference Signal and Horizontal Maximum Dynamic Displacement for Two-Mass Rotor at Station 4

MTI-13194

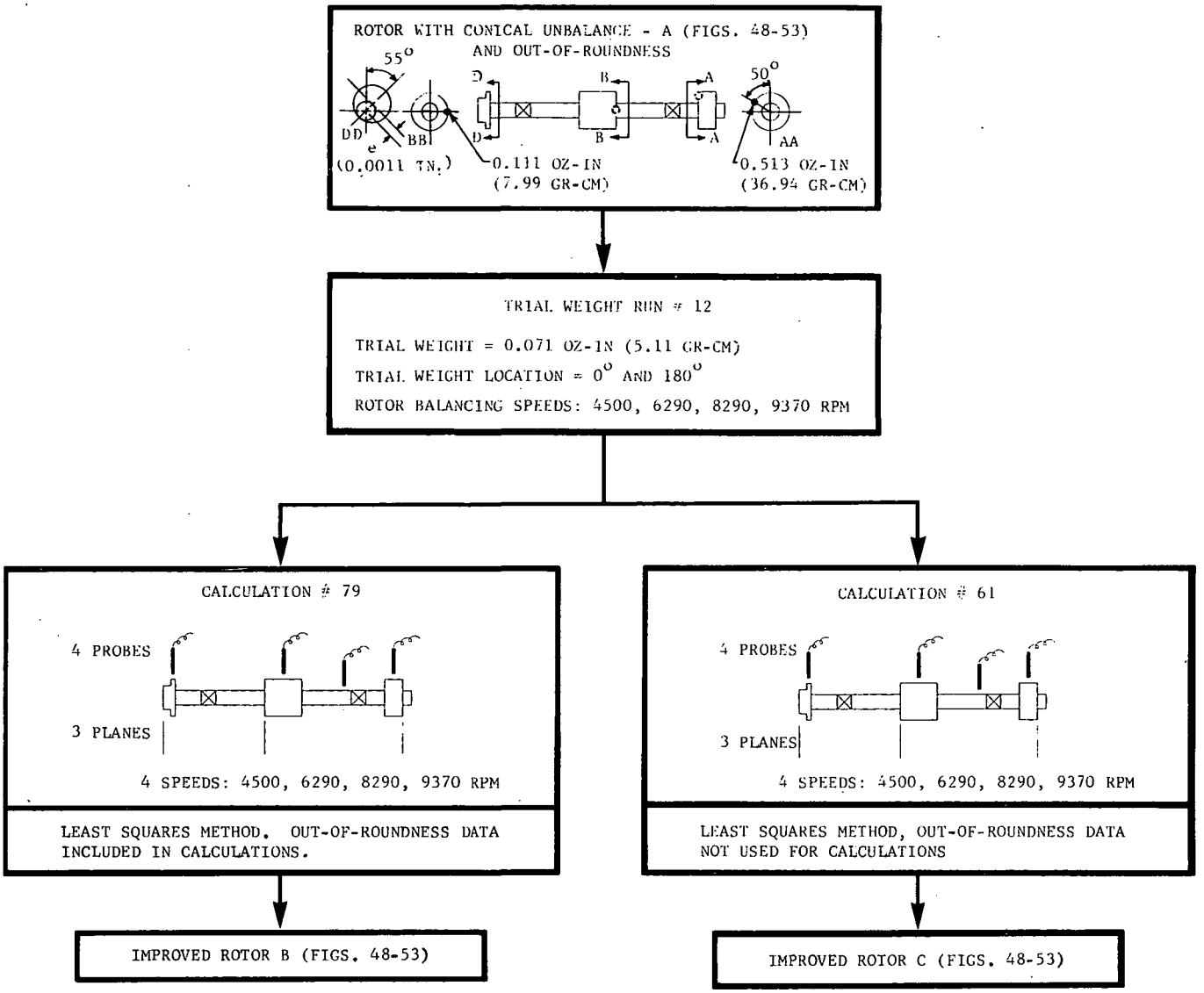

Fig. 47 Two-Mass Rotor With Conical Unbalance - With and Without Out-of-Roundness Data Included in Least Squares Balancing Calculations

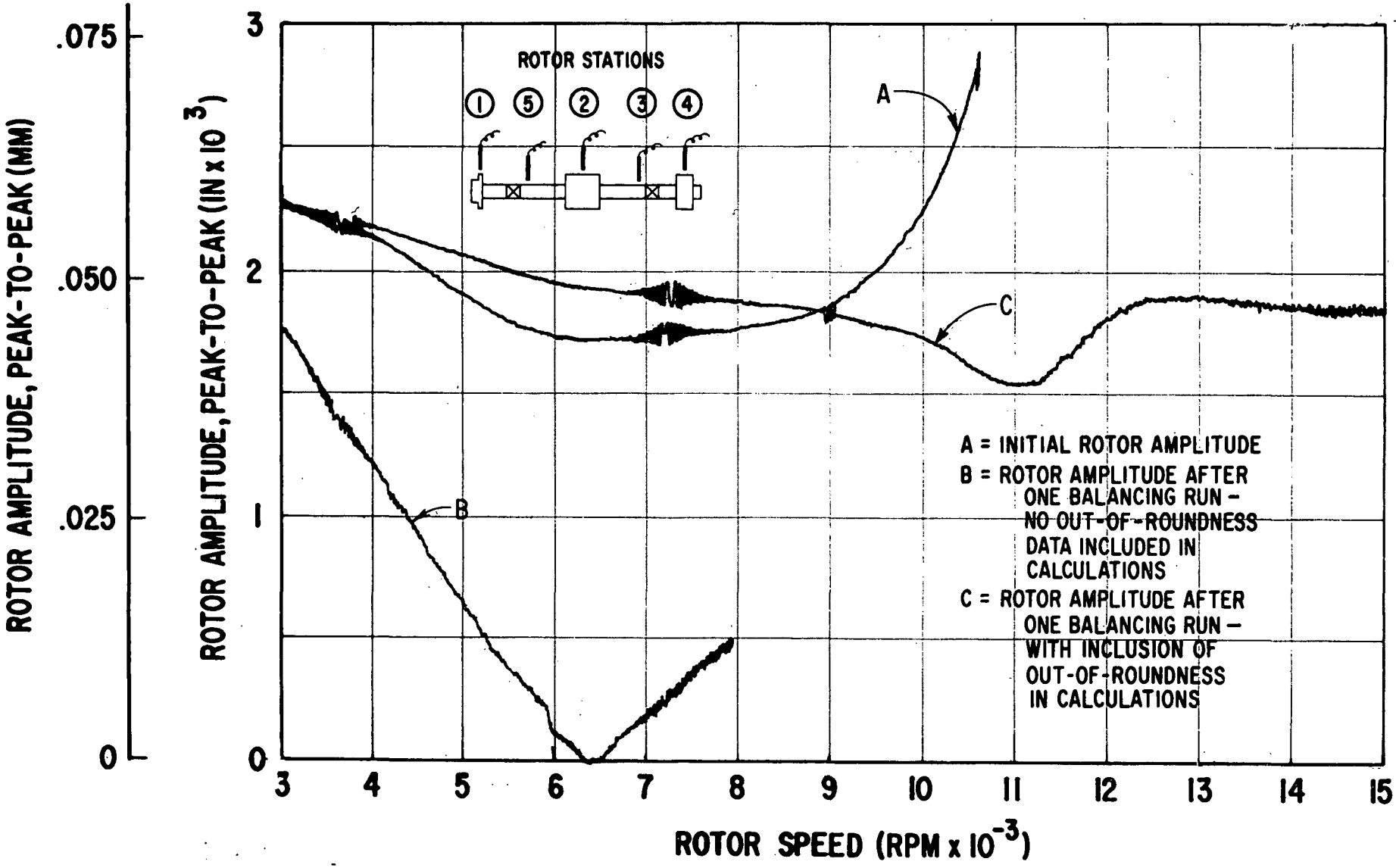

Fig. 48 Vertical Rotor Amplitudes at Station 1 - Initial Condition of Two-Mass Rotor (Conical Unbalance) and After One Balancing Run, With and Without Inclusion of Shaft Out-of-Roundness Data in the Correction Weight Calculations

MTI-13132

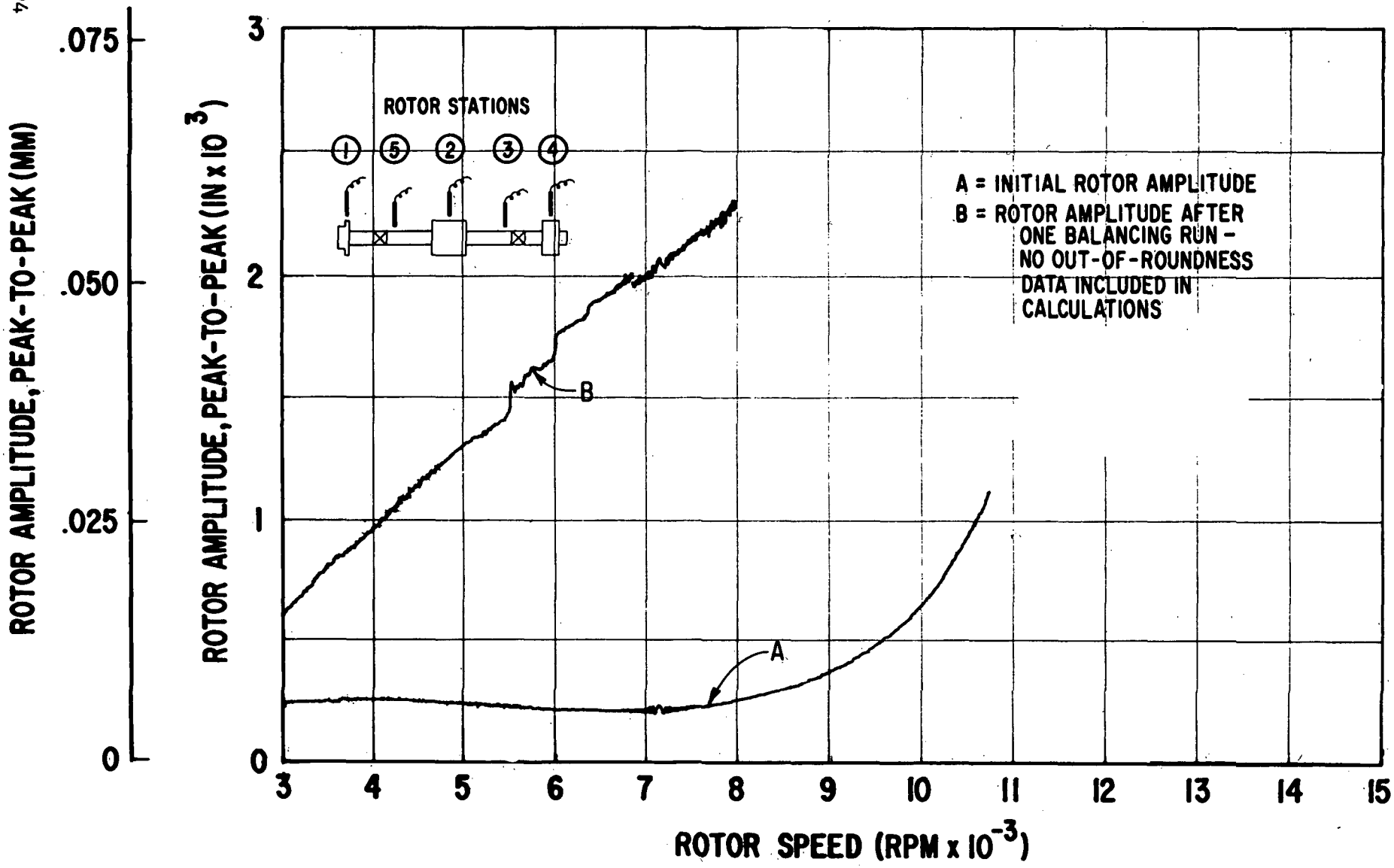

Fig. 49 Vertical Rotor Amplitudes at Station 5 – Initial Condition of Two-Mass Rotor (Conical Unbalance) and After One Balancing Run, Without Inclusion of Shaft Out-Of-Roundness Data in the Correction Weight Calculations

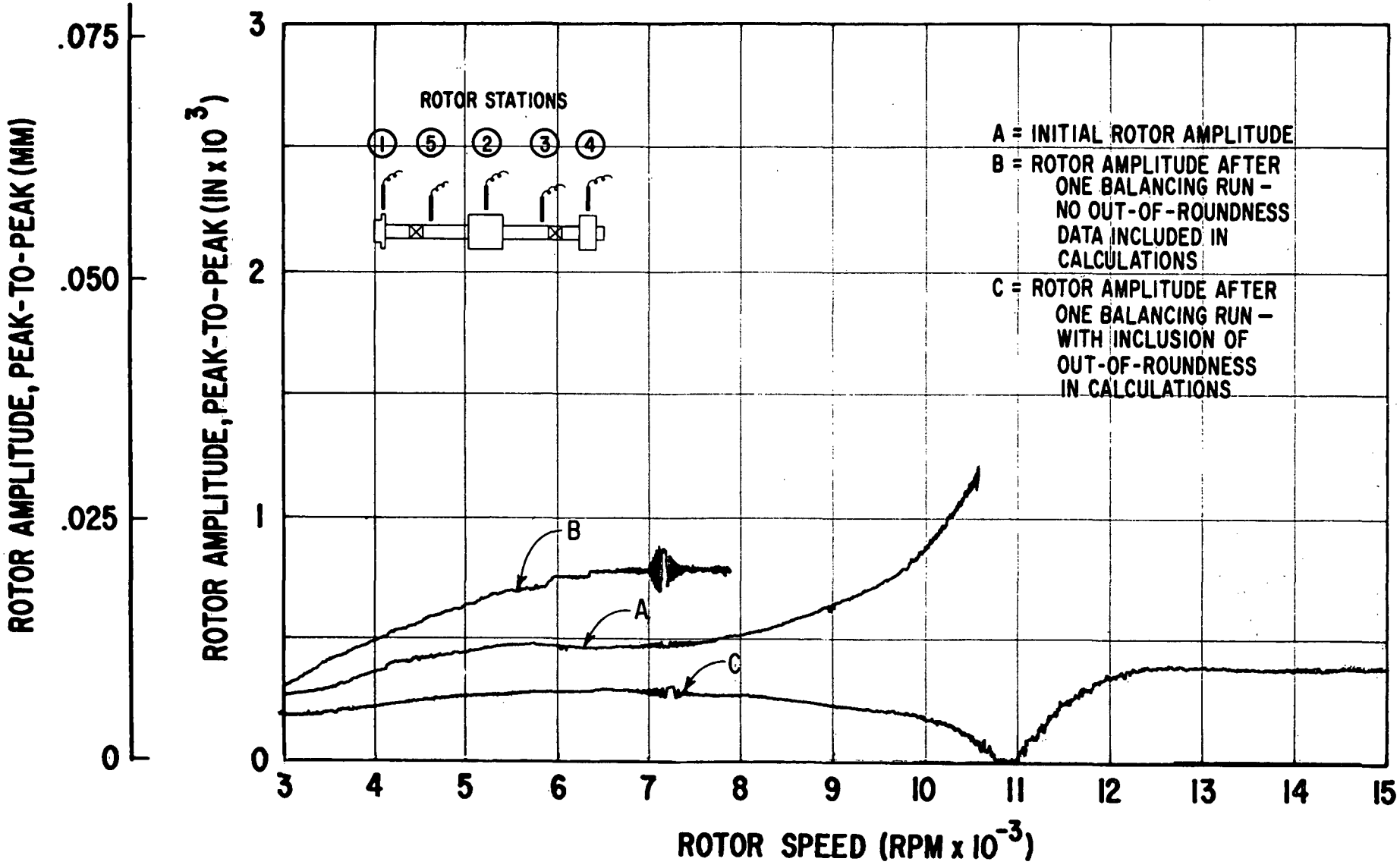

Fig. 50 Vertical Rotor Amplitudes at Station 2 - Initial Condition of Two-Mass Rotor (Conical Unbalance) and After One Balancing Run, With and Without Inclusion of Shaft Out-of-Roundness Data in the Correction Weight Calculations

MTI-13134

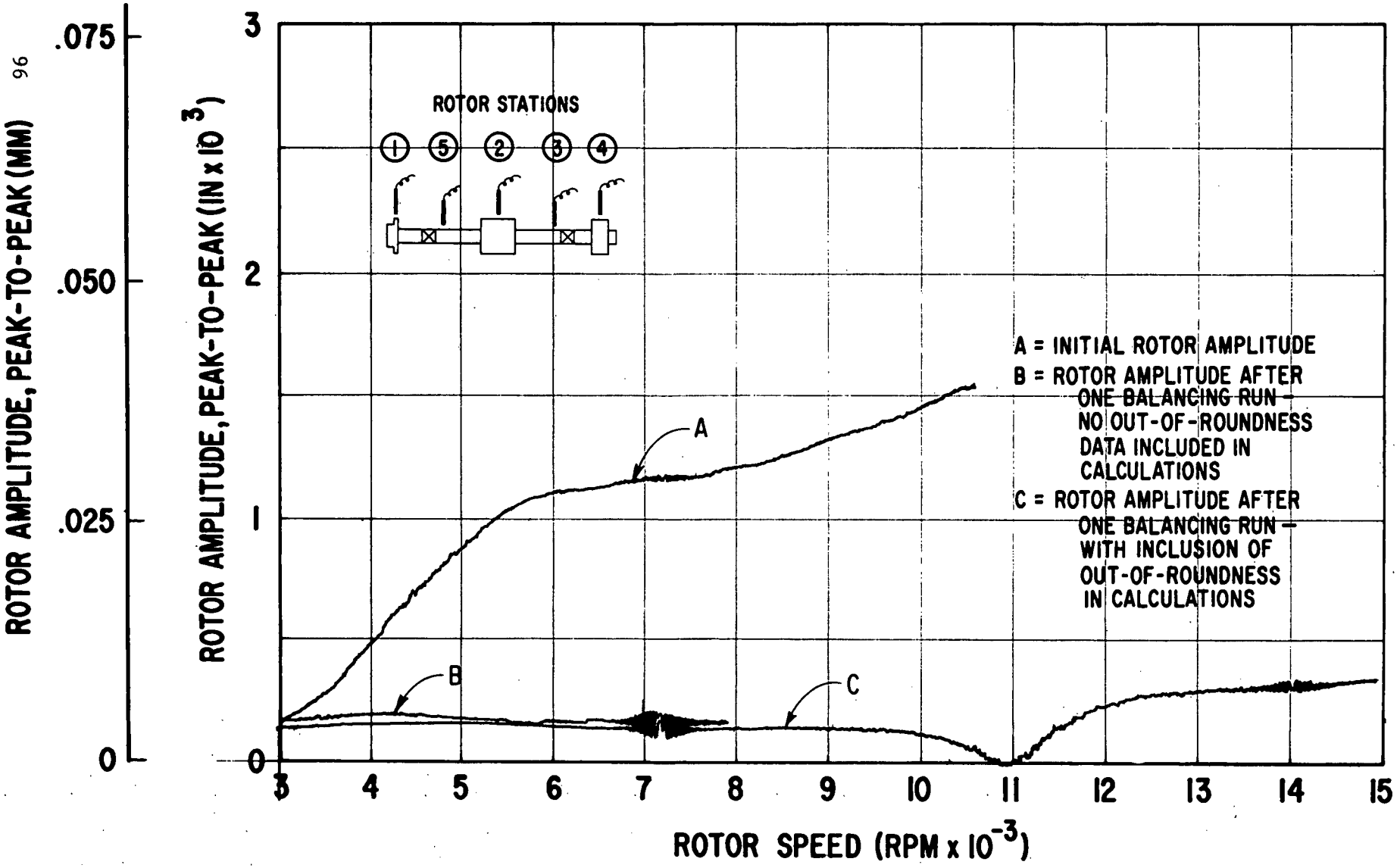

Fig. 51 Vertical Rotor Amplitudes at Station 3 - Initial Condition of Two-Mass Rotor (Conical Unbalance) and After One Balancing Run, With and Without Inclusion of Shaft Out-of-Roundness Data in the Correction Weight Calculations

MTI-13160

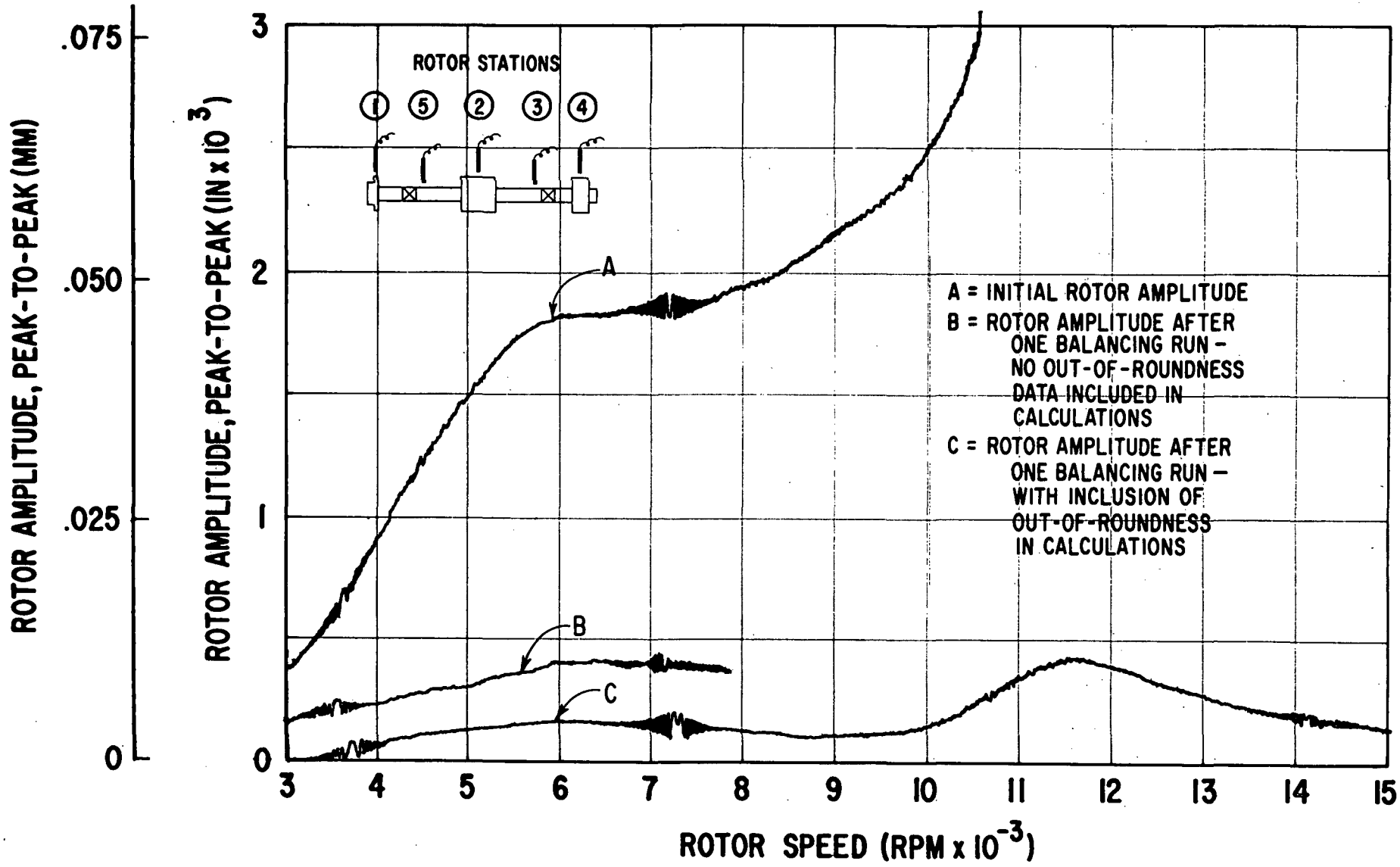

Fig. 52 Vertical Rotor Amplitudes at Station 4 - Initial Condition of Two-Mass Rotor (Conical Unbalance) and After One Balancing Run, With and Without Inclusion of Shaft Out-of-Roundness Data in the Correction Weight Calculations

MTI-13161

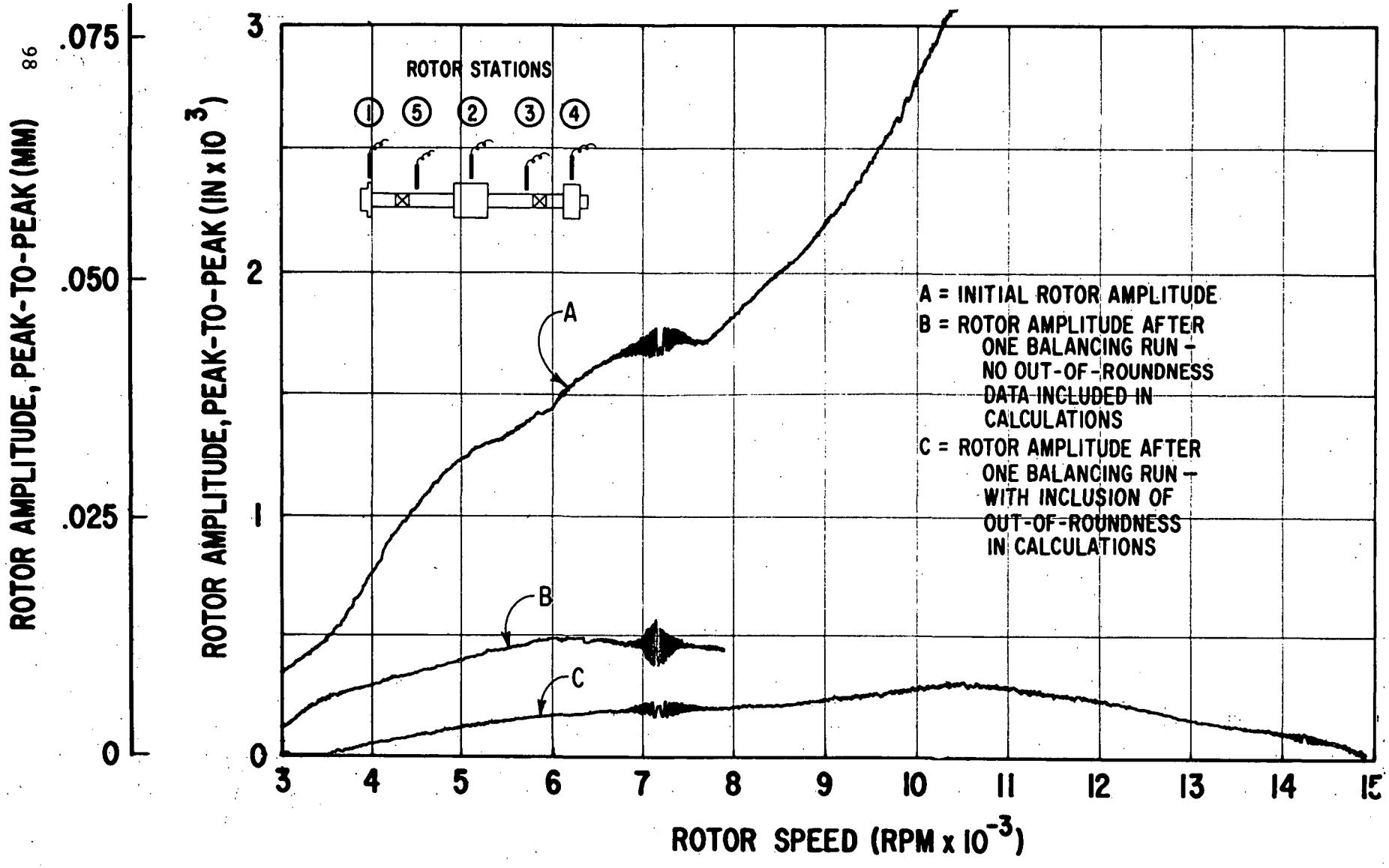

Fig. 53 Horizontal Rotor Amplitudes at Station 4 - Initial Condition of Two-Mass Rotor (Conical Unbalance) and After One Balancing Run, With and Without Inclusion of Shaft Out-of-Roundness Data in the Correction Weight Calculations

MTI-13162

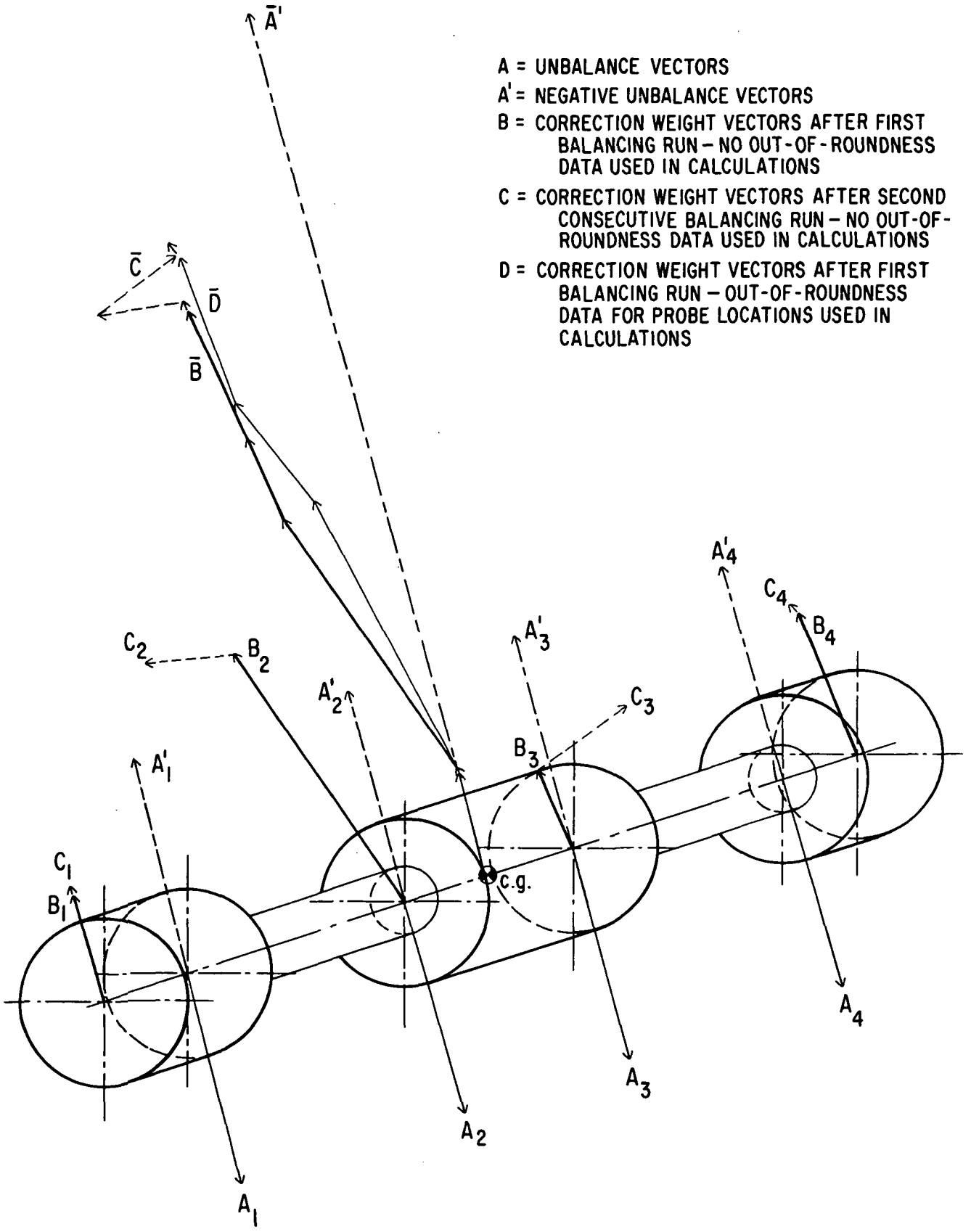

Fig. 54 Unbalance Vectors and Correction Weight Vectors For Test Rotor With In-Line, In-Phase Unbalance Condition (Second Test Case Data)

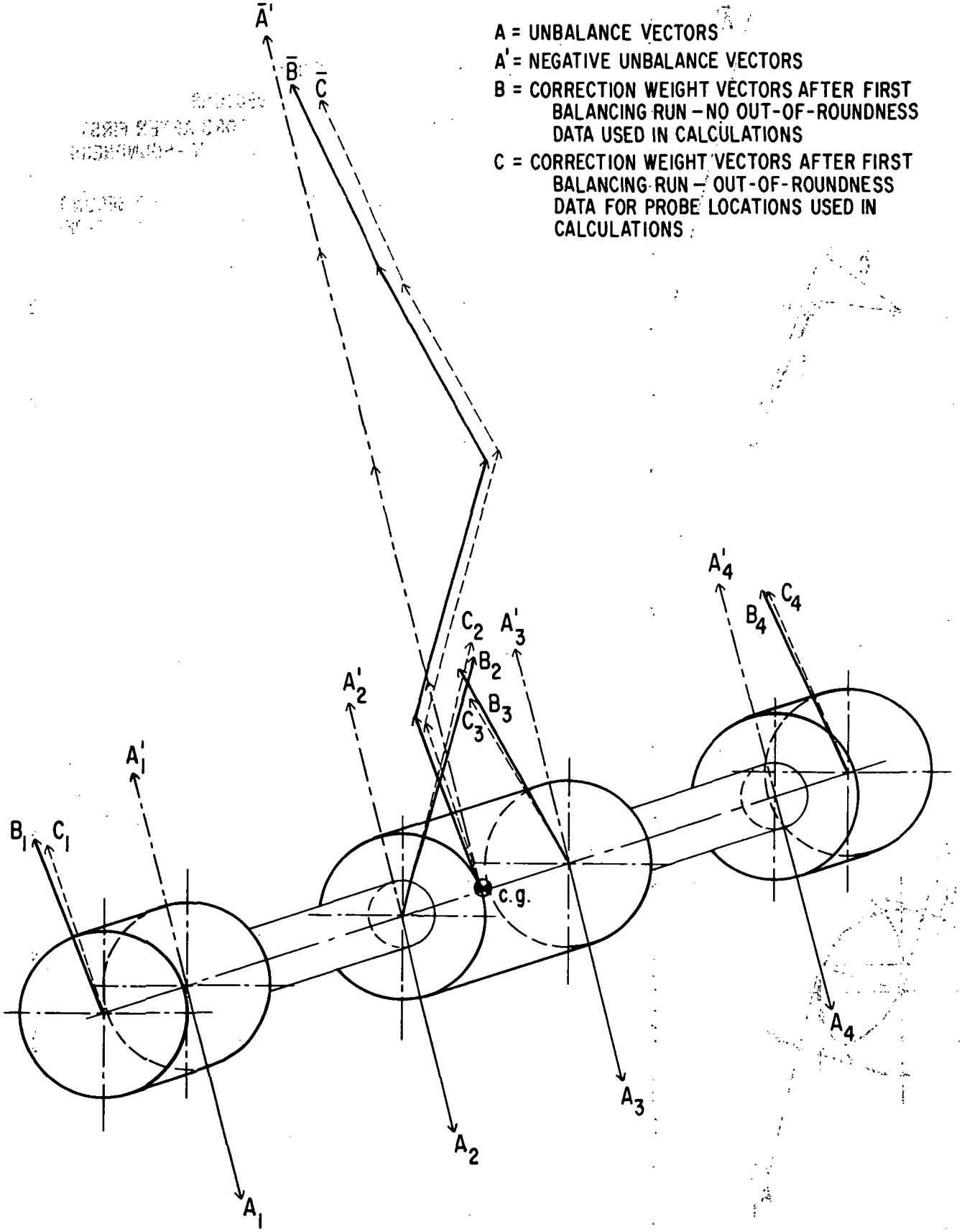

Fig. 55 Unbalance Vectors and Correction Weight Vectors for Test Rotor With In-Line, In-Phase Unbalance Condition

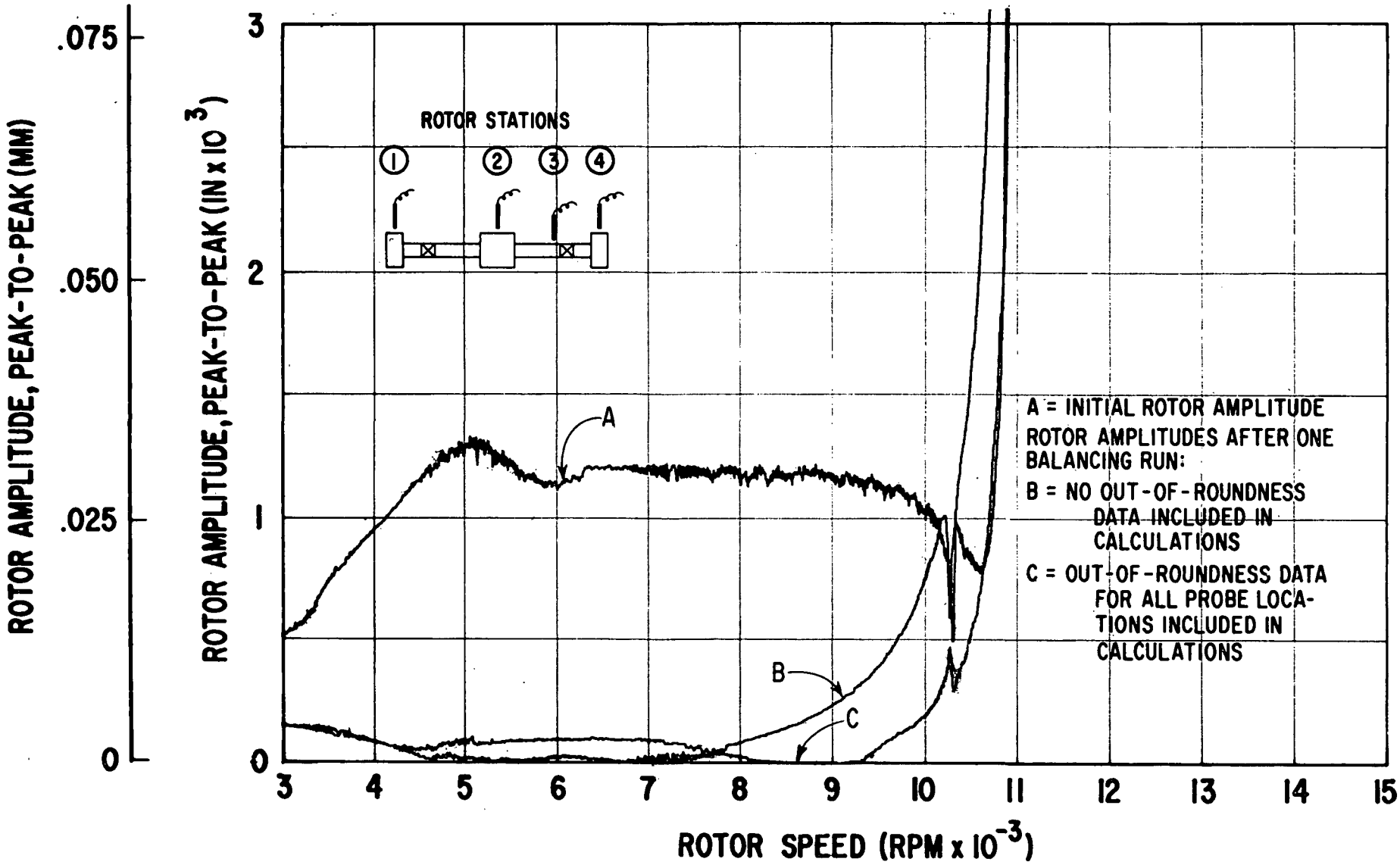

Fig. 56 Vertical Rotor Amplitudes at Station 1 - Initial Condition (In-Line, In-Phase Unbalance) and After One Balancing Run, With and Without Inclusion of Shaft Out-of-Roundness Data in the Correction Weight Calculations

MTI-13195

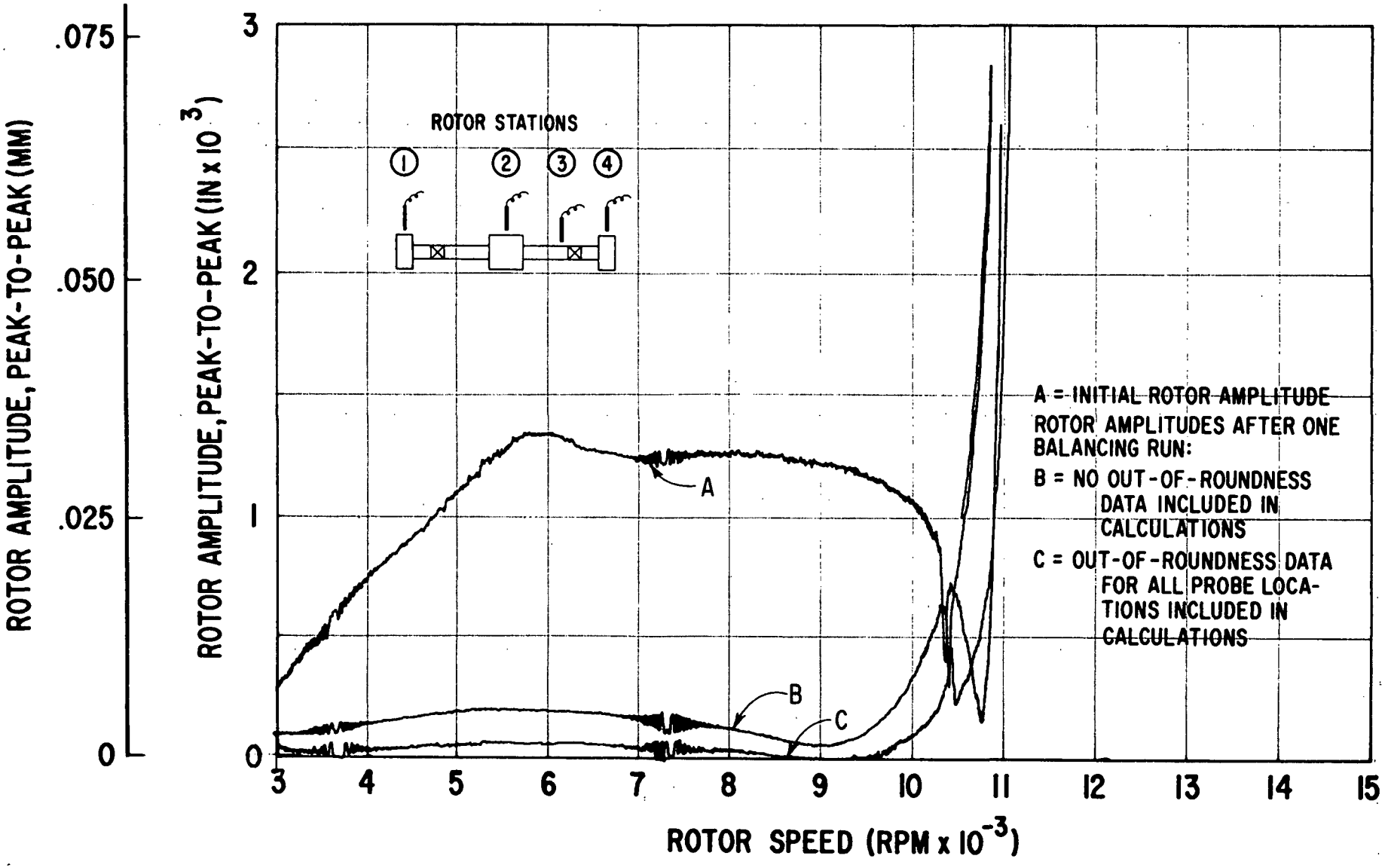

Fig. 57 Vertical Rotor Amplitudes at Station 2 - Initial Condition (In-Line, In-Phase Unbalance) and After One Balancing Run, With and Without Inclusion of Shaft Out-of-Roundness Data in the Correction Weight Calculations

MTI-13196

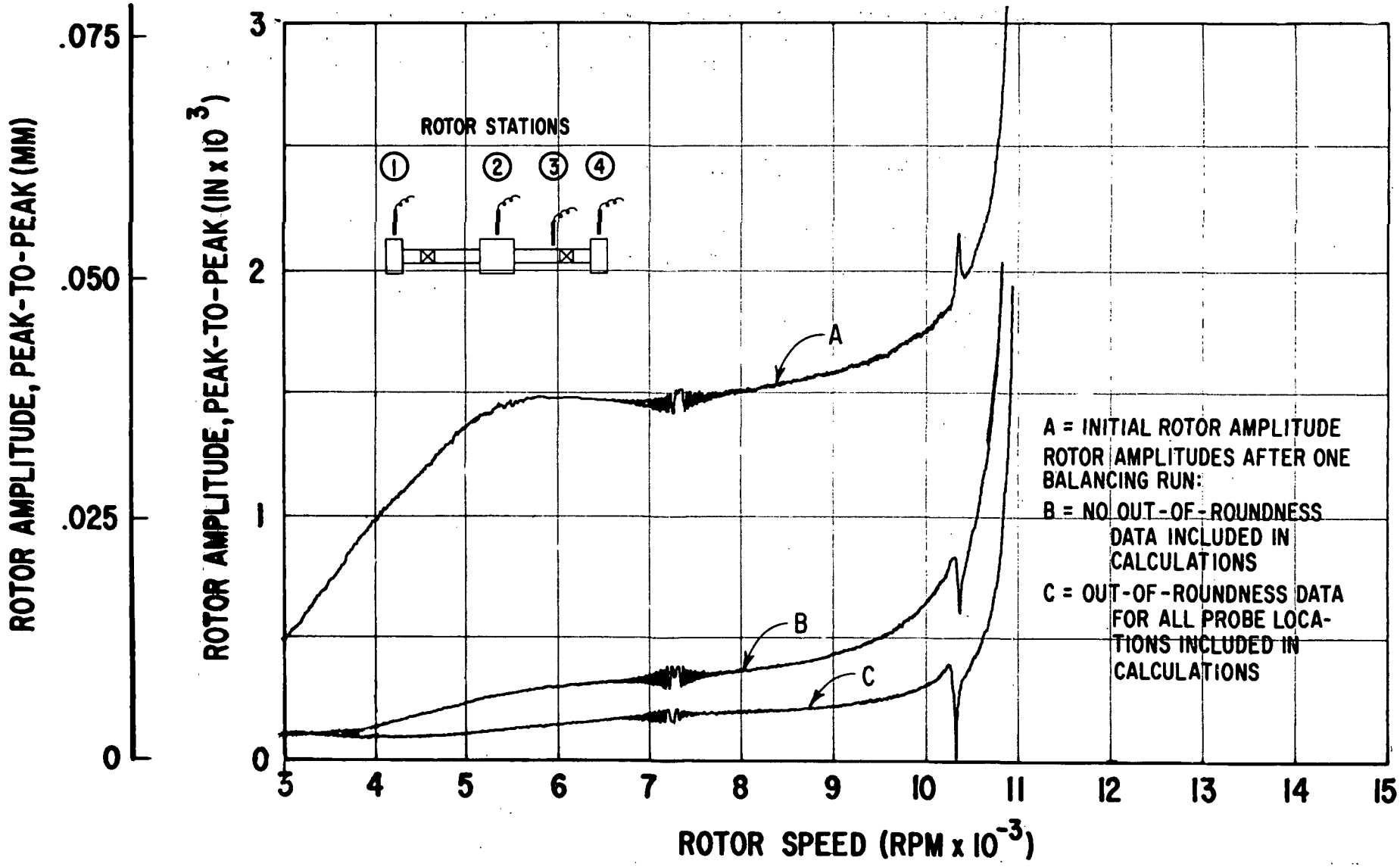

Fig. 58 Vertical Rotor Amplitudes at Station 3 - Initial Condition (In-Line, In-Phase Unbalance) and After One Balancing Run, With and Without Inclusion of Shaft Out-of-Roundness Data in the Correction Weight Calculations

MTI-13197

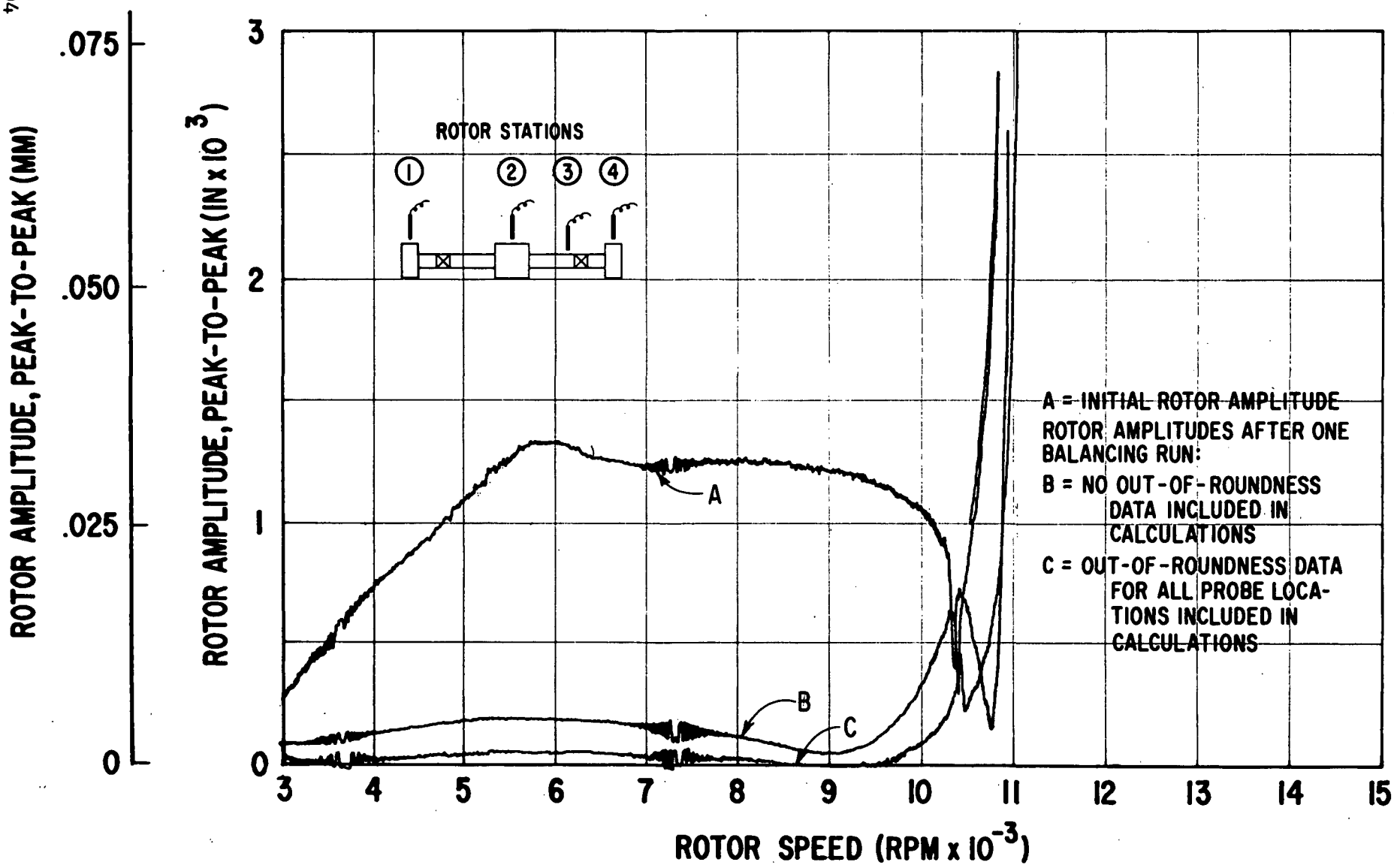

Fig. 59 Vertical Rotor Amplitudes at Station 4 - Initial Condition (In-Line, In-Phase Unbalance) and After One Balancing Run, With and Without Inclusion of Shaft Out-of-Roundness Data in the Correction Weight Calculations

MTI-13198

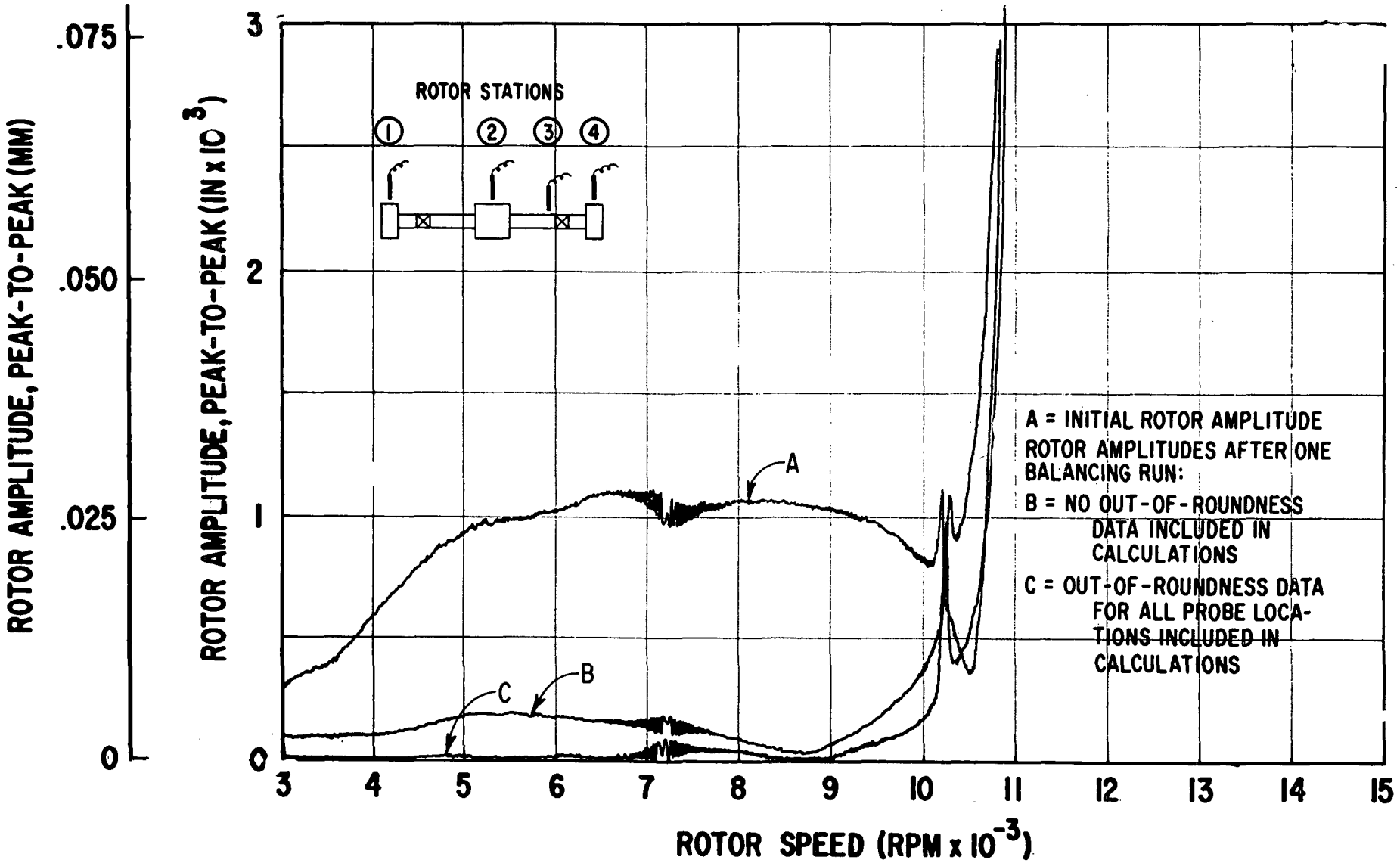

Fig. 60 Horizontal Rotor Amplitudes at Station 4 - Initial Condition (In-Line, In-Phase Unbalance) and After One Balancing Run, With and Without Inclusion of Shaft Out-of-Roundness Data in the Correction Weight Calculations

MTI-13199

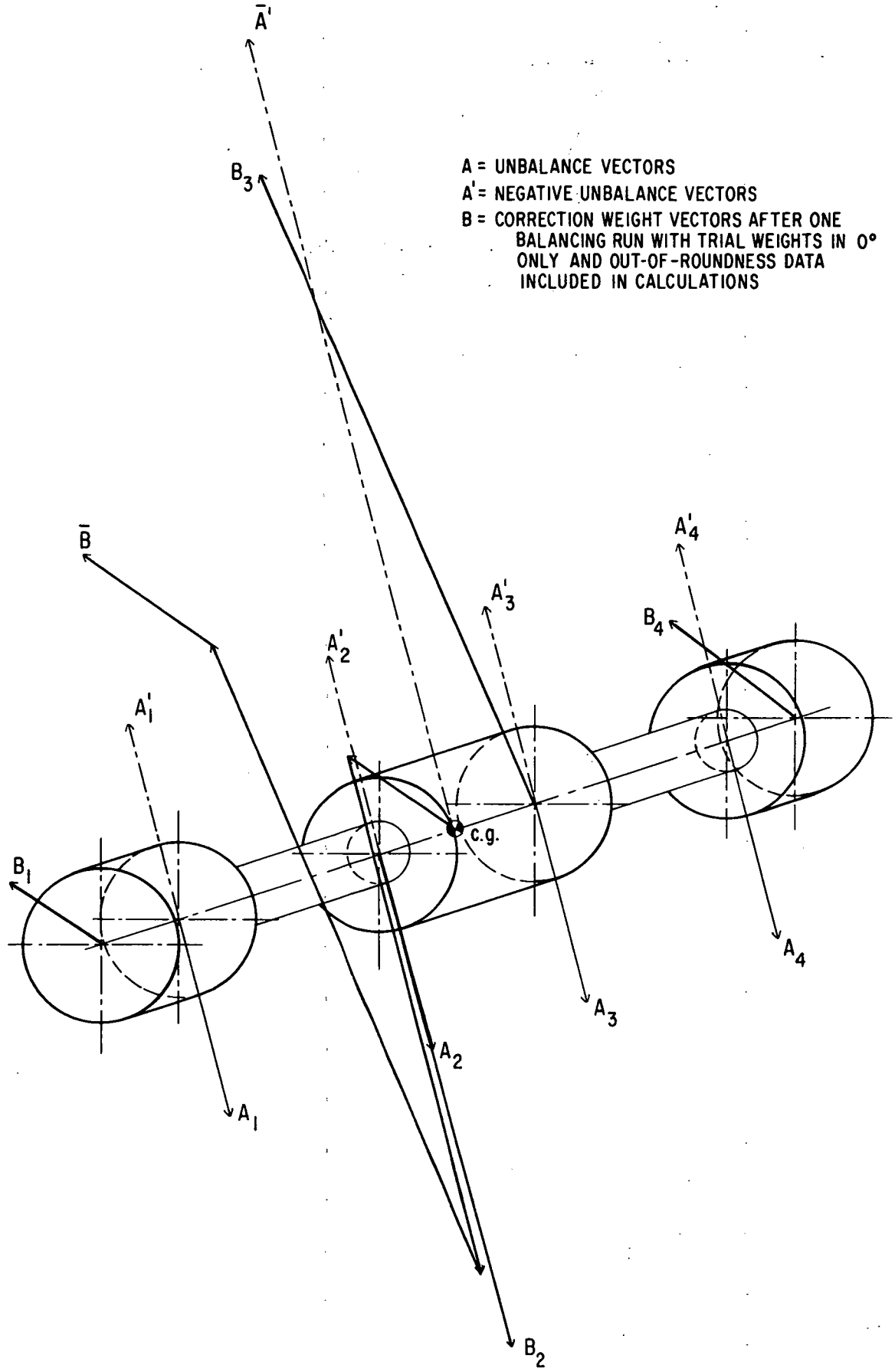

Fig. 61 Unbalance and Correction Weight Vectors for Test Rotor With In-Line, In-Phase Unbalance and Trial Weights in Zero-Degree Location Only

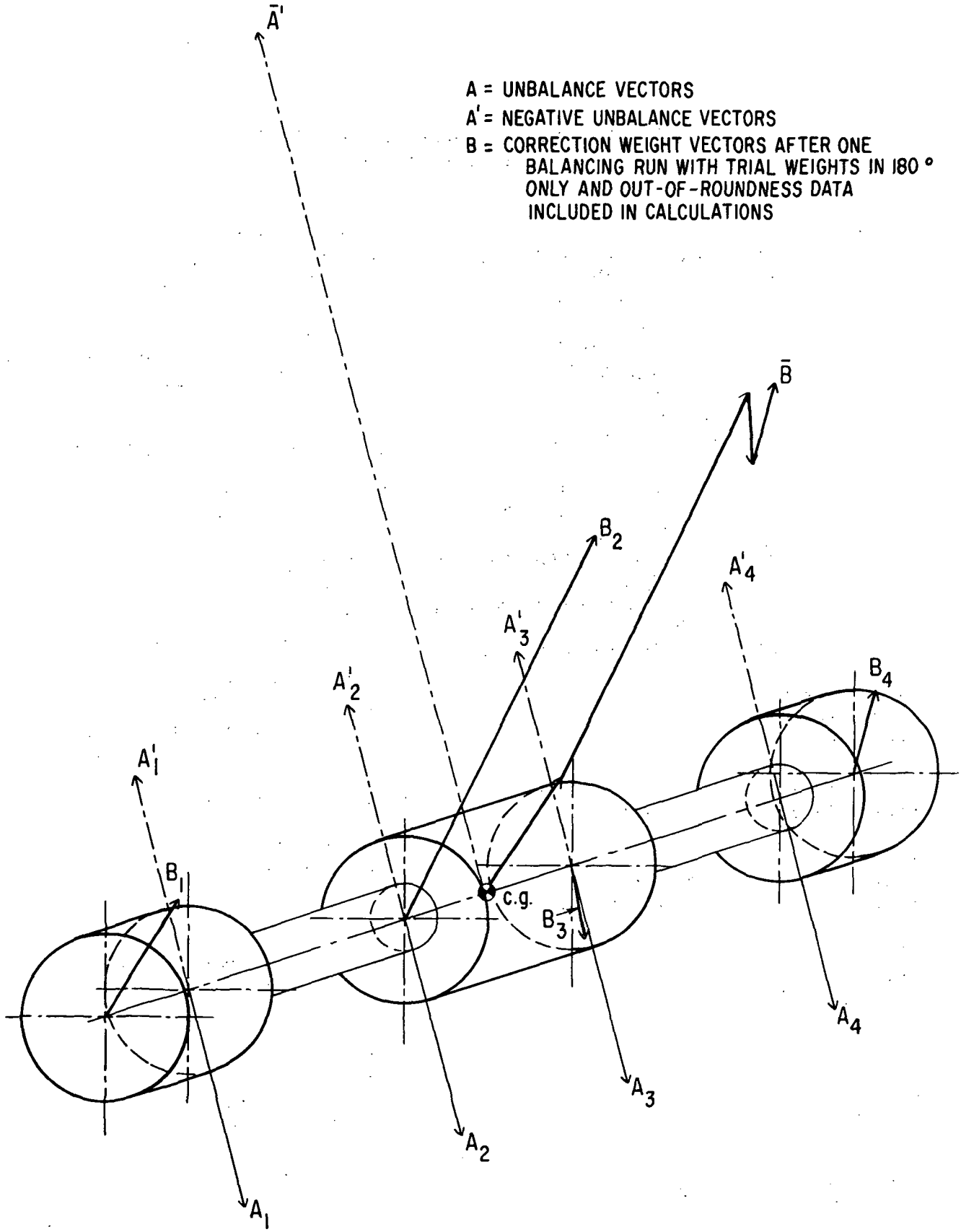

Fig. 62 Unbalance and Correction Weight Vectors for Test Rotor With In-Line, In-Phase Unbalance and Trial Weights in 180-Degree Location Only

BEARINGS BRANCH AERONAUTICS CONTRACTS
Final Report Distribution List

Attention:
Project Manager, MS 6-1
(10 + reproducible)
A. Ginsburg, MS 5-3
E.E. Bisson, MS 5-3
W.J. Anderson, MS 23-2
R.L. Johnson, MS 23-2
B. Lubarsky, MS 3-3
D.G. Beremand, MS 500-202
L.W. Schopen, MS 500-206
C.H. Voit, MS 5-3
D.W. Drier, MS 21-4
Report Control Office, MS 5-5
Library, MS 60-3
Reliability & Quality Assurance Office, MS 500-111
Technology Utilization Office, MS 3-19
Plans and Programs Office, MS 3-15
NASA Lewis Research Center
21000 Brookpark Road
Cleveland, Ohio 44135

National Technical Information Service (40)
Springfield, Virginia 22151

Attention: Library
NASA Ames Research Center
Moffett Field, California 94035

Attention: Library
NASA Flight Research Center
P. O. Box 273
Edwards, California 93523

Attention: Library
NASA Goddard Space Flight Center
Greenbelt, Maryland 20771

Attention: Library
Jet Propulsion Laboratory
4800 Oak Grove Drive
Pasadena, California 91103

Attention: Library
NASA Langley Research Center
Langley Station
Hampton, Virginia 23365

Attention: Library
NASA Manned Spacecraft Center
Houston, Texas 77058

Attention: Library
NASA Marshall Space Flight Center
Marshall Space Flight Center,
Alabama 35812

Attention: N.F. Rekos (RL)
W. Roudebush (RNP)
NASA Headquarters
Washington, D.C. 20546

Attention: Library
Aerojet-General Corporation
1100 West Hollyvale
Azusa, California 91702

Attention: Library
Aerojet-General Corporation
Aerojet Liquid Rocket Company
Sacramento, California 98509

Attention: Library
Aerospace Corporation
P.O. Box 95085
Los Angeles, California 91745

Attention: Library (1)
Lyle Six (1)
AiResearch Manufacturing Company
402 South 36 Street
Phoenix, Arizona 85034

Attention: Library
AiResearch Manufacturing Company
9851 Sepulveda Boulevard
Los Angeles, California 90009

Attention: N. Grossman
Atomic Energy Commission
Division of Reactor Development and Technology
Washington, D.C. 20767

Attention: N. Gerstein
Atomic Energy Commission
AEC-NASA Space Nuclear Systems Office
Washington, D.C. 20545

Attention: Library (1)
C.M. Allen (1)
Battelle Memorial Institute
Columbus Laboratories
505 King Avenue
Columbus, Ohio 43201

Attention: Library
Bendix Research Labs Division
Detroit, Michigan 48232

Attention: Library
Boeing Company
Aerospace Division
P.O. Box 3707
Seattle, Washington 98124

Attention: Library (1)
R. Gabel (1)
Boeing Company
Vertol Division, Boeing Center
P.O. Box 16858
Philadelphia, Pennsylvania 19142

Attention: Library
Continental Aviation and Engineering Corp.
12700 Kercheval Avenue
Detroit, Michigan 48215

Attention: Library
Curtiss-Wright Corporation
Wright Aero Division
Main & Passaic Streets
Woodridge, New Jersey 07075

Attention: Jeffrey V. LeGrow
MSTG Department
General Electric Company
Lynn, Massachusetts

Attention: W. Shapiro
Franklin Institute Research Labs
Benjamin Franklin Pkwy. at 20th St.
Philadelphia, Pennsylvania 19103

Attention: E.N. Bamberger
General Electric Company
Aircraft Engine Technical Division
Bearings, Fuels and Lubricants
Evendale, Ohio 45215

Commanding General
U.S. Army Aviation Systems Command
Attn: Dr. James Chevalier
Mail Stop AMC PM-HLS
P.O. Box 209
St. Louis, Missouri 63166

Attention: Library
General Electric Company
Mechanical Technology Laboratory
R & D Center
Schenectady, New York 12301

Attention: Library
General Motors Corporation
Allison Division
Indianapolis, Indiana 46206

Attention: Library
Hughes Aircraft Corporation
Centinda & Teale Avenue
Culver City, California 90230

Attention: Library
Institute for Defense Analyses
400 Army-Navy Drive
Arlington, Virginia 22202

Attention: Library
Lockheed Missiles & Space Company
P.O. Box 504
Sunnyvale, California 94088

Attention: Library
Massachusetts Institute of Technology
Cambridge, Massachusetts 02139

Attention: Library
Mechanical Technology Incorporated
968 Albany-Shaker Road
Latham, New York 12110

Attention: Library
National Science Foundation
Engineering Division
1800 G. Street, N.W.
Washington, D.C. 20540

Attention: S.M. Collegeman AIR 5365A
Naval Air Systems Command
Washington, D.C. 20360

Attention: W.C. Lindstrom NSC 613D4B
Naval Ship Engineering Center
Washington, D.C. 20360

Attention: W.V. Smith
Naval Ship Research & Development Center
Annapolis Division
Annapolis, Maryland 21402

Attention: J.E. Dray SNHIP 6148
Naval Ship Systems Command
Washington, D.C. 20360

Attention: F.A. Shen
North American Rockwell
6633 Canoga Avenue
Canoga Park, California 91304

Attention: Library
North American Rockwell Corporation
Space Division
12214 Lakewood Boulevard
Downey, California 90241

Attention: S.W. Doroff ONR/463
Office of Naval Research
Washington, D.C. 20360

Attention: Library
Sundstrand Denver
2480 West 70 Avenue
Denver, Colorado 80221

Attention: Library
TRW Accessories Division
23555 Euclid Avenue
Cleveland, Ohio 44117

Attention: Dr. Paul Trumpler,
President
Turbo Research Incorporated
Wayne, Pennsylvania 19087

Attention: Prof. D.F. Muster
Department of Mechanical Engineering
University of Houston
Houston, Texas 77004

Attention: W. Crim
U.S. Army Engineering R & D Labs
Gas Turbine Test Facility
Fort Belvoir, Virginia 22060

Attention: D. Hibner (1)
Library (1)
United Aircraft Corporation
Pratt & Whitney Aircraft Division
400 Main Street
East Hartford, Connecticut 06108

Attention: P.E. Maedel, Jr.
Development Engineering
Steam Division
Westinghouse Electric Corporation
Philadelphia, Pennsylvania

Attention: Lester Burroughs
United Aircraft Corporation
Sikorsky Aircraft Division
Stratford, Connecticut 06497

Attention: R. Givens
SAVFE-AS
U.S. Army Air Mobility R&D Labs
Ft. Eustis, Virginia 23604

Attention: Dr. E.J. Gunter
Department of Mechanical Engineering
University of Virginia
Charlottesville, Virginia 22901

Attention: E.A. Lake
Air Force Aero Propulsion
Laboratory (AFSC)
Wright-Patterson Air Force Base,
Ohio 45433

Attention: Harold Simmons
Pratt & Whitney Aircraft
Florida Research & Development Center
West Palm Beach, Florida 33402